# Hydrological Sensitivity of the Mkomazi River Basin (Tanzania) to Climate Change

Von der Fakultät für Mathematik und Naturwissenschaften
der Carl von Ossietzky Universität Oldenburg
zur Erlangung des Grades und Titels
eines Doktors der (Dr. rer. nat.)
angenommene Dissertation von

**Godfrey Mmbando**

geboren am 04. September 1977 in Tansania

Oldenburg 2015

1. Gutachter Prof. Dr. Michael Kleyer
2. Gutachter Prof. Dr. Gudrun Massmann

Tag der Disputation: 26.03.2015

# Contents

## Summary

The main objective of this study was to simulate hydrological responses to climate change for the southern Mkomazi river basin, a sub-catchment of the Pangani river basin, using the Hydrological Predictions for Environment (HYPE; Lindström et al., 2010) model. The model which best described the relationship between hydrological fluxes and catchment characteristics was influenced by topography, soils and land-cover or land-use. Input data for the model – spatiotemporally distributed rainfall, evapotranspiration, mean air temperature, soil depths profile and soil textures – were modelled by means of regression-based, digital elevation models (DEM) at 90 m spatial-resolution and geographic information system (GIS) techniques. In addition to the regression-based model, soil textures were estimated following the methodology described by Saxton and Rawls (2006).

For rainfall, the models accounted for orographic factors that strongly influenced the spatial variability of rainfall in the region. The area was divided into three zones: windward, leeward and transition zones. The transition zone was modelled as a function of windward and leeward zones. For maximum and minimum air temperatures, the models accounted only for the altitude gradient. Mean air temperature was calculated by using the arithmetic mean of maximum and minimum air temperatures. Incoming solar radiation ($R_s$) was modelled in ArcGIS based on DEM at 90x90 $m^2$ using a hemispherical upward-viewshed algorithm described by Fu and Rich (2002). Extraterrestrial radiation ($R_a$) was then calculated as a function of $R_s$. Reference evapotranspiration ($ET_o$) was calculated using an empirical equation described by Hagreaves and Samani (1985). The maps were made on a monthly basis for rainfall, $ET_o$, and mean, maximum and minimum air temperatures. One soil-depth profile maps and soil textures maps were also constructed. These maps are useful for the purpose of water resources studies.

A flow network connecting sub-basins to the outlet of a catchment was constructed based on DEM at 450x450 $m^2$ followed the methodology described by Jenson and Domingue (1988). Baseline or past-present hydrological response was simulated for the period 1964–1983. The simulation results were satisfactory as indicated by (i) the graphical plot of the estimated and observed hydrographs and the model efficiency $R^2$ a criterion suggested by Nash and Sutcliffe (1970), (ii) the percentage error by volume change ($\Delta V\%$) between observed and simulated total runoff, and (iii) the index of volumetric fit (IVF). The graphical plot revealed that the model captured the patterns of the observed riverflow such as the peak flow, time to peak, and the low flow. However, some peak and low flow were overestimated and others underestimated. Sensitivity of the model to the variation in the input data revealed that total runoff from the catchment is more sensitive to the rainfall than evapotranspiration and soil moisture. It was shown that to some extent inadequacies in these input data can be accommodated with the HYPE model without loss of the model performance.

Hydrological response under global climate change was simulated for the period 2046–2065 using the A2 greenhouse gas emissions scenario. The multimodel ensemble mean for rainfall and air temperatures from seven global circulation models, which were statistically downscaled by Pangani Water Basin Office in collaboration with International Union for Conservation of Nature (PWBO/IUCN, 2010), were used to drive the HYPE model. The ensemble mean runoff changes were mostly the result of precipitation changes, the annual riverflow is predicted to increase by 7%, and by 5% (4%) for maximum (minimum) monthly riverflows. There were insignificant relative changes in soil moisture (green-water) availability. However, green-water availability followed precipitation's changes patterns predicted by the ensemble mean.

**Thesis layout**

This study is divided into seven chapters. Chapter 1 discusses the background and overview of the study. Chapter 2 describes the study area. Chapter 3 describes the climate datasets, quality control of the datasets, and the methodology for modelling climate variables. Hydrological modelling for the past-present (baseline) conditions is described in Chapter 4, and hydrological modelling to climate change is given in Chapter 5. General conclusion of the study is provided in Chapter 6, and a synthesis is given in Chapter 7.

# Chapter 1

# General Introduction

## Background

Global demand for water has been increasing since the 1950s, driven by irrigated agriculture for food production, but the supply of fresh water has been declining (Gleick, 2003). Irrigated agriculture is the dominant user of water that causes water scarcity in many river basins (Molden et al., 2007). More than one billion people live in areas of water scarcity, which includes insufficient water to satisfy normal human needs e.g. drinking and washing (Seckler, 1999; Falkenmark et al., 2007; Hanjra and Qureshi, 2010). Increases in global population – of above nine billion people in the middle of 21$^{st}$ century (UN, 2013) – might intensify water scarcity. Worldwide cereals and meat demand has been projected to increase (de Fraiture et al., 2007) with increases in population (Alexandratos, 1999; Cassman, 1999). Meat demand will amplify water scarcity because meat products are mostly produced by grain-fed animals (Gilland, 2002; Rosegrant and Cline, 2003; Popkin, 2006).

In many parts of the Earth, human development activities include: (i) land degradation in irrigated areas (Carvalho, 2006; Khan and Hanjra, 2008), and (ii) ecosystems degradation (Cassman, 1999; Tilman et al., 2002, 2011), (iii) deforestation and excessive abstraction of river water (PWBO/IUCN, 2006), and (iv) groundwater depletion and pollution (Shah et al., 2008). With this current practices, water resources limits in many parts of the Earth will be reached soon (Falkenmark and Molden, 2008). This will affect not only the availability of water for domestic use, but also for food production.

Global climate change will affect the availability of water for human needs and food production in many parts of the world (Parry et al., 2001; Droogers and Aerts, 2005; Kurukulasuriya et al., 2006), by altering the spatial and temporal distribution of rainfall and evapotranspiration (Solomon et al., 2007). A decline in rainfall together with an increase in temperature will increase crop water requirement – due to high evapotranspiration. On the other hand, extreme rainfall can destroy ecosystems and irrigation schemes. Therefore, some parts of the most densely populated regions of the world such as sub-Saharan Africa might face severe food insecurity and water shortages (Postel and wolf, 2001; Rost et al., 2008).

In sub-Saharan Africa, about 95% of agriculture system is rain-fed (FAO, 2002), and agriculture makes up 20 to 40% gross domestic product (World Bank, 2000). This is the global hotspot region in terms of greater water challenges, high level of poverty and malnourishment (Molden et al., 2007). Secretary-General of the United Nations, Ban Ki-moon, in his article “The new face of hunger (Ki-moon, 2008)”, suggested that Africa should experience a green revolution which raised Asia from an agricultural crisis. However, such revolution considered only blue-water and not green-water. Blue-water is the water which occurs in aquifers, lakes, and reservoirs (Falkenmark and Rockström, 2004). Therefore, in addition to groundwater depletion and pollution, land degradation in irrigated areas, urbanization and loss of fertile soils due to erosion could undermine expansion of the irrigated agriculture systems. For that reason, rain-fed agriculture, which uses green-water, will continue to play a crucial role in providing food in most parts of the sub-Saharan Africa (Molden et al., 2007; Merrey and Sally, 2008).

Green-water is the rainfall infiltrated into the unsaturated soil layer. This infiltrated soil-water it may recharge the groundwater or partly returns to atmosphere by evaporation from soil and transpiration from plants. Combination of evaporation from soil and transpiration from plants is commonly termed evapotranspiration. In other words, the availability and variability of green-water is influenced by weather and climate conditions. Climate systems operating in the sub-Saharan Africa have been predicted to change due to increases emissions of greenhouse gases in the atmosphere (Solomon et al., 2007). It is therefore necessary that the availability and variability of green-water should be analysed in this region, in which the society in many countries e.g. Tanzania relies on the utilization of water resources to reduce short-term dependency.

In Tanzania, rain-fed is the main agriculture system for food production and riverflow for domestic water supply. In some parts of the country groundwater is a source of water for domestic purposes and irrigated agriculture schemes are used for food production. Climate change and weather variability affects many parts of the country, reduces the ability of the country to feed its people and preserve environment (Mongi et al., 2010).

An assessment of the availability and variability of soil moisture or green-water is a challenging issue, due to complex soil moisture dynamics, which are controlled by the interactions between the atmosphere and land-surface. Hydrological modelling is usually used to link the atmosphere and land-surface processes such that the availability and variability of green-water can be assessed. The availability and variability of green-water is influenced by the scale of the assessment. River basins are considered as useful units for the analysis of soil moisture or green-water. Also, the scale can be short- or long-term timescale. In most cases a scale of assessment depends on the availability of data and the timeframe available for a research.

## Understanding soil moisture dynamics

Soil is a complex porous media containing mineral particles, water and air, together with some amounts of organic matter (Kutílek and Nielsen, 1994). Soil water or soil moisture varies in space and time (Dingman, 1994). Soil moisture modulates interactions between the atmosphere and land-surface, by influencing evapotranspiration, runoff and drainage to the groundwater systems (Dunne et al., 1975; Binley and Beven, 2003). Therefore, soil moisture influences ecological patterns (Rodriguez-Iturbe, 2000) and soil processes related to agricultural production and plant growth (Brady, 1990; White, 2009).

The standard quantitative definitions of soil moisture are (i) gravimetric and (ii) volumetric (Kutílek and Nielsen, 1994; Hillel, 1998). Gravimetric is the mass of water divided by the mass of dry soil, whereas volumetric is the volume of water divided by the volume of soil. These two definitions are linked by the dry soil bulk density, which is the ratio between the volumetric and the gravimetric soil moistures. Soil moisture is a quantity that represents the average conditions in a finite volume of soil. Therefore, it is important to know the volume and depth range that represents a soil moisture value.

Theoretically, the range in soil moisture is bounded by zero values and the soil porosity values. Soil porosity is the ratio between the volume of soil pores and the volume of soil. In the field the practical lower limit on soil moisture is positive due to the inability of plants to extract water below a particular level, commonly called the wilting point (Kutílek and Nielsen, 1994; Hillel, 1998). A two-dimensional conceptualization of the soil profile and the fluxes influencing the soil moisture stored in the soil profile is illustrated in Figure 1.1a. In general, the exchange of energy between the atmosphere and soil control changes in soil moisture. The soil moisture store is replenished by infiltration and depleted by soil evaporation, plant transpiration, runoff and by groundwater discharge i.e. drainage (Figure 1.1a). The relative importance of evaporation and transpiration depends on the vegetation cover, with transpiration dominating in well-vegetated landscapes. Fluxes between the soil and groundwater can be important in some contexts. Drainage from the soil profile is the primary source of recharge for many groundwater systems, and capillary rise from shallow groundwater tables can be an important source of water replenishing the soil water store during drier periods. The energy and moisture fluxes are linked through the evapotranspiration processes. When soil moisture is evaporated or transpired a phase-change (latent heat of vaporization of water) from liquid water to water vapour occurs. Soil moisture availability, in conjunction with atmospheric conditions, controls the evapotranspiration and the partitioning of incoming solar energy into latent and sensible heat fluxes.

A general loamy-type soil moisture profile for the volume of soil moisture and its dynamics change with soil depth is shown in Figure 1.1b. Close to the surface, soil moisture is strongly influenced by the fluxes between the active root zone and the atmosphere, in which the soil moisture is more variable than the moisture at deep soil-depth. Soil moisture close to the surface responds more quickly and therefore has both short and long term variability, whereas at deep soil-depth soil moisture is less responsive to short term variations in the fluxes across the soil-atmosphere interface.

Changes in soil water tension and hydraulic conductivity with soil moisture content for a general loamy-type soil are shown in Figure 1.1c and 1.1d. As smaller pores are emptied of water the tension increases due to capillary effects, whereas the hydraulic conductivity declines as the soil dries. These two effects results in hydraulic gradients, dominated by gravity and conductive soils at high moisture contents. Provided a soil is free to drain, wet soils drain to the point where gravity can no longer remove water from the soil pores. The soil moisture at this point is the field capacity (Kutílek and Nielsen, 1994; Hillel, 1998). At lower soil moisture contents, the hydraulic gradients are dominated by soil water tension, and the resistance to flow increases rapidly. – Because of the rapidly decreasing flow velocities as soil dries, the spatial scale at which soil water flow processes operate is very much smaller for dry soils than for wet soils. The changes in soil water tension affect evapotranspiration by increasing the energy required to extract water from the soil as soil moisture decreases. This leads to a marked reduction in evapotranspiration under dry conditions. – Eventually the tension becomes so large that plants can no longer extract water from the soil and they wilt. This soil moisture content is referred to as the wilting point (Kutílek and Nielsen, 1994; Hillel, 1998).

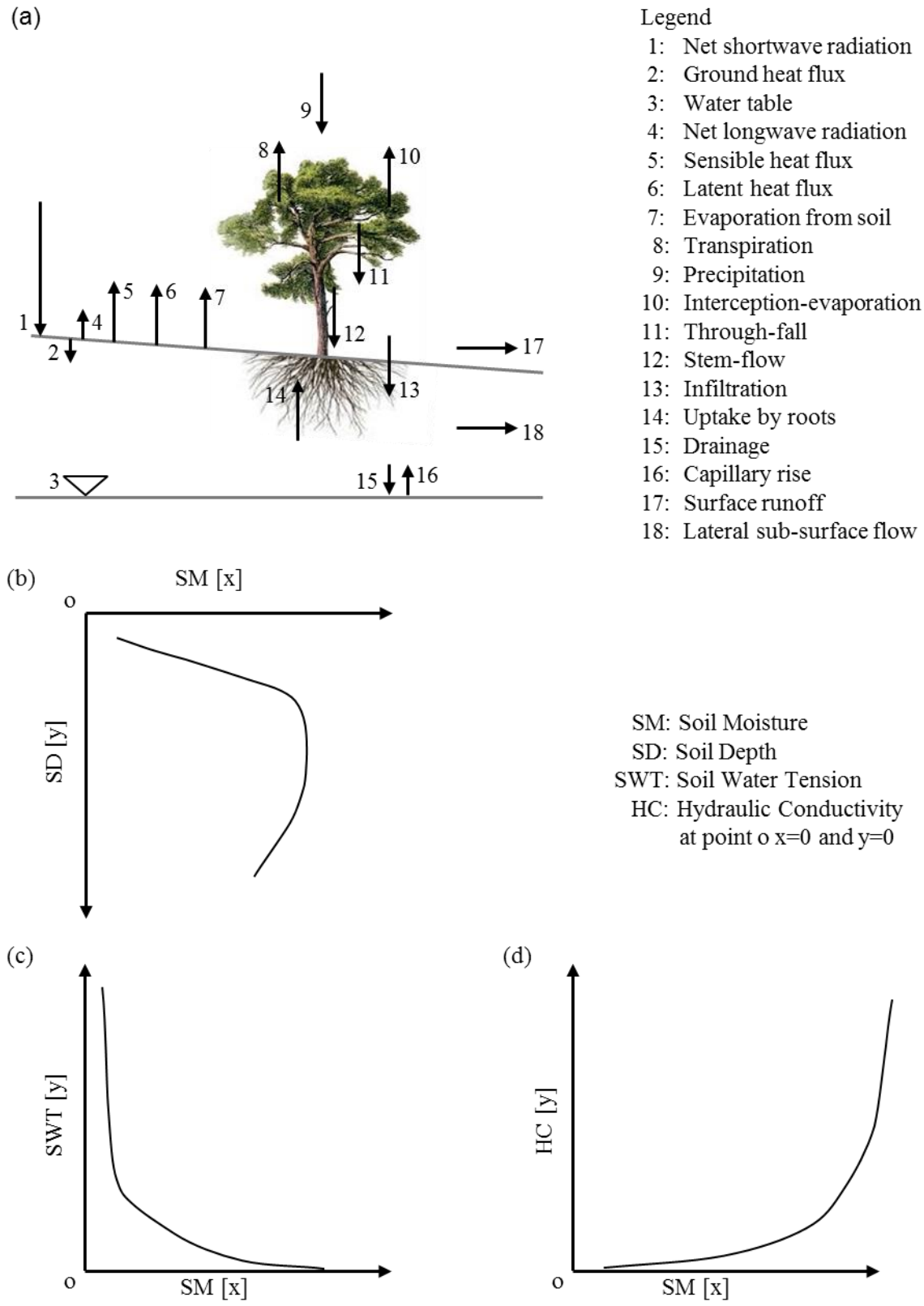


Figure 1.1. Soil-atmosphere interface: (a) a two-dimensional conceptualization of surface energy fluxes affecting soil moisture, and a general loamy-type soil moisture availability profile curves with varying (b) Soil depth, (c) soil water tension, and (d) hydraulic conductivity (modified from Western et al. (2002)).

## Hydrological modelling understanding

Hydrological modelling links hydrological cycle components. These components include precipitation, interception-evaporation, stem-flow, through-fall, infiltration, plant roots uptake, bare soil evaporation and runoffs (Freeze and Harlan, 1969). In other words, hydrological modelling partitions water among various pathways of the hydrological cycle components (see Fig. 1.1a for the components). Lateral sub-surface flow takes place where: (i) the topographic relief has a surface slope greater than a few percent, (ii) anisotropy between vertical and horizontal hydraulic conductivities (Zaslavsky and Sinai, 1981), and (iii) soil moisture content is sufficiently high for a long period.

Different spatiotemporally scales in formulating water pathways have significant impact on a final hydrological response results. For example, the small-scale hydrodynamics theories such as that described by Eagleson (1978) cannot be easily extended to make predictions at large scale, because of the heterogeneity and variability existing in natural catchments. At a small-scale, variability in the catchment characteristics such as steepness and orientation of slopes, snow patches, vegetation and soils have significant influence on hydrological response. This is illustrated, for example, by Blöschl and Sivapalan (1995) that (i) the influences of vertical (vadose-zone) processes dominates at a small plot scales, (ii) topography begins to dominate runoff processes at the hillslope scale, and (iii) stream network begin to dominate at spatial soil moisture variations. At large-scale this variability is usually averaged out.

When moving towards a larger-scale, hydrological processes appear to become more regular than the processes at a small-scale (Blöschl and Sivapalan, 1995). Therefore, there are two hydrological modelling approaches: downward and upward. In the downward approach, hydrological response of a catchment is derived from the observed annual hydrological response e.g. runoff is equal to the difference between rainfall and evapotranspiration. As a time-scale decreases to a month and day scales, the complexity of the model is increased by addition of pathways. These pathways include: (i) separation of runoff into surface flow and lateral sub-surface flow, (ii) separation of lateral sub-surface flow into shallow sub-surface flow and deeper baseflow, (iii) introduction of delays in saturated zone, (iv) separation of total evapotranspiration into bare soil evaporation, transpiration and interception-evaporation, and (v) introduction of channel flow routing. Examples of downward hydrological modelling approaches include studies by Klemês (1983), Jothityangkoon et al. (2001), Atkinson et al. (2002) and Farmer et al. (2003).

In upward approach a hydrological model is developed by incorporating fluxes describing water movements across a land-atmosphere interface (see Fig. 1.1a). The inclusion of these fluxes such as (i) interception-evaporation, (ii) surface flow, (iii) unsaturated soil moisture movement in both vertical and lateral directions, and (iv) groundwater movement in both unconfined and confined conditions. Depend mainly on topography, vegetation or land cover, and the objective or purpose of a model. There are many hydrological models with a varying complexity that have been developed for different purposes and regions of the earth (Singh, 1995). Therefore, the objectives of the study, availability of data, and research timeframe including funds are major factors in choosing a suitable complexity of a hydrological model.

## Objectives

This study aimed to understand the linkages between the atmosphere and land surface in the Mkomazi river basin, using an upward hydrological modelling approach. This approach enabled to assess the availability of soil moisture (green-water) under the influence of global increases in emissions of greenhouse gases in the atmosphere concentrated in the middle of 21$^{st}$ century.

The following specific objectives were identified:

1) To analyse rainfall, temperature and evapotranspiration patterns, and construct respective maps on a monthly basis.
2) To simulate hydrological response for the Mkomazi river basin for the past-present (baseline) conditions, and draw the simulated soil moisture availability maps on a monthly basis.
3) To simulate hydrological response for the Mkomazi river basin for the predicted effects of global increases emissions of greenhouse gases in the atmosphere, and draw the simulated soil moisture maps on a monthly basis.

# Chapter 2

# Study Area

## Introduction

Because the study area is part of the Pangani river basin, many issues in the study area are applicable to the entire Pangani river basin. The description of the Pangani river basin is thus given followed by the description of the Mkomazi river basin.

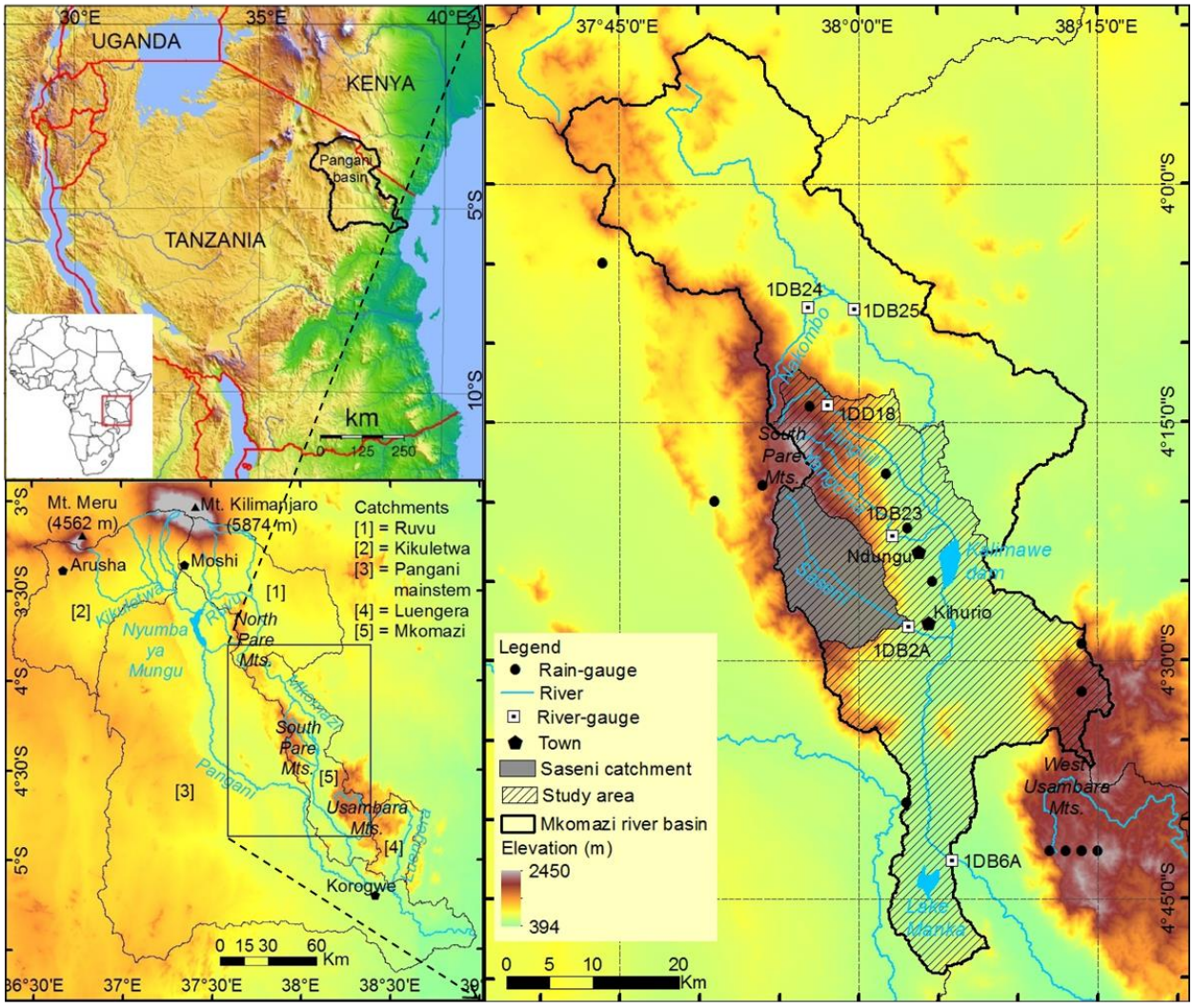


Figure 2.1. A map shows the location of the Pangani river in Tanzania and the location of the study area in the Mkomazi river basin.

## Pangani River Basin

The Pangani river basin, located in northern Tanzania, is one of the nine major river basins in the country, with a size of approximately 43000 $km^2$. About 5% of this area is located in Kenya (Fig. 2.1). The Pangani river basin can be divided into five main catchments called (i) Ruvu, (ii) Kikuletwa, (iii) Pangani main stem, (iv) Luengera, and (v) Mkomazi (PBWO/IUCN, 2006). These catchments have distinct hydrological characteristics. The Ruvu river originates from the North Pare mountains and receives tributaries from South-eastern slopes of the Mt. Kilimanjaro. The Kikuletwa river originates from the Mt. Meru and receives tributaries from South-western slopes of the Mt. Kilimanjaro. The Ruvu and Kikuletwa catchments are characterized by many perennial springs. These catchments flow into the Nyumba ya Mungu dam of a surface area of 100 $km^2$, which was constructed in the 1960s mainly for hydropower generation. Currently this dam generates about 17% of the country's hydropower (IUCN, 2003).

The area upstream of the Nyumba ya Mungu dam also named as the Upper Basin and the Lower Basin for an area downstream of the dam. From the outlet of the Nyumba ya Mungu dam to the Indian Ocean, the river is called Pangani and is fed by only two major tributaries called Luengera and Mkomazi rivers. The Luengera river drains the eastern Usambara mountains, while the Mkomazi river drains the Pare and the eastern slopes of the West Usambara mountains. These rivers join the Pangani river in Korogwe town with the Mkomazi river upstream of the Luengera river. The intermittent flow originating from the western sides of Pare mountains during the rainy seasons, recharges the local groundwater and wetlands, and thus makes insignificant contribution to Pangani river. Springs account for almost half of the total dry season discharge in the basin (IUCN, 2003).

Most of the estimated 3.7 million people in the Pangani river basin rely directly or indirectly on agricultural activities for their livelihoods (IUCN, 2003). The urban population in the Pangani river basin is growing rapidly. Particularly in the two major cities of Arusha and Moshi which are the most developed areas economically. Despite the rapidly growing urbanization, 90% of the population in the Pangani river basin live in rural areas. Reliable rainfall and springs originating from the foot of the Mt. Kilimanjaro and Mt. Meru provide sufficient livelihoods to the society in the Upper Basin with Arusha and Kilimanjaro regions.

Traditionally, agriculture or crop productions in the Pangani river basin were mainly in the elevated and easily accessible areas. These were areas where people lived. The irrigation furrows were traditional, and the flow of water was not regulated, because water was plenty and the population were low. Increases in population in mountainous areas forced people to the lower lands, and further far away from the source of water. This led to the construction of many furrows for irrigation. According to Turpie et al. (2003) more than 2000 indigenous irrigation furrows were found in the Upper Basin on the slopes of Mt. Kilimanjaro and Mt. Meru. There are also many indigenous irrigation furrows in the Lower Basin (downstream of the Nyumba ya Mungu dam), which were observed during our field observations, in the Pare and Usambara mountains. According to the United Republic of Tanzania (URT, 1977), 90% of water consumption by irrigation users in the Pangani river basin are indigenous smallholder

irrigation schemes. Also, about 85% of water consumption in the Kilimanjaro region is attributed to irrigation. In general, the efficiency of many of these indigenous irrigation canals and intakes, which are made of logs, mud and stones, is very poor. Most of these canals and intakes are unlined earthen furrows (Adams et al., 1994; Fleuret, 1985) with water losses above 80% (IUCN, 2003). But note that the abstraction of water is legal in the Pangani river basin with the possession of the water right.

Over the past decades, water abstraction and climatic factors have reduced instream flow into the Nyumba ya Mungu dam from several hundred to less than 40 $m^3 s^{-1}$ (IUCN, 2003), which is affecting the production of power supply. Demand for irrigation water escalates to meet requirements of an increasing population in the Pangani river basin (Grove, 1993; Potkanski and Adams, 1998). With competition over water between the irrigation systems still remains, there are intensifications of the land-use in the basin. The forest cover in the Pangani river basin is threatened not only because of agriculture for food production, but also to meet the growing semi-urban requirements for timber, charcoal and firewood. Over the second half of the last century alone, natural forest area in Kilimanjaro declined by 41 $km^2$ (IUCN, 2003). Also, it is estimated that about 80% of Pare and Usambara mountains, which historically have been known to be covered with forests, has been lost due to human development (IUCN, 2003). Although many households in the Pangani river basin use charcoal, firewood is still a major source of energy for cooking. The Pare and Usambara mountains occupy some of the most densely populated areas of the Pangani basin (IUCN, 2003). In the West Usambara mountains, populations have grown more than twenty-fold since 1900 (Newmark, 1998).

Many parts of the Pangani river basin have been instrumented with meteorological stations, and major tributaries have been gauged (IUCN, 2003). However, the Pangani river basin lacks long-term records in many of its major catchments (IUCN, 2003), particularly river flow data compared to rainfall. This can be attributed to the management. Before the Pangani Basin Water Office (PWBO) initiated, the Ministry of Water was responsible for collection and management of hydrological and meteorological data, through its Regional Offices. It is fair to say that there was not much attention in taking readings and then in keeping records. This responsibility has now devolved to the PWBO. Below the Ministry of Water and Irrigation (MoWI) at the national level, the authorities responsible for Pangani river basin are (i) the Pangani Basin Water Board (PBWB) which comprise representatives of non-government organizations, and (ii) the PBWO which deals with technical matters and implementation. The PBWO apportions water rights within the basin and is responsible for the monitoring of streamflow and water quality, but for the meteorological stations, the in charge is the Tanzania Meteorological Agency (IUCN, 2003).

## Mkomazi River Basin

*Physiography*

The research focuses in the southern Mkomazi river basin, which is in the mid-reaches of the Pangani river basin. This mountainous catchment is located at latitude (4°10'S–4°50'S) and longitude (37°50'E–38°20'E), with a size of approximately 1188 $km^2$ (Fig. 2.1). The elevation above sea level ranges from 400 m along the Mkomazi valley to 2300 m and 2450 m in the West Usambara and South Pare mountains. Physiography varies from plains along the valley to rugged escarpments and steep slopes formed by erosion in the surrounding mountainous range.

*Geology*

The geology of the area is characterized by weathered metamorphic igneous rocks and superficial deposits (Bagnall, 1963), associated with the granulite-gneiss complexes in the Mozambique belt (Muhongo and Lenoir, 1994; Mutakyahwa et al., 2001). Rocks have undergone regional metamorphism, resulting in the development of a strong foliation almost parallel to the bedding, with a predominant granulite-pyroxenes facies (URT, 1965). The steep scarps observed in the catchment are retreated fault scarps, with the actual faults buried under superficial deposits. Differences in topography and climate give rise to a spatial variation in soil depth, colour and composition. Soils on the forests and on mountains valleys are loamy clays with dark-red to red-brown colour (Anderson, 1963; Johansson, 2001), whereas soils on scraps slopes are predominately yellowish. Reddish soils consisting of unconsolidated deposits and limestones are found along the Mkomazi valley. The alluvial deposits are found in the flood plains and along the river beds, which are mainly due to soil erosion and deposition (Mul et al., 2007).

*Climate*

The southern Mkomazi river basin is characterized by an extreme weather variability, particularly in rainfall. Peasant farmers cultivation is based on the following rainfall patterns (i) ‘vuli’ (the short-rains) from October to January, (ii) ‘masika’ (the long-rains) from March to May sometimes up to June, and (iii) ‘mluati’ (the intermediate-rains) from August to September. This latter rainfall pattern is mainly on high mountains areas, depending on the orientation of the mountain slopes. In general, the climate of the southern Mkomazi river basin is largely influenced by the equatorial East African climate systems.

*Agricultural, land and water use*

The South Pare and West Usambara mountains are covered with the tropical rainforests exhibiting a high diversity of species (Bjorndalen, 1992). Some species have been reduced or deforested, due an increasing land demands for agricultural related activities. However, there

are parts of the reserved forests areas, and the degradation continues on remains of the reserved forest areas (Kaoneka and Solberg, 1994; Conte, 1999; Johansson, 2001; Kashimbiri et al., 2005; PWBO/IUCN, 2007). It is estimated that about 73% of the natural forest cover in the South Pare mountains has been reduced and 84% for the West Usambara mountains (Newmark, 1998).

Peasant farmers in the area produce first to meet their basic domestic food requirements. They produce mainly maize, beans, Irish-potatoes, sweet-potatoes, bananas, cassava and vegetables including cabbages, carrots, tomatoes and onions (Johansson, 2001). However, over the last three decades agriculture has remained the backbone of the local economy and become a source of important cash income (Johansson, 2001).

In the West Usambara mountains, agriculture activities are dominated by small-scale farming and livestock keeping. Different farming systems exist in the area, depending on topographic conditions. On the steep slopes down to the Mkomazi valley, agriculture is rain-fed and often without erosion control. Maize and beans are regularly washed away by flash floods. On the slopes down to the West Usambara mountains floodplains, hedges are often planted with forage grass for cattle and preventing soils against erosion, agriculture is also rain-fed with maize and beans. The most productive area with diverse crops is in the floodplains, in which natural riparian vegetation was cleared and eventually streams are not apparent any more (Johansson, 2001). In addition to rain-fed, irrigation agriculture is common in these areas.

In the Mkomazi valley, in the areas surrounding Ndungu and Kihurio towns (Fig. 2.1) water is available. These areas are characterized by a variation of agriculture activities, and intensive grazing. During the rainy seasons, particularly the long-rains season, rain-fed agriculture is practiced in all parts of the Mkomazi valley, with cultivation of maize, beans and rice as major crops. During the dry season, crop production depends on irrigation systems. Competition of river-water during the dry season is extremely high (based on field observations). An abstraction of water ranges from using indigenous furrows by peasant farmers to concrete furrows owned by the Ndungu rice scheme. The Mkomazi valley has sharp spatial contrasts in water availability. The areas to the South of the Mkomazi river are very dry during the dry season or for a prolonged dry spells during rainy seasons. Norbert et al. (2002) noted that the probability of crop failure in the South Pare and West Usambara mountains is high because of soil types and rainfall variability. This indirectly explains the intensification of suitable land on the mountains.

Small-scale farming systems also play a significant role in the South Pare mountains. In contrast to the situation in the West Usambara mountains, agricultural systems in the South Pare mountains are integrated into the natural forest ecosystems. In fact in many agricultural areas forests had been cleared. Nevertheless, in some areas where bananas, maize, sugar cane, ginger, and vegetables are grown some forest trees exist. Crop production is practiced throughout the year in many parts of the South Pare mountains. Indigenous furrows are used to divert water to meet plant-water requirements during the dry spells. During the dry season, agriculture in South Pare mountains can be termed as fully irrigated, with indigenous furrows abstract water at their maximum capacity (Makurira et al., 2007). Land users on the lower mountain slopes and in Mkomazi valley receive less water than in the past. Particularly during

the dry spells due to the increased cultivation of highly water consuming crops like ginger and sugar cane on the South Pare mountains.

*Runoff*

The Mkomazi river basin is fed by four tributaries called Saseni, Yangoma, Hingilili and Nakombo. However, currently the southern Mkomazi river is fed by two perennial tributaries, the Saseni and Yangoma rivers (see Fig. 2.1). According to PBWO/IUCN (2006), the Mkomazi river basin is the most developed catchment of the Pangani river basin. It is estimated that about 58% of the generated runoff in the Mkomazi basin is used. For the southern Mkomazi basin, the rivers flows originating from the eastern slopes of the South Pare mountains are reduced by increasing agriculture activities, which reduces the flow to the mid- and low-lands, and thus reduce flow to the southern Mkomazi river.

Figure 2.2 shows the difference in the "current day" flows and "naturalized" flows. Current day flow represents the flows that can be expected under current water use levels, subject to a long-term variable rainfall. Naturalised flow represents flows that could have occurred prior to the start of development in the catchment. Not only the flows are reduced during the dry season, the river now is drying (Fig. 2.2). Population increase and resultant water-use increase have triggered these changes. Increasing population density has increased the necessity for agricultural lands. In mountains areas, forests areas have been reduced and mountains slopes cleared for agriculture purpose but also for timber and firewood. Deforestation usually increases surface runoffs, particularly in mountainous or elevated areas. PBWO/IUCN (2006) noted that the Mkomazi river basin is the only catchment of the Pangani river basin which experiences large flood events during the short-rains season.

*Social-issues*

The sourthern Mkomazi basin is the home of three main tribal groups (i) the WaPare, (ii) the WaShambaa, and (iii) the WaMbughu people (Egger, 1980). The WaPare and WaShambaa are Bantu-speaking people and the WaMbughu a very small Hamitic-speaking group. The WaPare people are the dominant group in the South Pare mountains. The West Usambara mountains are historically known as the home of the WaShambaa. With their unique Shambaa mountain kingdom and chiefdoms (Shambalai) of the 19$^{th}$ century which existed until the arrival of German colonials, when widespread land alienation spelt the beginning of the end of the kingdom (Johansson, 2001). The WaMbughu are mostly in the West Usambara mountains. The WaPare are also in the West Usambara mountains. During the 1960s many of the WaPare people migrated from the South Pare mountains to the West Usambara, largely due to inter-clan conflicts wars with the WaChagga and land pressure conflicts with the WaMaasai (Egger, 1980). These three groups live in harmonious manner working and trading among each other.

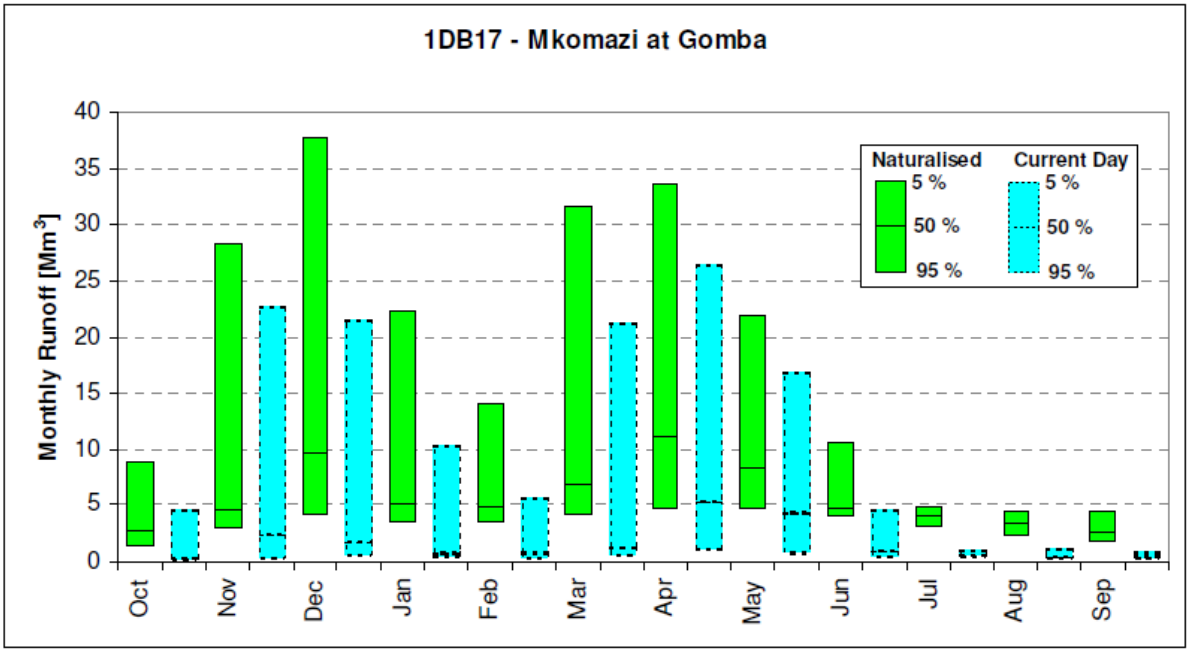


Figure 2.2. Comparison of naturalised and current day flows for the Mkomazi river catchment (source: PBWO/IUCN, 2006). Monthly runoff [M $m^3$] is equal to [$10^6$ $m^3$].

# Chapter 3

# Mapping Precipitation, Temperature and Evapotranspiration: a case study Mkomazi river basin in Tanzania

## Abstract

It is still a challenge to provide spatially explicit predictions of climate parameters in African regions of complex relief, where meteorological information is scarce. Here we predict rainfall, temperature and reference evapotranspiration ($ET_o$) for the southern Mkomazi river basin in north-eastern Tanzania, Africa, by means of regression-based, digital elevation models (DEM) at 90 m spatial-resolution and geographic information systems (GIS) techniques.

We mapped rainfall for the period 1964–2010. The models accounted for orographic factors which strongly influenced the spatial variability of rainfall in the region. According to orography, the area was divided into three zones for modelling rainfall: windward, leeward and transition zones. The transition zone was modelled as a function of windward and leeward zones. Rainfall indicates high spatial and temporal variability dominated by equatorial East African region climate circulation systems.

Maximum and minimum temperatures were modelled for the period 1989–1994, the models accounted only for the altitude gradient. Mean temperature was calculated by arithmetic mean of maximum and minimum temperatures maps in ArcGIS. $ET_o$ was estimated following the method described by Hargreaves and Samani (HS). Solar radiation was modelled in ArcGIS based on DEM using a hemispherical upward-viewshed algorithm. HS equation was then applied by layer algebra in ArcGIS to calculate $ET_o$.

The maps were made on a monthly basis for rainfall, $ET_o$, and mean, maximum and minimum temperatures. The obtained maps are useful for the purpose of agriculture, ecological and water resources management.

**Keywords:** linear regression, mapping, rainfall, temperature, reference evapotranspiration, DEM, GIS, Mkomazi river basin

## Introduction

Accurate precipitation, temperature and evapotranspiration maps at landscape scales are needed for many applications in agriculture, climate forecasting, irrigation schemes, and water provisioning. These climatic maps are important in ecological studies because precipitation, temperature and evapotranspiration strongly influence the transfer of moisture between the surface and the atmosphere at local and regional level. Precipitation is the main source of water in the terrestrial water cycle, while evapotranspiration returns about 65% of precipitation into the atmosphere, depending on the vegetation cover (Trenberth et al., 2007a). The sun as a black body emits energy at 5800 K (5530 °C), averaged over the year and of all surfaces of the Earth this amounts to 342 W $m^{-2}$. Some amount of such solar energy is used for all plant physiological processes and sets up large-scale climatic conditions and patterns.

Precipitation and temperature are mostly measured at meteorological stations. Evapotranspiration is commonly assessed indirectly by either (i) considering the energy

balance at land surface (Ward and Trimble, 2004), (ii) by measuring eddy covariance at some distance above the land surface (Mu et al., 2007), (iii) by a water balance approach for watersheds when precipitation, change in storage, and stream discharge are known (Ward and Trimble, 2004), or (iv) by estimating reference evapotranspiration ($ET_o$) from a hypothetical surface of green grass cover of uniform height of 0.12 m adequately watered with surface resistance of 70 s $m^{-1}$ and albedo of 0.23 (Allen et al., 1998).

In general, precipitation and temperature patterns on the earth's surface are determined by the combination of geographic factors including altitude, latitude, aspect and exposure, atmospheric circulations, the effect of continentality and characteristics of ocean currents (Aguado and Burt, 2001). Mountain climates are controlled by the same factors, with their hydrological and ecological systems being sensitive to climate variability (Beniston, 2003; Diaz et al., 2003), compounded by local infinite variety of combinations created by orientation, spacing, and steepness of slopes, along with the presence of complex patterns of snow patches, shade, vegetation and soil. By acting as a barrier, mountains themselves affect local and regional climate and modify passing storms. When mountain ranges are oriented perpendicular to the prevailing winds, forced ascent of air is usually most effective, the more exposed the slope, the more rapidly air will be forced to rise and cool (adiabatic), which results in precipitation. Great variations in precipitation and temperature occur over relatively short distances; one slope may be excessively wet with more precipitation at higher elevations while another is relatively dry (Barry, 1992; Whiteman, 2000).

Different interpolation or extrapolation methods can be envisaged to map climate variables in a spatially explicit way. Over the last few decades, geostatistic interpolation methods (Li and Heap, 2008) became commonly used and recognized to have several advantages (Isaaks and Srivastava, 1989; Atkinson, 1997; Goovaerts, 1997; Zhang and Srinivasan, 2009) over non-geostatistic methods such as Thiessen polygon, inverse distance weighting, or isohyetal methods (Thiessen, 1911; Shepard, 1968; McCuen, 1989).

Many research studies have used geostatistic techniques which consider topographic variations in mapping climatological variables on mountains terrain. Studies exemplifying these approaches are (Phillips et al., 1992; Pardo-Igúzquiza, 1998; Prudhomme and Reed, 1999; Goovaerts, 2000; Drogue et al., 2002; Diodato, 2005; Buytaert et al., 2006; Moral, 2010; Westerberg et al., 2010; Mair and Fares, 2010) for precipitation and (Martinez-Cob, 1996; Mardikis et al., 2005; Noshadi and Sepaskhah, 2005) for evapotranspiration. However, most of these interpolation techniques do not take into account the effect of relief and other geographic factors.

For that reason, interpolation techniques should take into account the potential effects of topographical factors on the spatial distribution of climatic variables. Such interpolation techniques (universal techniques) use geographic information systems (GIS) and digital elevation models (DEM) for spatial analyses (Burrough and McDonnell, 1998; Chapman and Thornes, 2003).

Several researchers have demonstrated the potential of universal techniques on mapping precipitation (Daly et al., 1994; Drogue et al., 2002; Guan et al., 2005; Ranhao et al., 2008;

Um et al., 2010), temperature (Ninyerola et al., 2000; Hong et al., 2005; Gómez et al., 2008) and evapotranspiration (Vicente-Serrano et al., 2007; McVicar et al., 2007). In these regression-based techniques, geographic and topographic factors that control the spatial distribution of climate are used as independent variables (Basist et al., 1994), and dependence models are created between the climate data and independent variables. The main advantage of this technique is that maps are compiled from weather stations and auxiliary information that describes geographic and topographic variables which improves the accuracy and spatial detail of the maps. A goal of the present study is to apply universal interpolation methods and GIS technologies in mapping precipitation, temperature and evapotranspiration of the southern Mkomazi river basin, an East-African mountainous region. The region is typical for remote East-African rural areas, where most of the population settles on the slopes of the mountains and in the vicinity of the river, whereas the semi-arid plains are scarcely populated.

The climate of the southern Mkomazi river basin is characterised by two distinct rainfall seasons. Long-rains in March–May are commonly abundant (Camberlin and Philippon, 2002) whereas short-rains in October–December reveal more interannual variability (Hastenrath et al., 1993; Nicholson, 1996; Mutai and Ward, 2000; Philippon et al., 2002). This bimodal pattern is largely related to the seasonal migration of the inter-tropical convergence zone (ITCZ) across the equator (Mutai et al., 1998; Slingo et al., 2005).

There are two essential phenomena influencing the interannual rainfall variability in this region: (i) the El Niño-Southern Oscillation (ENSO; Janowiak, 1988; Ogallo, 1988; Indeje et al., 2000; Hastenrath et al., 2004; Kijazi and Reason, 2005), and (ii) the Indian Ocean dipole (IOD; Saji et al., 1999; Webster et al., 1999; Behera et al., 2005; Marchant et al., 2007) or Indian Ocean zonal model (IOZM; Black et al., 2003; Clark et al., 2003; Fischer et al., 2005). Both extreme weather events can bring large floods (Birkett et al., 1999; Behera et al., 1999; Latif et al., 1999; Murtugudde et al., 2000) or strong droughts (Hastenrath et al., 2007; 2010), which severely affect the livelihoods of the people.

Therefore, better knowledge of the spatial distribution of precipitation, temperature and evapotranspiration is required, particularly in areas with strong variations in topography and elevation (Daly et al., 1994; Vicente-Serrano et al., 2007; Gómez et al., 2008). To address this, the present study uses regression-based techniques and GIS knowledge to construct monthly maps of precipitation, temperature and evapotranspiration, accounting for major topographic influences, particularly elevation, surface orientation and obstruction by surrounding topographic features.

Unfortunately, the number of meteorological stations where precipitation, air temperature, wind speed, humidity and solar radiation are observed is limited in many parts of the globe, particularly in developing countries. Many sub-Saharan countries continue to experience difficulties with the availability of long-term climatic data and available information is sparse with numerous prolonged gaps both in time and space. These limitations in the quantity and quality of site observations impose substantial constraints on studies of the climatic variability, particularly in the southern Mkomazi river basin in Tanzania. Therefore, our study involved additional efforts of data correction and dealing with missing data.

## Methods

*Data source and data cleaning*

We used two climatic datasets: (i) monthly rainfall averages from 23 stations provided by the Tanzania Meteorological Agency (TMA) (hereafter dataset1) and (ii) Pangani-NRM-version-2.0 (hereafter dataset2) daily rainfall and temperature records. Dataset2 consolidates climatological records collected from Tanzania Ministry of Water and Livestock Development, TMA, Pangani river basin district and regional offices and institutions.

For rainfall, the two datasets of most but not all stations show similar characteristics in terms of record lengths, monthly averages sums and missing data. We used datset1 for our analysis since most of its records lengths spanned to recent years and used dataset2 to fill gaps in dataset1. With this procedure, we were able to replace 10% of the missing rainfall data.

Both systematic and random errors exist in station data-observations (Sevruk, 1986; Xu and Vandewiele, 1994; Xu et al., 2006). Errors can be caused by wind, wetting and evaporation losses, type and location of the weather gauge station (Dingman et al., 1988). In addition, there are human associated errors like misread and mistyped records (Reek et al., 1992). Such erroneous station data have been identified as inhomogeneous data or outliers (Eischeid et al., 1995; Gonzalez-Rouco et al., 2001; Feng et al., 2004). Quality control of climatological data constitutes a key point in climate research (Begert et al., 2005), and it depends on the quality of the reference series (Rhoades and Salinger, 1993; Peterson and Easterling, 1994; Keiser and Griffiths, 1997), in which high correlation and vicinity is a general agreement on how to select neighbour stations for reference series (Vincent and Gullet, 1999; Mitchell and Jones, 2005; Auer et al., 2005; Brunetti et al., 2006). Some examples of statistical methods for identifying outliers include the biweight mean and standard deviation method (Lanzante, 1996), and the traditional methods based on the mean and standard deviation.

In the present study, all rainfall stations were selected for constructing reference series. The traditional statistical method was used to identify outliers: Estimate the mean and standard deviation, and transform the original values through standardization into ‘Z-scores’, then discard all values greater than a predefined limit. We used such method for each calendar month of each year separately based on the premise that an individual station’s value should be similar in a statistical sense. Knowing that there is a sample size dependent on the largest Z-score that can occur in a finite sample (Shiffler, 1988), we predefined a standard deviation limit of greater than 50% Z-score to pass for outliers.

Very few stations in dataset1 had complete records from 1930s to recent years. Therefore, our analysis concentrated on the period 1964–2010 as it comprised 75% of all rainfall records of dataset1. Temperature was analysed for the period 1989–1994 because of limited availability of temperature records in higher altitude. Note that we aimed to establish a relationship between climate variables and altitude. Seven stations, of records end-date before 1964, and of less than 30% of available records relative to the period 1964–2010, were not included into the dataset for analysis of rainfall. The dataset (at month scale) included sixteen rainfall and

three temperature stations (Tab. 3.1). We used mean values (MV) and standard deviations (SD) to describe rainfall, and maximum and minimum temperatures temporal variability.

Table 3.1. Rainfall and temperature gauge network. Temperature stations are marked *, whereas 'w' and 'r' are windward and ridge rainfall stations, respectively. Missing data are described relatively to start-end-date for each gauge station, and values in parentheses are relatively to the period 1964–2010 for rainfall and 1989–1994 for temperature.

| Station number | Gauge name | Gauge ID | Elevation (m a.s.l) | Latitude | Longitude | Record length | Missing (%) |
|---|---|---|---|---|---|---|---|
| 1 | Suji Mission | 9437004 | 1371 | -4.317 | 37.850 | 1923−2008 | 18 (32) |
| 2 | Mazinde Factory | 9438019 | 1996 | -4.700 | 38.217 | 1929−2010 | 6 (7) |
| 3 | Hassan Sisal Estate | 9437001 | 914 | -4.333 | 37.850 | 1933−2007 | 21 (29) |
| 4 | Same Met | 9437003 | 860 | -4.083 | 37.733 | 1934−2011 | 1 (0) |
| 5 | Buiko Hydromet | 9438009 | 534 | -4.650 | 38.050 | 1962−2005 | 1 (11) |
| 6 | Shume Forest | 9438012 | 1889 | -4.700 | 38.200 | 1937−1997 | 5 (6) |
| 7 | Gologolo Forest House | 9438047 | 1920 | -4.700 | 38.233 | 1964−2009 | 41 (41) |
| 8 | Gologolo | 9438037 | 1882 | -4.700 | 38.233 | 1955−1986 | 7 (56) |
| 9 | Mlomboza[r] | 9438046 | 2286 | -4.700 | 38.250 | 1964−1997 | 1 (29) |
| 10 | Mtae Pr Court | 9438066 | 1559 | -4.483 | 38.233 | 1971−2010 | 22 (22) |
| 11 | Shagavu Forest Nursery | 9438049 | 1981 | -4.533 | 38.233 | 1964−2011 | 6 (6) |
| 12 | Shagavu | 9438034 | 1828 | -4.533 | 38.217 | 1955−2011 | 5 (3) |
| 13 | Gonja Estate[w] | 9438011 | 584 | -4.300 | 38.033 | 1937−1988 | 10 (50) |
| 14 | Kalimawe[w] | 9438040 | 488 | -4.417 | 38.083 | 1963−2010 | 40 (41) |
| 15 | Ndungu Sisal Estate[w] | 9438051 | 533 | -4.367 | 38.050 | 1966−2002 | 16 (34) |
| 16 | Tia Dam[w] | 9437010 | 1676 | -4.233 | 37.950 | 1962−2010 | 32 (31) |
| 101 | *Lushoto Hydromet | 9438076 | 1631 | -4.783 | 38.267 | 1989−1994 | 1 (1) |
| 102 | *Moshi Airport | 9337004 | 854 | -3.350 | 37.333 | 1958−1993 | 2 (18) |
| 103 | *Same Met | 9437003 | 860 | -4.083 | 37.733 | 1958−2010 | 8 (2) |

Station elevations ranged from 488 m for station 14 in the Mkomazi valley to 2286 m for station 9 in the West Usambara mountains. Gauge altitude was corrected using DEM at 90 m spatial-resolution for discrepancy greater than 500 m for station 2 and 10. The dataset was cleaned for outliers, such as too high rainfall in February (1965 for station 1, 1984 and 1985 for station 9), May 1975 for station 8, June (1966, 1969, 1971) for station 3, and zero values during the entire year 1994 for station 9. Daily rainfall records were aggregated to monthly values for station 5, and missing data for station 16 were filled by accumulated daily records. The dataset included eight rainfall stations within the study area boundary, thus the network density was 74 $km^2$ $gauge^{-1}$ when all rainfall stations in the dataset counted.

Unlike for rainfall data quality control and outlier's limit rejection, monthly maximum and minimum temperature were compared only to ensure that the latter do not exceed the former, as temperature possesses less spatial-temporal variability than does rainfall (New et al., 2001;

Mitchell and Jones, 2005). Missing data for maximum and minimum temperatures ($T_{i,\ j}$), in which maximum temperature in February 1992 were filled for station 101 was calculated as

$$T_{i,j} = 0.5\left(T_{i,j-1} + T_{i,j+1}\right) \quad (3.1)$$

where $T_{i,j-1}$ and $T_{i,j+1}$ are temperature (°C) data followed and preceded by the missing data, and j is the month of year i.

*Spatial interpolation of rainfall*

The precipitation-elevation relationships on mountains can vary noticeably from terrain to terrain, and are influenced by factors such as steepness and orientation of the terrain, upward wind effects, among others. Rainfall stations were divided into three groups according to orographic barriers: (i) stations on the eastern slopes of South Pare mountains (windward side), (ii) stations on the western slopes of West Usambara mountains (leeward side), and (iii) stations located at the ridge. Grouped stations result in strengthening precipitation-elevation relationships (Houghton, 1979; Osborn, 1984; Daly, 1994).

To effectively predict the spatial pattern of orographic precipitation in complex terrain, the model should include physical elements such as airflow dynamics in both vertical and horizontal scales (Hobbs et al., 1973; Collier, 1975; Smith, 1979; Barros and Lettenmaier, 1993; Sinclair, 1994; Kuligowski and Barros, 1999; Neiman et al., 2002; Jiang, 2003; Smith and Barstad, 2004). However, relatively high data demands limit the use of airflow dynamics in most areas of data scarcity like in the Mkomazi river basin. Therefore, to predict the spatial pattern of rainfall, we considered only altitude and aspect correction, and assumed that condensed water falls immediately to the ground.

The landscape was divided into three topographic zones which reflect different orographic precipitation regimes; windward, leeward and transition zones. We used the ArcGIS to hypothetically determine the surface illumination and the shadow surface of the West Usambara mountains. According to our field observations, the transition zone (local variability of rainfall distribution) is between the towns of Ndungu and Kihurio (see Fig. 2.1 for the location), and increasing northward of the former while decreasing southward of the latter. The shadow surface contours attained the best fit line between Ndungu and Kihurio towns, and the transition zone was obtained as a buffered zone around the line.

Local increases in rainfall with elevation often approximate a linear or curved distribution (Hay et al., 1998; Goovaerts, 2000; Weisse and Bois, 2001; Ninyerola et al., 2007) in many regions. Under some conditions climate variables can best be estimated by non-linear regression models (Goodale et al., 1998; Marquínez et al., 2003; Ranhao et al., 2008). However, the linear form is easy to use where there are precipitation-elevation relationships and appears to be an acceptable approximation in most situations (Daly et al., 1994).

We modelled windward and leeward zones by means of linear regression-based interpolation, and constructed rainfall maps using DEM at 90 m (www2.jpl.nasa.gov/srtm/) spatial

resolution in ArcGIS. Monthly precipitation, $P_{i,j}$ (mm), for windward and leeward zones was calculated as

$$P_{i,j} = b_0 + b_1 E_{i,j} \quad (3.2)$$

where $b_1$ and $b_0$ are respectively, the monthly regression slopes (mm $m^{-1}$) and intercepts, $E_{i,j}$ is the DEM elevation above-sea-level (m), and i is latitude of longitude j. Monthly rainfall maps for the transition zone were modelled by means of layer algebra in ArcGIS as a function of the constructed windward and leeward monthly rainfall maps, latitude and longitude. Thus, the transition zone rainfall maps, $Pt_{i,j}$ (mm), were calculated as

$$Pt_{i,j} = b_{0s} + (b_{0n} - b_{0s})\omega + (b_{1s} + (b_{1n} - b_{1s})\omega)E_{i,j} \quad (3.3)$$

where $b_{1n}$ and $b_{1s}$ are monthly regression slopes (mm $m^{-1}$) for windward and leeward zones, $b_{0n}$ and $b_{0s}$ are regression intercepts, and ω is the distance weighting between windward or leeward and transition zone at latitude i of longitude j.

*Spatial interpolation of temperature and evapotranspiration*

Several methods such as Thornthwaite (1948), Blaney-Criddle (BC; 1950), Penman-Monteith (PM; 1965), Priestly-Taylor (PT; 1972) and Hargreaves and Samani (HS; 1985) were developed to calculate reference evapotranspiration ($ET_o$). The Food and Agriculture Organization of the United Nations (FAO-56; Allen et al., 1998) has recommended PM as the standard method for computing $ET_o$ from climate data. The PM model, which incorporates thermodynamic and aerodynamic aspects, has proved to be a relatively accurate method in both humid and arid climates. However, a relatively high data demand is a major drawback to the application of PM. In addition to air temperature available at most meteorological stations, PM requires measurements of wind speed, humidity and solar radiation, which are observed at relatively few weather stations globally.

In locations like Mkomazi river basin, where only maximum and minimum temperatures are available, it is impractical to use the PM. Instead, methods considering only temperature appeared feasible. Hargreaves and Samani (HS; 1985) developed an empirical method using only air temperature (mean, maximum and minimum) and extraterrestrial radiation. The latter can be calculated for a certain latitude and day of a year. Various studies showed that HS ranked best among methods that require air temperature data only (Xu and Singh, 2001, 2002; Droogers and Allen, 2002; Bautista et al., 2009; Maeda et al., 2011). The HS method is defined as

$$ET_0 = 0.0023 * 0.408 R_a (T_{mean} + 17.8)\sqrt{T_{max} - T_{min}} \quad (3.4)$$

where $ET_o$ is the monthly averaged reference evapotranspiration (mm $day^{-1}$), $R_a$ is the extraterrestrial radiation (MJ $m^{-2}$ $day^{-1}$), $T_{mean}$ is averaged monthly temperature (°C), and $T_{max}$ ($T_{min}$) are maximum (minimum) monthly temperature (°C). To obtain monthly evapotranspiration, $ET_o$ must be multiplied by the number of days in the month.

Monthly maximum and minimum temperatures were modelled by means of regression-based interpolation and from DEM at 90 m spatial-resolution in ArcGIS to obtain continuous temperature maps respectively. Such temperatures, T (°C) were calculated as

$$T = b_0 + b_1 E_{i,j} \quad (3.5)$$

where $b_1$ and $b_0$ are respectively, the monthly regression slopes (°C $m^{-1}$) and intercepts, $E_{i,j}$ is the DEM elevation above-sea-level (m), and i is latitude of longitude j. Monthly mean temperature, $T_{mean}$ (°C), was then calculated by arithmetic mean of maximum and minimum temperature as

$$T_{mean} = 0.5(T_{max} + T_{min}) \quad (3.6)$$

Global solar radiation ($R_s$) was modelled in ArcGIS using DEM at 90 m spatial-resolution and the hemispherical upward-viewshed algorithm developed by Fu and Rich (2002), in which such radiation is calculated as the sum of direct Sun map and diffuse sky map solar radiations. Direct Sun and diffuse sky maps solar radiations were measured for each feature on the topographic surface on a monthly basis, assuming a clear sky for diffuse proportion and transmittivity. Extraterrestrial solar radiation ($R_a$) was then calculated as

$$R_a = R_s/(a_s + b_s\frac{n}{N}) \quad (3.7)$$

where $a_s$ and $b_s$ are fraction of extraterrestrial radiation reaching the earth. These Angstrom values vary depending on atmospheric conditions (e.g. humidity) and solar declination such as latitude and month. However, where no calibration has been carried out, the values $a_s$ = 0.25 and $b_s$ = 0.50 are recommended (Allen et al., 1998). Also, the assumption n=N is recommended (Allen et al., 1998) where no number of sunshine hour n of possible maximum N are available. The HS equation was then applied in ArcGIS to construct continuous monthly $ET_o$ maps.

We used two statistical estimators to determine performance of the constructed models for rainfall and maximum and minimum temperatures, the coefficient of determination ($R^2$) (Draper and Smith, 1998) and the probability of F distribution (Johnson and Balakrishnan, 1995).

## Results

*Dataset*

The mean values of monthly rainfall ranged from 1 mm (July) for station 15 (533 m a.s.l.) along the Mkomazi valley to 250 mm (December) for station 16 (1676 m a.s.l.) in the South Pare mountains (Tab. 3.2). Monthly rainfall variability was high for both long- and short-rains with standard deviations approximating mean values for most stations. However, short-rains showed more variability as standard deviations exceeded the mean values in October for station 2 (1996 m a.s.l.), 3 (914 m a.s.l.), 9 (2286 m a.s.l.), 15 (533 m a.s.l.), and in November

and December for station 5 (534 m a.s.l.). Monthly maximum temperatures in higher altitude ranged from 21 °C (July) to 29 °C (February) and minimum 7 °C (August) to 14 °C (April) for station 101 (1631 m a.s.l.) in the west Usambara mountains. In contrast, maximum temperatures in low altitudes ranged from 26 °C (July) to 33 °C (February) and minimums from 16 °C (August) to 19 °C (April) for station 102 (854 m a.s.l.) in Moshi town.

*Spatial modelling and mapping rainfall, $ET_o$ and temperature*

$R^2$ values for rainfall and maximum and minimum temperatures showed that there was an overall relationship between elevation and such climatic variables (Tab. 3.3). When modelling rainfall, station 9 was included into both windward and leeward groups based on the assumption that because station 9 was located at the ridge it had both windward and leeward side's rainfall characteristics. Subdividing zones according to relief for spatial estimation of rainfall provided important information about rainfall variability at the local scale, which can be shown by differences between $R^2$ values for rainfall, both for leeward and windward sides. Particularly for the long-rains season (March, April, May), in which $R^2$ was greater for the windward-side (0.43, 0.83, 0.86) than for the leeward-side (0.38, 0.76, 0.42). Likewise, $R^2$ values increased towards the long-rains season except in May for the leeward side, when it decreased. In contrast, for the short-rains season (October, November, December), the strength of the relationship between elevation and rainfall decreased towards the short-rains season, and $R^2$ values in the windward-side (0.66, 0.21, 0.05) was smaller than in the leeward-side (0.52, 0.43, 0.22) except in October. Moreover, during the transition period towards the wet seasons in (February, September), $R^2$ values in the windward-side were smaller (0.36, 0.15) than the leeward-side (0.53, 0.32). The analysis of probability of F distribution both for rainfall and temperature passed the F test at significance level of 0.01, except for rainfall in August (leeward-side) and September (windward-side) where it passed at 0.1.

The constructed rainfall maps showed that monthly rainfall along the valley and on mountains ranged between 2 to 15 mm and 68 to 194 mm per month (Fig. 3.1). The results also showed that rainfall was abundant for the long-rains season in March–May centred in April. Nevertheless, during such period mountain areas received more rainfall than in the valleys. In contrast, rainfall during the short-rains season in October–December revealed high spatial variability in the leeward-side than in the windward-side. The valley in the windward-side received rainfall amounts similar as on mountains, particularly for the period November to December.

Table 3.2. Statistical descriptive of gauge stations. Station number: see Table 3.1.

| Station number | Jan | Feb | Mar | Apr | May | Jun | Jul | Aug | Sep | Oct | Nov | Dec |
|---|---|---|---|---|---|---|---|---|---|---|---|---|
| | MV ± SD | MV ± SD | MV ± SD | MV ± SD | MV ± SD | MV ± SD | MV ± SD | MV ± SD | MV ± SD | MV ± SD | MV ± SD | MV ± SD |
| | Rainfall (mm) | | | | | | | | | | | |
| 1 | 92 ± 71 | 72 ± 53 | 142 ± 97 | 120 ± 61 | 52 ± 35 | 12 ± 14 | 5 ± 7 | 8 ± 11 | 10 ± 15 | 31 ± 40 | 129 ± 105 | 165 ± 89 |
| 2 | 55 ± 58 | 57 ± 46 | 82 ± 62 | 142 ± 69 | 131 ± 77 | 31 ± 31 | 16 ± 21 | 15 ± 19 | 13 ± 29 | 41 ± 57 | 66 ± 46 | 75 ± 50 |
| 3 | 60 ± 50 | 43 ± 35 | 87 ± 79 | 71 ± 45 | 40 ± 28 | 7 ± 17 | 5 ± 10 | 5 ± 15 | 8 ± 15 | 23 ± 29 | 63 ± 62 | 81 ± 59 |
| 4 | 54 ± 53 | 43 ± 41 | 91 ± 89 | 107 ± 62 | 64 ± 52 | 12 ± 17 | 4 ± 7 | 10 ± 15 | 13 ± 22 | 39 ± 43 | 62 ± 62 | 63 ± 51 |
| 5 | 42 ± 46 | 34 ± 32 | 59 ± 55 | 71 ± 46 | 46 ± 38 | 10 ± 13 | 7 ± 14 | 6 ± 10 | 4 ± 10 | 27 ± 34 | 32 ± 41 | 45 ± 56 |
| 6 | 74 ± 60 | 56 ± 37 | 129 ± 83 | 149 ± 71 | 72 ± 40 | 14 ± 16 | 8 ± 17 | 5 ± 7 | 10 ± 18 | 37 ± 36 | 91 ± 59 | 95 ± 57 |
| 7 | 64 ± 47 | 53 ± 39 | 101 ± 67 | 115 ± 59 | 67 ± 37 | 17 ± 16 | 12 ± 25 | 8 ± 19 | 13 ± 29 | 38 ± 34 | 85 ± 58 | 76 ± 56 |
| 8 | 89 ± 80 | 75 ± 62 | 134 ± 91 | 170 ± 91 | 90 ± 59 | 22 ± 26 | 13 ± 26 | 11 ± 19 | 15 ± 33 | 50 ± 31 | 116 ± 53 | 102 ± 54 |
| 9 | 86 ± 71 | 83 ± 51 | 141 ± 92 | 172 ± 70 | 142 ± 113 | 41 ± 41 | 20 ± 30 | 14 ± 23 | 15 ± 23 | 54 ± 58 | 113 ± 102 | 129 ± 90 |
| 10 | 47 ± 41 | 43 ± 36 | 75 ± 67 | 144 ± 61 | 92 ± 58 | 13 ± 13 | 9 ± 10 | 12 ± 14 | 15 ± 24 | 51 ± 46 | 100 ± 57 | 147 ± 101 |
| 11 | 83 ± 58 | 61 ± 45 | 120 ± 72 | 140 ± 56 | 55 ± 36 | 7 ± 9 | 4 ± 5 | 5 ± 7 | 9 ± 13 | 52 ± 51 | 127 ± 71 | 167 ± 93 |
| 12 | 102 ± 81 | 75 ± 55 | 132 ± 68 | 150 ± 51 | 61 ± 39 | 7 ± 10 | 4 ± 6 | 7 ± 9 | 9 ± 14 | 53 ± 51 | 140 ± 71 | 186 ± 108 |
| 13 | 107 ± 67 | 84 ± 77 | 141 ± 124 | 118 ± 95 | 44 ± 36 | 8 ± 13 | 4 ± 8 | 9 ± 12 | 18 ± 24 | 39 ± 36 | 148 ± 82 | 229 ± 128 |
| 14 | 47 ± 51 | 40 ± 36 | 63 ± 56 | 70 ± 51 | 25 ± 21 | 4 ± 5 | 2 ± 3 | 5 ± 6 | 13 ± 36 | 21 ± 15 | 38 ± 36 | 61 ± 45 |
| 15 | 74 ± 84 | 62 ± 57 | 93 ± 98 | 86 ± 67 | 32 ± 31 | 3 ± 8 | 1 ± 4 | 3 ± 6 | 11 ± 20 | 28 ± 31 | 85 ± 77 | 127 ± 93 |
| 16 | 117 ± 127 | 81 ± 75 | 153 ± 96 | 172 ± 70 | 62 ± 50 | 11 ± 16 | 5 ± 6 | 13 ± 16 | 22 ± 29 | 69 ± 59 | 244 ± 172 | 251 ± 162 |
| | Maximum temperature (°C) | | | | | | | | | | | |
| 101 | 28.1 ± 1.0 | 28.5 ± 0.8 | 27.6 ± 0.9 | 25.4 ± 0.4 | 23.2 ± 0.7 | 21.9 ± 0.6 | 21.4 ± 0.4 | 21.9 ± 0.4 | 23.9 ± 0.3 | 26.0 ± 0.6 | 26.6 ± 0.4 | 27.0 ± 0.4 |
| 102 | 31.3 ± 1.4 | 32.8 ± 1.2 | 32.2 ± 1.8 | 29.7 ± 1.3 | 27.3 ± 1.1 | 26.0 ± 0.4 | 25.5 ± 0.3 | 26.0 ± 0.5 | 28.5 ± 0.4 | 30.8 ± 0.5 | 31.9 ± 0.7 | 31.1 ± 0.8 |
| 103 | 30.9 ± 1.6 | 32.4 ± 1.2 | 31.7 ± 1.5 | 29.1 ± 1.0 | 26.7 ± 1.0 | 26.2 ± 0.5 | 25.8 ± 0.3 | 26.1 ± 0.6 | 28.2 ± 0.4 | 30.2 ± 0.5 | 30.7 ± 0.8 | 29.9 ± 1.1 |
| | Minimum temperature (°C) | | | | | | | | | | | |
| 101 | 12.9 ± 1.0 | 12.9 ± 0.3 | 12.2 ± 0.5 | 13.7 ± 0.7 | 13.2 ± 0.4 | 10.1 ± 1.1 | 8.7 ± 0.9 | 8.0 ± 0.5 | 7.6 ± 0.3 | 9.5 ± 1.4 | 10.8 ± 0.6 | 12.8 ± 0.9 |
| 102 | 17.7 ± 0.5 | 17.8 ± 0.9 | 18.5 ± 0.4 | 19.1 ± 0.2 | 18.5 ± 0.2 | 16.8 ± 0.4 | 16.0 ± 0.5 | 15.6 ± 0.5 | 16.0 ± 0.7 | 17.3 ± 0.4 | 18.3 ± 0.4 | 18.4 ± 0.7 |
| 103 | 18.4 ± 1.0 | 18.4 ± 0.9 | 18.3 ± 1.0 | 17.9 ± 0.8 | 16.9 ± 0.9 | 15.2 ± 0.9 | 14.4 ± 0.9 | 14.6 ± 1.0 | 15.1 ± 0.8 | 16.8 ± 1.0 | 18.1 ± 0.7 | 18.6 ± 0.8 |

The modelled monthly maximum and minimum temperature maps (Figs. 3.2 & 3.3) by an arithmetic mean were then drawn by layer-algebra in ArcGIS to construct monthly mean temperature maps (Fig. 3.4), all based on the digital elevation model (see Fig. 2.1). Mean monthly temperature strongly decreased with altitude, as expected. This effect was most pronounced in June–September, whereas the valley was characterised by similar temperatures throughout the year. The mean temperatures ranged from 9 °C (July–September) to 28 °C (February, March and November). The period December–February was warmer where the temperature in the south Pare and West Usambara mountains was above 15 °C. Figure 3.4 also showed that the temperature was lower in July–September, particularly in higher altitudes. Moreover, the results showed that temperature in the Mkomazi valley was in excess of 23 °C throughout the year. Maximum and minimum temperatures ranged from -1 to 35 °C (Figs. 3.2 & 3.3) with patterns and trend similar to that described for mean temperature.

The constructed monthly $ET_o$ maps values ranged from 28 to 165 mm (Fig. 3.5). Result showed that except for the period May–July, $ET_o$ surpassed 50 mm, and greater than 150 mm (January, March and October–December) and below 150 mm (February, April, August and September). In May–July $ET_o$ ranged between 40 and 126 mm. Maximum $ET_o$ occurred in March in which the lowest was 100 mm. In general, $ET_o$ decreases with altitude. The results also showed that in January, November and December some slopes had greater amounts of $ET_o$ than on the plains, which primarily was associated with the effects of seasonal variations in the position of the Sun on the slopes than on the plains. The constructed monthly extraterestrial radiation maps are shown in Figure 3.6.

Table 3.3. Results of the monthly precipitation, maximum and minimum temperature models by means of regression-based interpolation. $R^2$ values in parentheses for rainfall were calculated when leeward and windward rainfall groups were modelled with an absence of the stations at the ridge.

| | Rainfall (mm) | | | | Temperature (°C) | | | |
|---|---|---|---|---|---|---|---|---|
| | Leeward | | Windward | | Maximum | | Minimum | |
| | $R^2$ | F | $R^2$ | F | $R^2$ | F | $R^2$ | F |
| January | 0.32 (0.28) | 81.0 | 0.17 (0.47) | 17.8 | 0.99 | 28.6 | 0.98 | 33.1 |
| February | 0.53 (0.43) | 128.9 | 0.36 (0.28) | 29.8 | 0.99 | 38.6 | 0.98 | 39.3 |
| March | 0.38 (0.30) | 145.9 | 0.43 (0.48) | 76.3 | 0.99 | 38.5 | 0.99 | 27.1 |
| April | 0.76 (0.72) | 543.7 | 0.83 (0.85) | 333.9 | 0.98 | 27.9 | 0.96 | 20.1 |
| May | 0.42 (0.31) | 187.7 | 0.86 (0.89) | 373.2 | 0.98 | 25.9 | 0.93 | 13.1 |
| June | 0.31 (0.18) | 41.1 | 0.79 (0.75) | 94.0 | 0.99 | 68.6 | 0.95 | 20.9 |
| July | 0.35 (0.22) | 24.2 | 0.77 (0.56) | 42.6 | 0.99 | 51.0 | 0.96 | 25.7 |
| August | 0.12 (0.04) | 4.5 | 0.75 (0.65) | 24.0 | 0.99 | 66.6 | 0.98 | 48.4 |
| September | 0.32 (0.25) | 14.2 | 0.15 (0.66) | 2.6 | 0.99 | 92.4 | 0.99 | 65.9 |
| October | 0.52 (0.43) | 84.0 | 0.66 (0.93) | 76.5 | 0.98 | 33.3 | 0.99 | 40.4 |
| November | 0.43 (0.39) | 199.4 | 0.21 (0.80) | 66.1 | 0.95 | 17.2 | 0.99 | 45.4 |
| December | 0.22 (0.22) | 123.0 | 0.05 (0.47) | 14.8 | 0.91 | 9.6 | 0.99 | 44.8 |

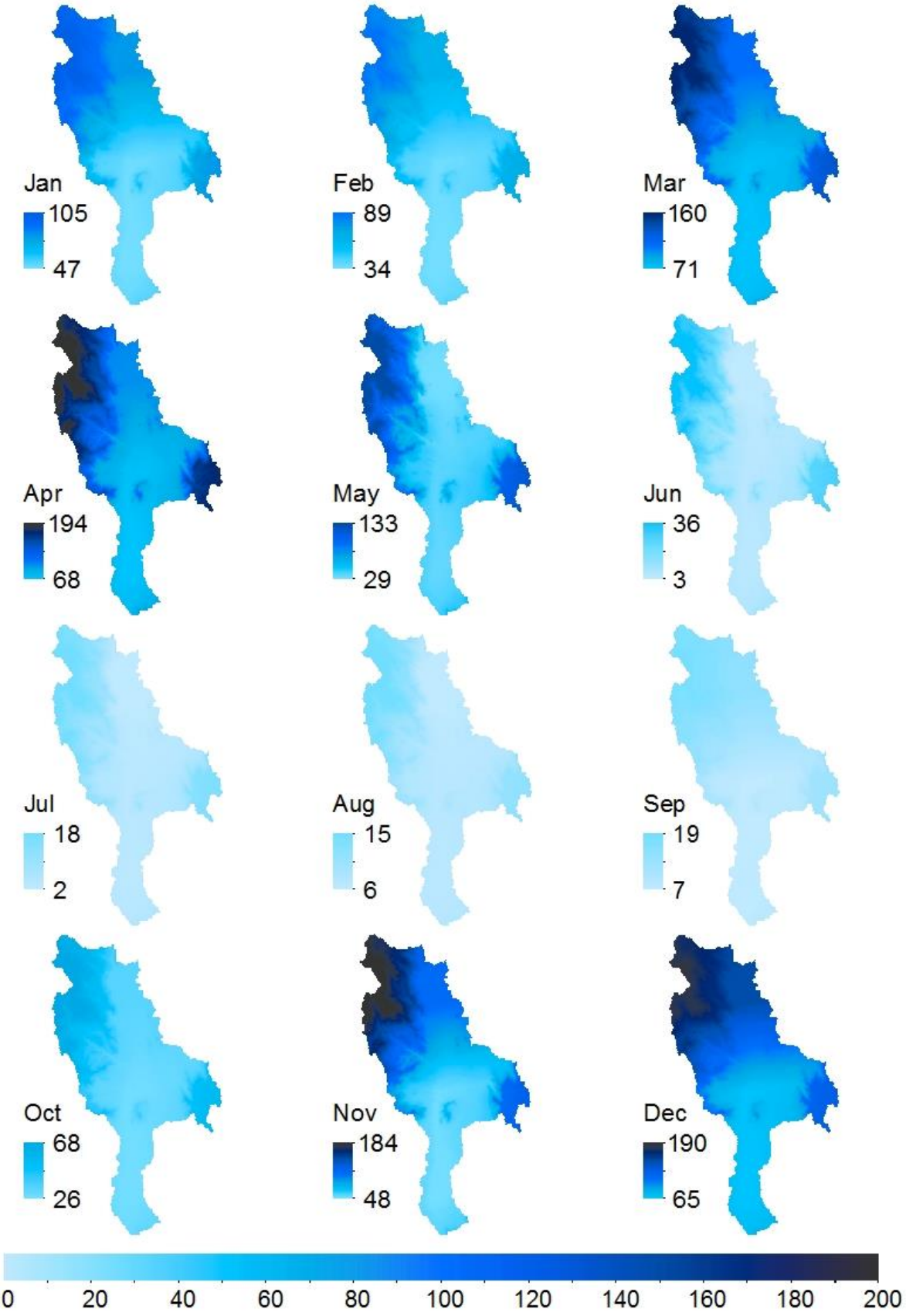

Figure 3.1. Monthly mean rainfall (mm) maps for the southern Mkomazi river basin averaged for the period 1964–2010.

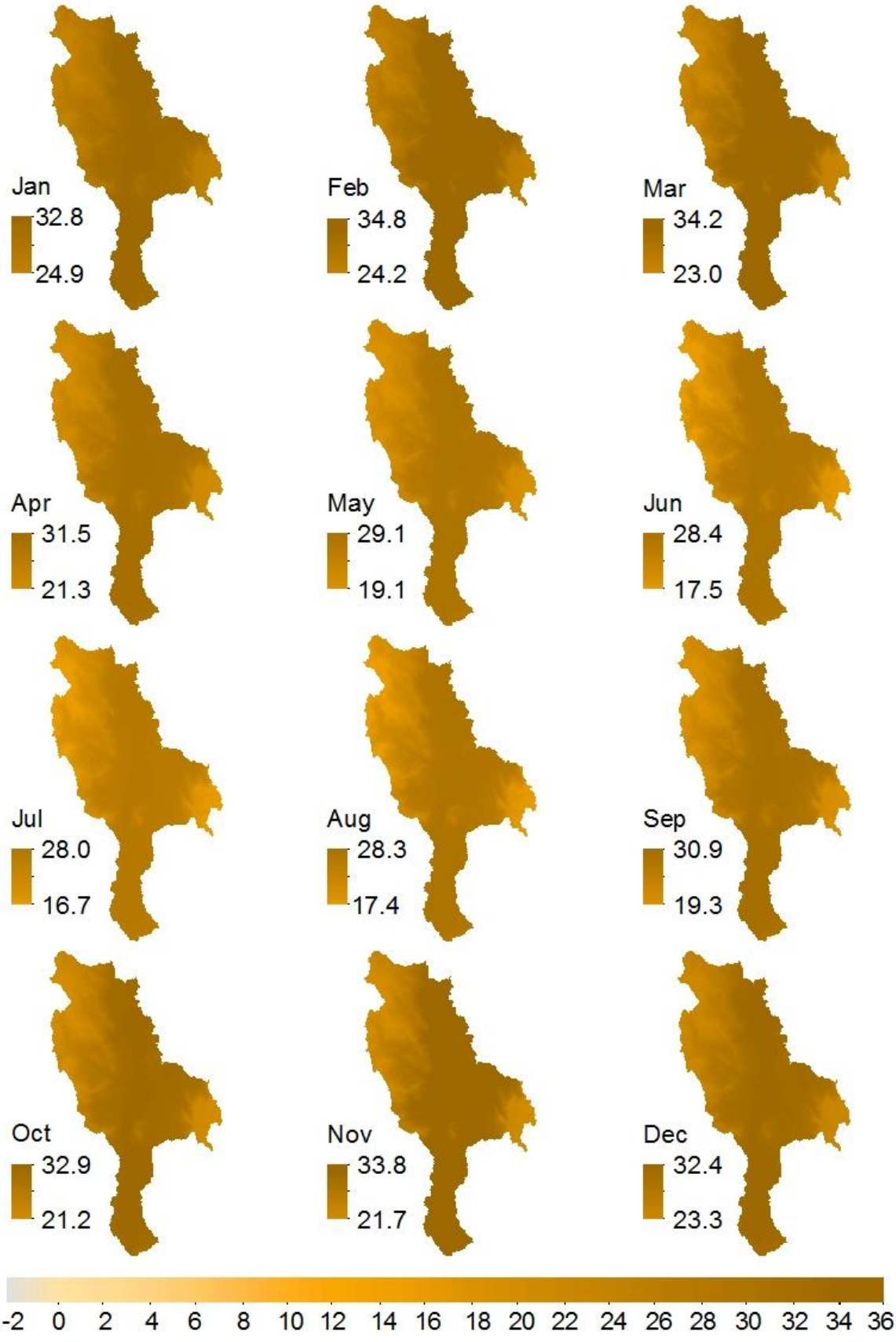


Figure 3.2. Monthly averaged maximum temperature (°C) maps for the southern Mkomazi river basin for the period 1989–1994.

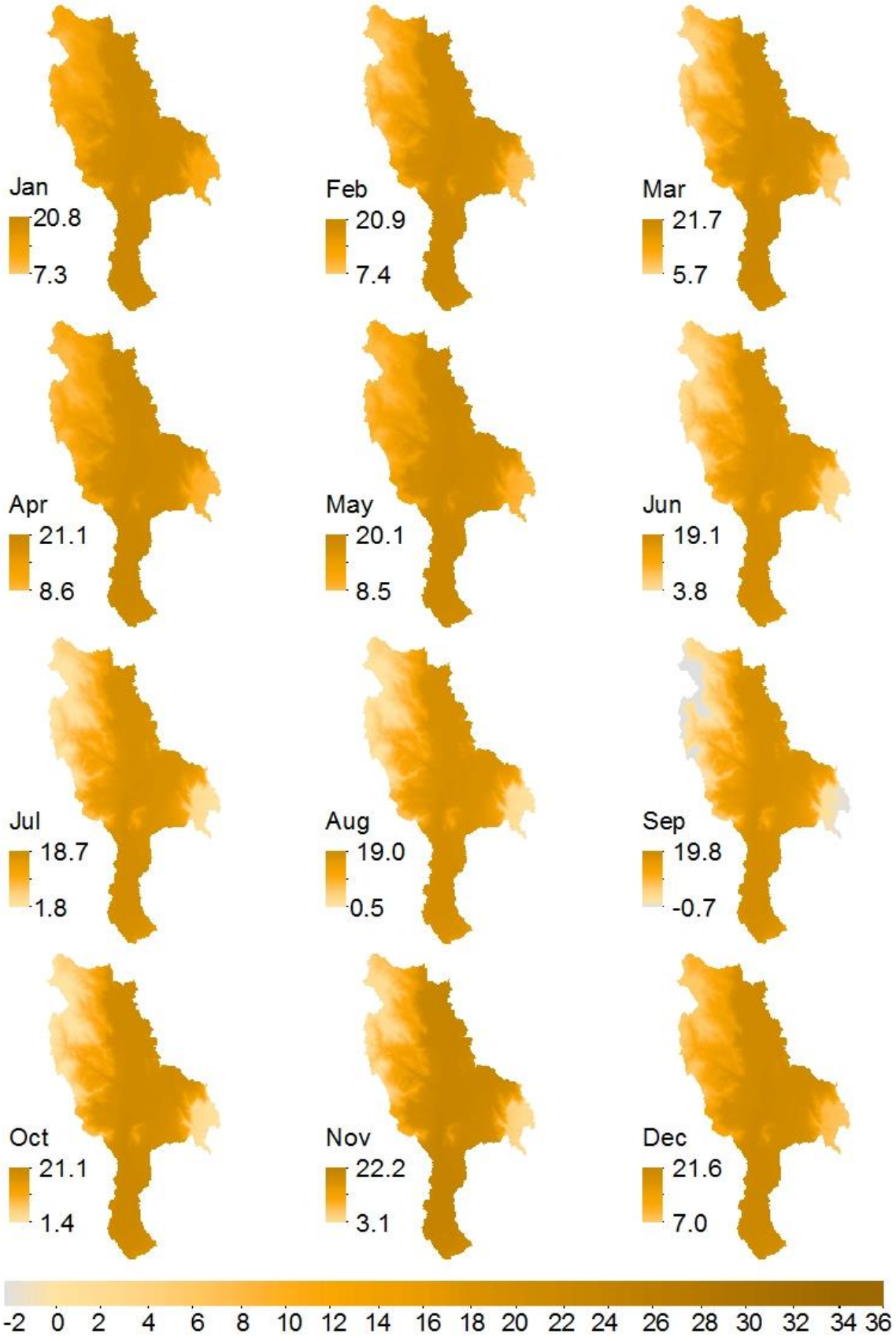


Figure 3.3. Monthly averaged minimum temperature (°C) maps for the southern Mkomazi river basin for the period 1989–1994.

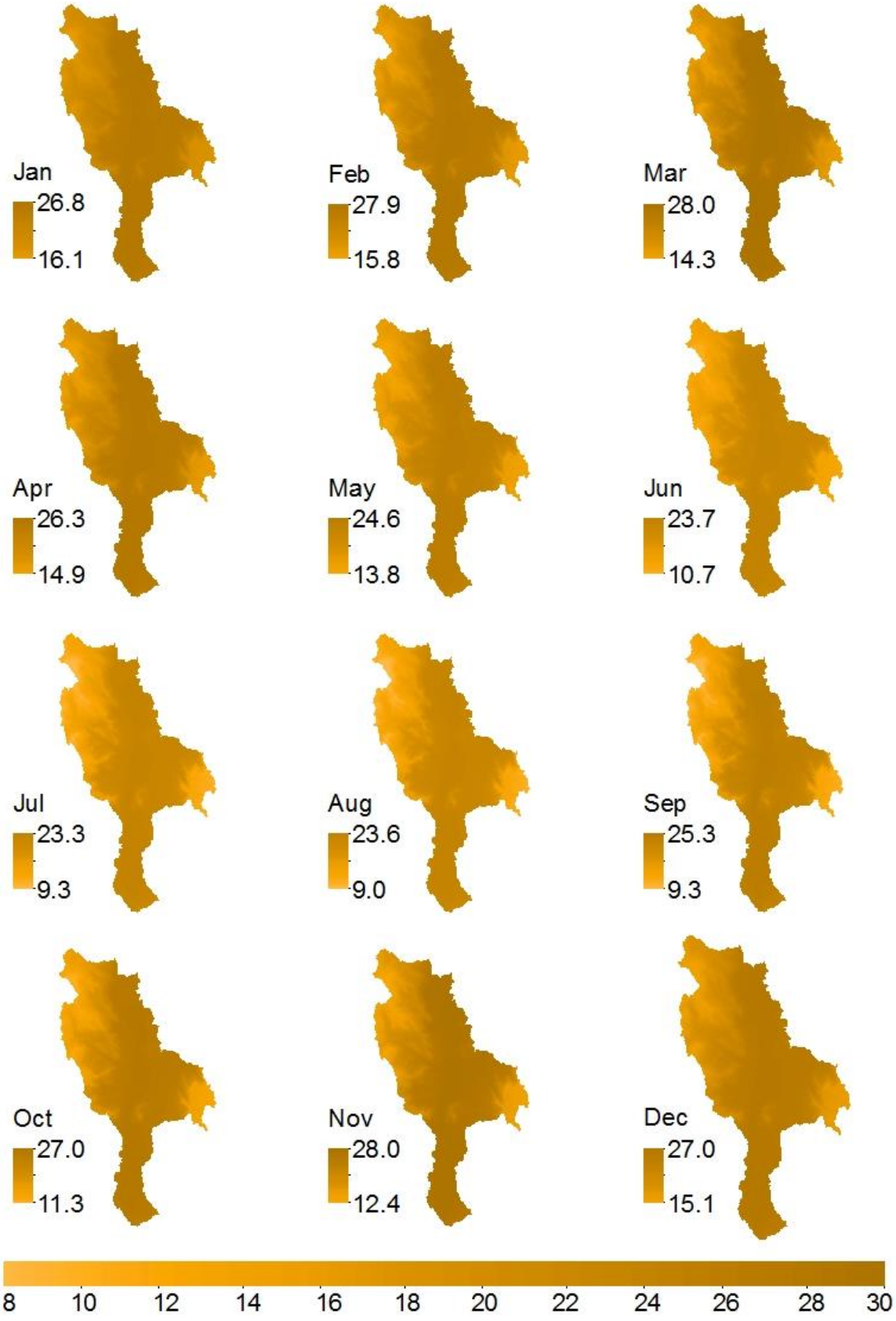


Figure 3.4. Monthly mean temperature (°C) maps for the southern Mkomazi river basin averaged for the period 1989–1994.

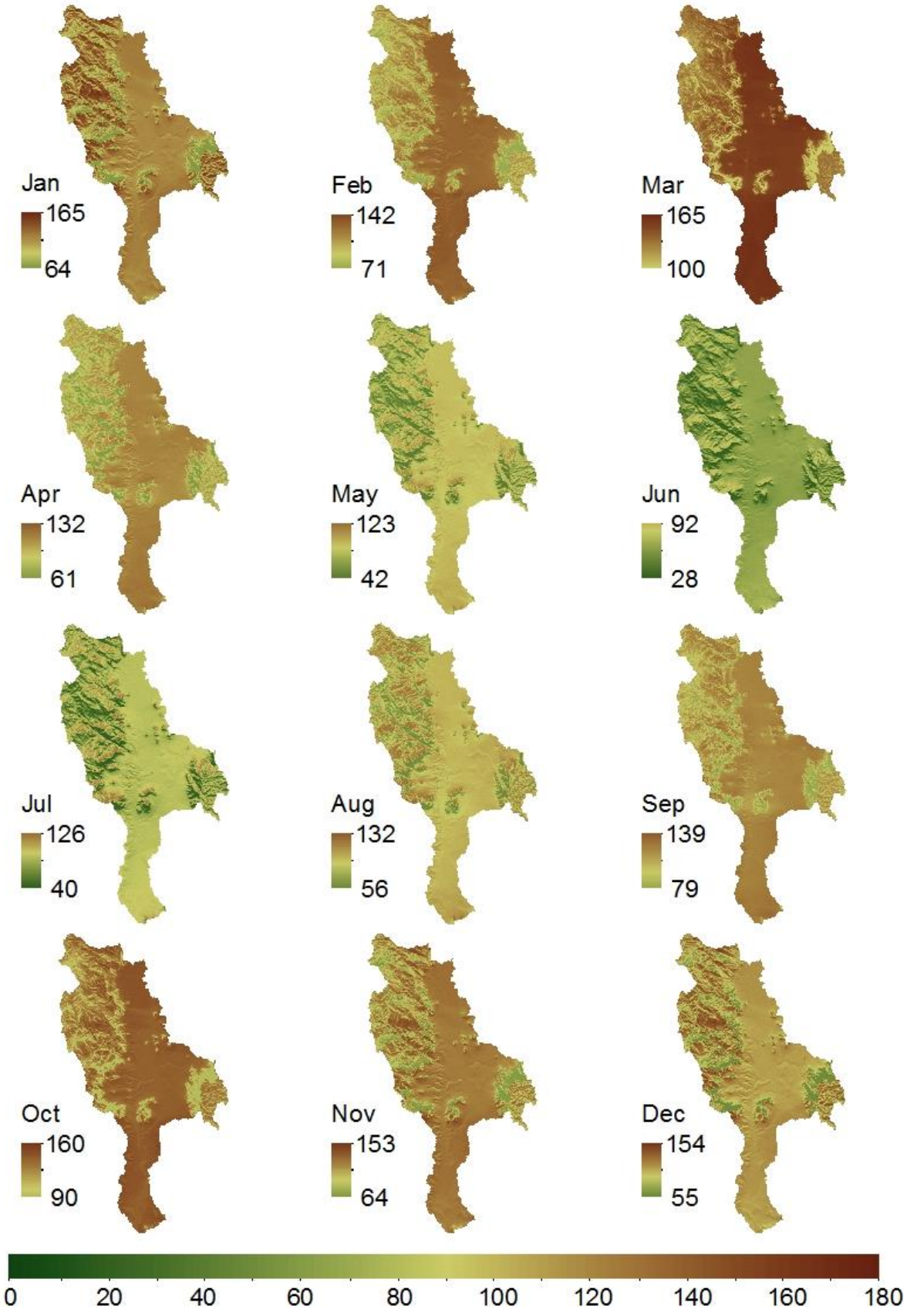


Figure 3.5. Monthly reference evapotranspiration (mm) maps for the southern Mkomazi river basin averaged for the period 1989–1994.

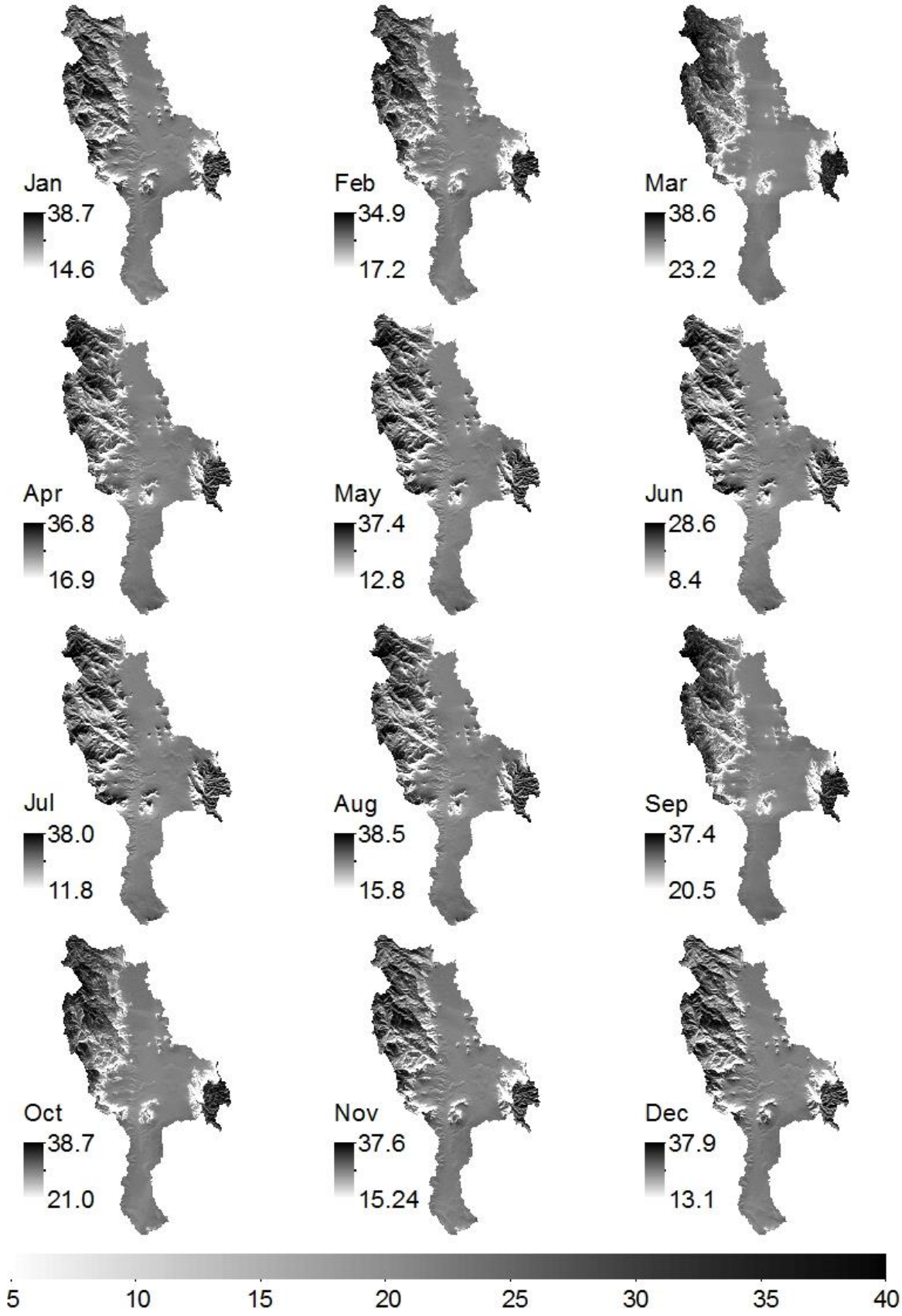


Figure 3.6. Monthly extraterrestrial solar radiation (MJ $m^{-2}$ $day^{-1}$) for the southern Mkomazi river basin.

## Discussion

In agronomic studies, calculations of $ET_o$ following the HS equation are generally performed using values of extraterrestrial radiation ($R_a$) calculated assuming a planar surface and solely as a function of latitude, according to the method described by Allen et al. (1998), which does not take relief into account. This study reveals the potential of regression-based models, DEM and GIS modelling techniques to map $ET_o$, precipitation and temperature, the climate variables that are important in many environmental and water resources studies (Postel et al., 1996; Pereira et al., 1999; Ward and Trimble, 2004; Mu et al., 2007; Trenberth et al., 2007). We have modelled $R_a$ using DEM and ArcGIS. The usefulness of this approach might not be for flat terrain, in which relief does not significantly affect $R_a$. However, in complex terrain, for high resolution $ET_o$ maps used for ecological and water resources management, spatial variations in relief are commonly very important and significantly affect the values of $R_a$ estimates because, radiation flux are especially dependant on the geometry of terrain (Vicente-Serrano et al., 2007), and this has a significant effect on local $ET_o$ values (Häntzschel et al., 2005).

The dataset was collected from many institutions, and cleaned for inhomogeneous data. Obvious outliers were removed by means of traditional methods based on the mean and standard deviation and a predefined limit. The largest risk of making a type I error (erroneously removing good data) was in the subjective decision to remove too high rainfall in dry months for dry years.

There was an overall relationship between elevation and both rainfall and temperature, as expected. The results of the precipitation models showed that, for the long-rains season in March–May, $R^2$ values for the period March–April increased for leeward and windward, and were great in April for both sides, in which rainfall peaked in April. In contrast, for short-rains season in October–December, in which rainfall peaked in December, $R^2$ values decreased and were very low in December. From the constructed rainfall maps and the analysis of temporal rainfall variability, precipitation patterns regimes agreed well with results from equatorial East African studies showing that the rainfall is abundant in most areas for the long-rains season (Camberlin and Philippon, 2002), while short-rains season reveal more interannual variability (Mutai and Ward, 2000). High and low $R^2$ values corresponded with the temporal patterns in rainfall variability.

Rainfall was modelled in a linear form assuming that condensed water falls immediately to the ground and no influence of horizontal-movements was included, which is somewhat violating mountain wave theory for modelling orographic precipitation (Smith, 1979). It does not include the physical elements such as airflow dynamics, advection and fallout, condensed water convection, and downslope evaporation (Smith and Barstad, 2004). However, it is a usable assumption to obtain a relationship between elevation and precipitation in most situations, an example showing such an assumption is shown in the study by Daly et al. (1994). In addition to general usable assumptions on climatic model development, one has to increase the complexity and performance of such models upon availability of other parameters.

An attempt to improve $R^2$ values for rainfall was to exclude stations at the ridge (station 9 in this case) for analysis of elevation-rainfall relationship and seasonal trends. The results showed significant improvement of $R^2$ values for windward-side, particularly for the short-rains season in comparison to the long-rains season. In contrast, there was no significant improvement of $R^2$ values for the leeward-side, particularly in December. Also, the elevation-rainfall relationship for the long-rains season for both windward and leeward models showed no significant $R^2$ differences with or without station 9. Low $R^2$ values indirectly indicate climate mechanisms for rainfall distribution in particular for the period November to January. The rainfall distribution form during this period is yet unknown. However, the climate of the Mkomazi river basin is largely influenced by equatorial East African climate systems. Slingo et al. (2005) noted that over the Western Indian Ocean the inter-tropical convergence zone (ITCZ) makes its greatest north–south excursions, dominated by the Asian monsoon with its reversals of the wind from northeasterly in December–February to southwesterly in June–August periods. As such, during the transition periods in March–May as the northeast monsoon relaxes, the ITCZ from its southernmost position over the southern Western Indian Ocean progresses northwards bringing equatorial East Africa long-rains season, and as the Asian summer monsoon retreats in September–November, the ITCZ progresses south again bringing equatorial East Africa short-rains season. Therefore, we considered local prevailing winds, especially their trend and strength, associated with the ITCZ excursions, also to be an important variable for rainfall patterns.

A number of temperature records available within the study area were not sufficient. Therefore, it was necessary to include nearby meteorological stations to increase understanding of the temperature gradient, which resulted into highly satisfactory estimations for this variable. This can be explained by high $R^2$ values for temperature. However, although maximum and minimum temperatures are commonly more easily modelled because of low measurements uncertainties compared to rainfall, very high $R^2$ values for temperature were influenced by the little number of temperature stations used to model these climatic variables. These few stations were located in high- altitude and low-altitude, which supported the linear relation closely.

We used the Hargreaves and Samani (HS) method to map $ET_o$ for the reason that, to construct reliable maps, it is necessary to use a dense database of the climatic variables. Although the most accurate method is the one that is physically based on the Penman-Monteith equation, it is impossible to produce reliable $ET_o$ maps using the Penman-Monteith equation in the area of data scarcity because of a relatively high data demand of such an equation. Apart from our specific study area, this may be the case for many Africa regions. In addition, numerous researchers (e.g. Droogers and Allen, 2002; Hargreaves and Allen, 2003) have demonstrated that, for $ET_o$ estimates for periods longer than one week, the HS method provides similar results to those obtained using the Penman-Monteith equation.

## Conclusion

Our study has demonstrated the potential use of linear-regression-based, DEM and GIS techniques in modelling and construction of reliable climate maps. These maps were made on a monthly basis for rainfall, temperatures and evapotranspiration.

Both rainfall and temperature showed a linear correlation form with elevation. Temperature linear correlation form with elevation was stronger than that showed by rainfall with elevation. However, the coefficients of determination ($R^2$) for temperature with elevation were very high. Because of the few number of temperature stations used to model maximum and minimum air temperature. These temperature stations were located on two different altitudes (low and high), which supported the linear form strongly. For rainfall, the linear form was more pronounced for the long-rains seasons than for the short-rains season. For the long-rains season, the rainfall-elevation relationships showed no significant changes in $R^2$values, both for the leeward- and windward-side, when the station at the ridge was not included for the analysis of rainfall-elevation relationship. In contrast, for the short-rains season, $R^2$ values improved substantially when station at the ridge was not included into rainfall models. Therefore, rainfall distribution for the southern Mkomazi river basin particularly for the short-rains season deserves further attention, when other variables affecting rainfall distribution e.g wind speed and direction become available.

The constructed maps for $ET_o$, rainfall and temperatures can be useful for environment and water resources studies in the region as climate variability affects riverflows, which has in turn implications on livelihoods of the people which depend directly or indirectly on rain-fed agriculture.

# Chapter 4

# Hydrological Modelling: a case study Mkomazi river basin in Tanzania

## Abstract

Sufficient water is essential for drinking and food production, particularly in tropical and subtropical regions where rainfall is often scarce or has strong inter-annual variation. Hydrologic modelling of a river catchment in north-eastern Tanzania has been simulated using a semi-distributed conceptual rainfall-runoff model known as the HYPE model. Spatiotemporally distributed rainfall, mean air temperature, evapotranspiration, soil depth profile and soil textures were constructed by means of regression-based, digital elevation models (DEM) and geographic information system (GIS) techniques. The DEM created a flow direction and accumulation network at 450x450 $m^2$ spatial-resolution. The model satisfactorily captured the hydrograph of the observed runoff based on the performance efficiency $R^2$, criterion suggested by Nash and Sutcliffe of 0.85 and 0.68 for calibration and validation periods, respectively.

The sensitivity of the model to the variation in the input data revealed that total runoff from the catchment is more sensitive to rainfall than to evapotranspiration and soil moisture. The catchment exhibits considerable inter-annual variability in runoff volumes, in which this variability turns out to be the seasonality of the climate. The water balance is also affected by the nature of the soils and soil depths, and the underlying geology. We produced averaged monthly soil moisture maps useful for environmental studies in the catchment.

**Keywords:** HYPE model, Mkomazi river basin, modelling, soil moisture

## Introduction

Hydrological simulation, commonly termed rainfall-runoff modelling, aims to predict the behaviour of the real world system under a certain set of naturally-occurring circumstances (Beven, 1989). For example, Lidén and Harlin (2000) predicted riverflow for the catchments called Hagafiro (Tanzania), Locotoa (Bolivia), Ruwa (Zimbabwe) and Yassidere (Turkey); riverflow was also predicted for the Kilombero river basin in Tanzania (Yawson et al., 2005), and for multi-basins in Europe (Donnelly et al., 2009). Nikolopoulos et al. (2011) forecasted flood-events for the Fella river basin in Italy. Hydrological simulations are also used to assess the effects of land-use changes (e.g. afforestation/agriculture, deforestation and urbanization) to riverflow. Examples of hydrological modelling to land-use changes include studies by Fahey and Jackson (1997) for the Glendhu catchment in New Zealand; Kirkby et al. (2002) for the Nogalte catchment in Spain; Legesse et al. (2003) for the Ketar river basin in Ethiopia; and Palamuleni et al. (2011) for the Shire river catchment in Malawi. In addition, rainfall-runoff modelling is used to evaluate performance of hydrological models, for example Obled et al. (1994) analysed sensitivity of the TOPMODEL to spatial rainfall patterns for a well monitored mountainous catchment – the Réal Collobrier catchment in France.

The outputs of hydrological simulations have been used for many environment-related studies dealing with water-resources of a river basin such as soil moisture availability and variability (Ronda et al., 2002; Western et al., 2002), and nutrients and sediments transport (Syvitski et

al., 1998). It is therefore important that hydrological response should be investigated for river basins that support many different water-resources users, particularly in Tropical Africa, in which the society relies directly or indirectly on the utilization of basins' water-resources for their livelihoods (PBWO/IUCN, 2007).

Hydrologic modelling approaches that encapsulate the transformation of rainfall into runoff have been widely documented by many authors (e.g. Freeze and Harlan (1969), Clarke (1973), Pilgrim et al. (1988), Todini (1988), Beven (1989, 2001), Singh (1995), Sorooshian and Gupta (1995), Bergtröm and Graham (1998), Boyle et al. (2000) and Wheater (2002)). These authors discusses (i) hydrologic models classifications, (ii) uncertainties associated with hydrologic model structure and parameterization, (iii) hydrologic models data demands, and (iv) calibration and verification of hydrologic models.

Hydrological models are classified as physically-based or conceptual (Bergtröm and Graham, 1998). These models are further classified as lumped or distributed depending on the degree of discretization when describing the terrain in the basin. At least it is possible to understand the hydrology of a small and well monitored catchment using fully distributed physically-based hydrological models such as SHE (Abbott et al., 1986), IHDM (Beven et al., 1987) and THALES (Grayson et al., 1992). This type of models uses classical continuum mechanics and represents hydrological processes based on principles of conservation of mass, energy and momentum. In addition, fully physically-based models demand less calibration or tuning of the parameters, since their parameters are usually obtained from field measurements. However, using fully distributed physically-based models is impractical in many locations of the globe, because of limitations and uncertainties associated with over-parameterization and large demands of data input (Beven, 1989; Grayson et al., 1992; Kirkby, 1993). Particularly in Tropical Africa, input data for hydrological models are often scarce. The density of climate stations is very low and the data they produce is often limited, in terms of recorded parameters as well as spatial and temporal resolution and continuity (Pilgrim et al., 1988; PBWO/IUCN, 2007). Moreover, map data on soil texture, leaf area index, and extension of groundwater aquifers are hardly available.

In choosing between the hydrologic models, the optimum model should meet the data availability in the study region and still achieve the expected objectives (Bergström, 1991). Additionally, such a model should have a parsimonious structure to avoid over-parameterization (Beven, 1989) and should be distributed (Obled et al., 1994). Conceptual semi-distributed models have been widely used in hydrology, because their structures require fewer observed data compared to fully-distributed hydrological models. Conceptual semi-distributed models represent the hydrologic cycle by linking together process components which described physical concepts, on the presumption that the model parameters would also bear physical meaning, so that they could be assigned values without reference to the observed data (Todini, 1996). In other words, the latter type of the models assumed that most of their parameters such as runoff coefficients could be defined from the physiographic characteristics of the basins. Parameters are estimated either manually or using optimization algorithms by maximizing objective functions such as criterion suggested by Nash and Sutcliffe (1970) or combined criterion suggested by Lindström (1997). Manual procedure of

tuning model parameters is dependent on familiarity of the model structure and study catchment.

A semi-distributed hydrologic modelling approach minimizes computational demands, the number of model parameters and data input for hydrologic simulation in large catchments (Becker, 1992; Becker and Braun, 1999; Flügel, 1995). Examples of conceptual semi-distributed models include TOPMODEL (Beven and Kirkby, 1979; Beven et al., 1984), ARNO (Todini, 1996), and HYPE (Lindström et al., 2010). The structures of these conceptual semi-distributed models show similarity in runoff formation and catchment discretization. However, the infiltration processes of the TOPMODEL are described by the Green-Ampt (1911) equation, while for the ARNO and HYPE they are described by the empirical relationships of the soil moistures contents. Also, input data demand is different between these models. The TOPMODEL requires rainfall and evapotranspiration at one hour time scale. The ARNO requires rainfall and number of sunshine hour also at one hour time scale, and for a catchment of the order of 1000–2000 $km^2$, the ARNO requires three hour time scale input data. The HYPE requires only rainfall and mean surface air temperature at day time scale as forcing. For that reasons, HYPE appear to be a suitable model for simulation of the hydrologic response in the Mkomazi river basin where only rainfall and temperature data are available at daily and monthly scales.

The present study aimed to simulate hydrological response (rainfall–runoff) of the Mkomazi river basin in north-eastern Tanzania using HYPE (Lindström et al., 2010), digital elevation models data at 90 m (www2.jpl.nasa.gov/srtm/) spatial-resolution, and spatially distributed climatological maps constructed in Chapter 3. The Mkomazi river basin is particularly challenging to hydrological modelling, due to strong variations in rainfall and evapotranspiration, rugged terrain and different land uses. However, rural livelihood depends strongly on available water for both rain-fed and irrigated agriculture. The output of the hydrological simulation was used to produce soil moisture availability maps for the catchment.

## Methods

*Model Description*

The HYdrological Predictions for Environment (HYPE; Lindström et al., 2010) was developed for the simulation of basin hydrological processes, nutrients transport and water quality. Parts of HYPE are based on the HBV models by Bergström (1976), Lindström et al. (1997), Andersson et al. (2005), Arheimer et al. (2005) and Lindström et al. (2005). The HYPE model requires daily rainfall and temperature data as forcing. Model parameters are either general or related to soil type, or land cover. A basin is divided into sub-basins with up to three (if greater than one) soil layers and of possible different soil layers depths (Fig. 4.1). The sub-basins resolution is the resolution of the input forcing data and the geographic input data such as elevation and slope. Within each sub-basin the proportion of each soil land-use combination (SLC) is specified (Fig. 4.1a). Digital elevation models (DEM) data in addition to soil and land cover maps is used for such inputs.

For each SLC, the processes of snow melt, evapotranspiration, infiltration and surface runoff, percolation and macropore flow, tile drainage, and groundwater flow to the stream from soil layers with water contents above field capacity are simulated (Fig. 4.2). The maximum water content of a soil layer is determined by three model parameters coupled to soil texture: (i) the portion not available for evapotranspiration, (ii) the portion available for evapotranspiration but not for runoff, (iii) the portion available for runoff. The first two fractions correspond to the soil wilting point and field capacity. Soil moisture above the threshold determined by the portion of water available for runoff may percolate down to the next layer. The percolation through underlying soil layers is restricted by the maximum percolation capacity of the soil moisture and by the available pore space in the soil layers below.

Evapotranspiration occurs from the two top soil layers and is assumed to decrease with depth. It is divided between the two layers based on a decreasing exponential function at the midpoint of each layer. Reference evapotranspiration depends on temperature and a seasonal adjustment factor, if not given as input. The outflow from soil layers is routed within and between sub-basins using a river routine. Runoff can drain from any soil layer, if the soil moisture in that layer exceeds the threshold for runoff.

The model has two types of rivers and lakes, internal and main rivers and lakes. The internal rivers and lakes are lumped together into one river and one lake, which are connected in series, and receive only local runoff from sub-basin. The lake can be bypassed by a fraction of the local runoff. The second type, main rivers and lakes, constitutes the coupling between sub-basins. These rivers and lakes receive the local runoff – after it has passed internal rivers and lakes – and the riverflow from upstream sub-basins. The riverflow is delayed in time, according to the river length and a flood wave velocity. The river lengths are approximated as the square root of the sub-basin area, if not given as input. The outflow from the basin is determined by a rating curve. The structure of the HYPE is as shown in Figure 4.3.

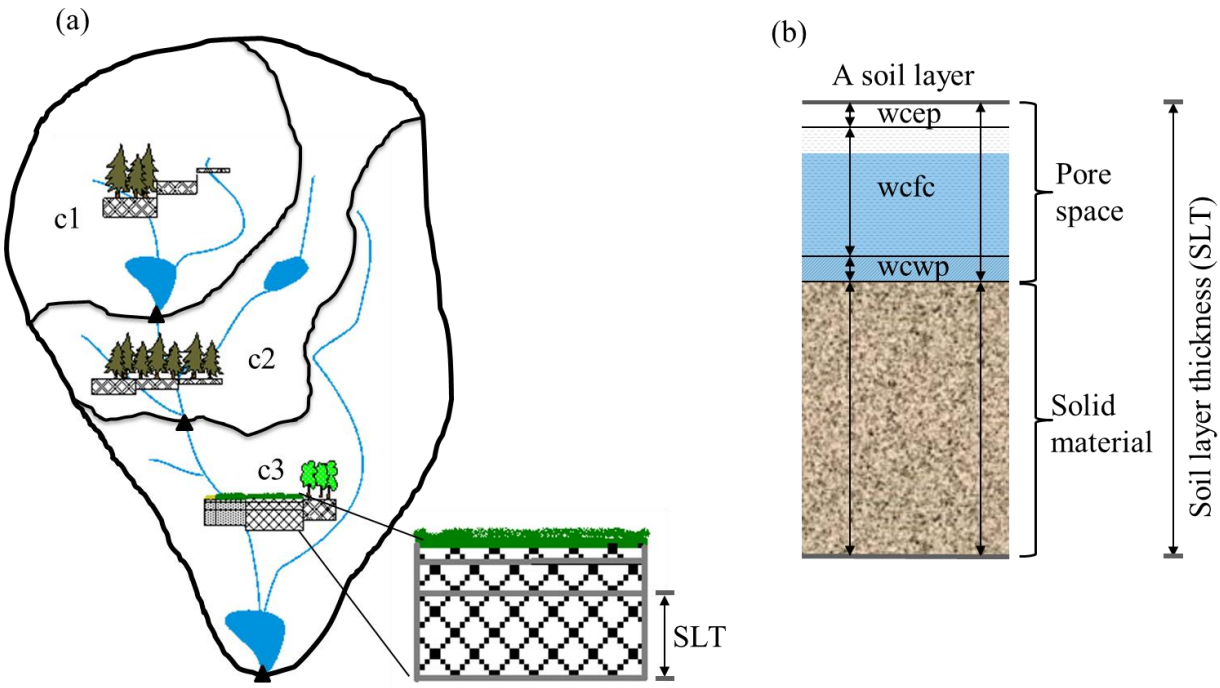


Figure 4.1. An example of a basin divided into three sub-basins. Each sub-basin can be with different (i) soil depth and land-use classes – c1, (ii) soil type and land-use – cl2, and (iii) soil and land-use types – c3. Soil depth profile can be of three soil layer thicknesses (SLT) of different soil types. The parameters of water retention in the soil are effective porosity (wcep), field capacity (wcfc) and wilting point (wcwp).

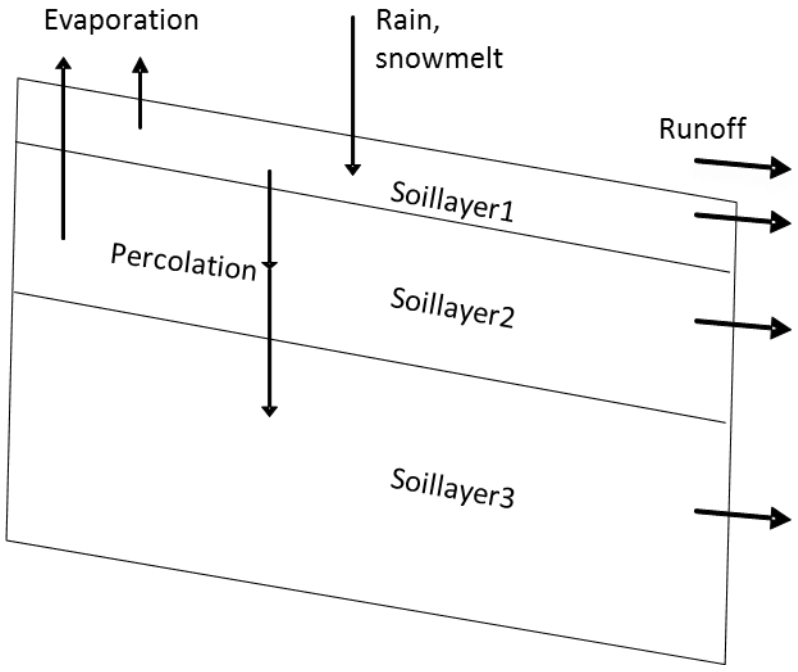


Figure 4.2. A two-dimensional water movement within a soil profile of three soil layers. Evaporation occurs from the topmost two soil layers. Surface runoff occurs due to infiltration excess. Infiltrated rainfall percolates through the soil layers causing saturation excess runoffs.

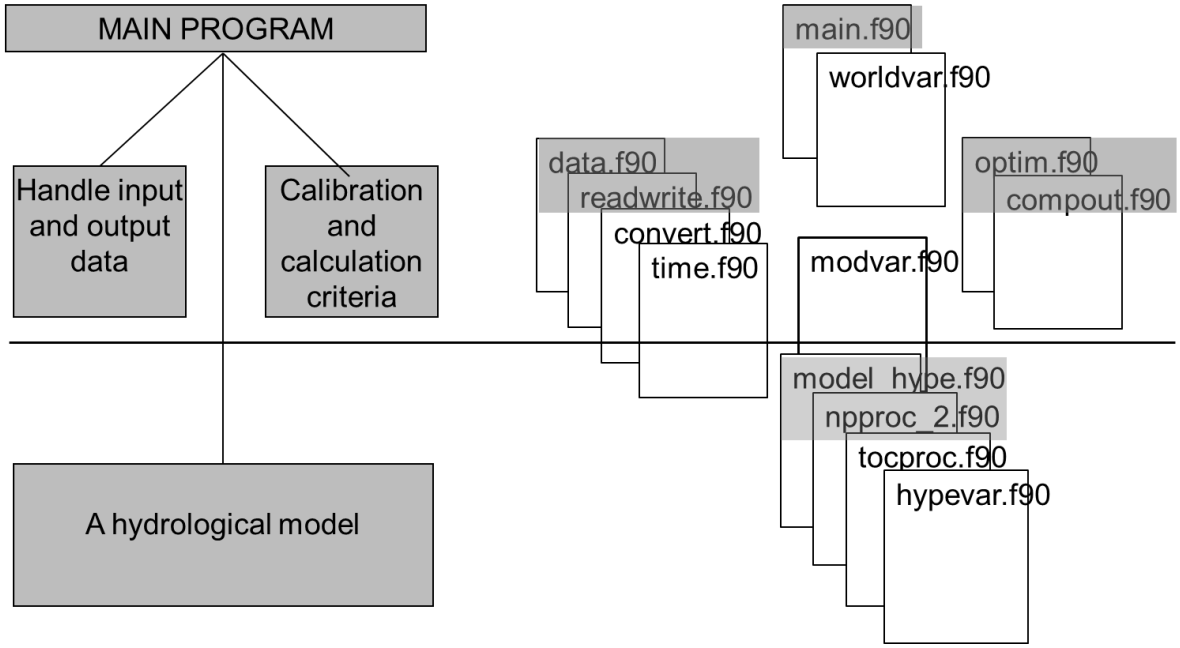


Figure 4.3. Modules structure of a hydrological model. Top part: hydrological simulation system (HYSS) handles input and writes output, provides routines for calibration using different optimisation criterions. Bottom part: hydrological predictions for environment (HYPE) model. Right part: main program (main.f90), variables for HYSS (worldvar.f90), subroutines for input-data and print-out (data.f90), subroutines for read and write to file (readwrite.f90), subroutines for conversion and time (convert.f90 and time.f90), subroutines for optimization (optim.f90), subroutines for calculations and criteria (compout.f90), subroutines for interface between HYSS and HYPE (modvar.f90), subroutines for water (model_hype.f90), subroutines for nitrogen and phosphorus (npproc2.f90), subroutines for organic carbon (tocproc.f90), and variables for HYPE (hypevar.f90).

*Data used and model setup*

The HYPE model setup requires (i) a flow network connecting sub-basins to the outlet of a catchment, (ii) distributed soil land-use combination (SLC) parameters, and (iii) spatiotemporally distributed climatological data. A DEM at 90 m (www2.jpl.nasa.gov/srtm/) spatial-resolution was fundamental for spatial data development and model parameters. This DEM was aggregated to 450 m spatial-resolution. Watershed boundary, flow direction and flow accumulation, were then delineated according to the procedure described by Jenson and Domingue (1988). Based on the aggregated DEM, we calculated local slope and mean elevation for each 450x450 $m^2$ pixel. Flow direction and flow accumulation maps were linked to create a streamflow network by connecting pixels from upstream to the outlet. These pixels are sub-basins according to the HYPE model requirements for the present study area.

Soil depth profile and soil texture classes were estimated from literature and in situ measurements of 150 observations plots covering the most important soil features (Petzold and Kleyer, [in prep.]), which include: (i) soil type (e.g. sand, clay and silt), (ii) soil depth, (iii) organic matter content, (iv) gravel content, and (v) bulk density. One soil-depth profile map was constructed by means of linear regression-based and GIS techniques with DEM at 90 m spatial resolution, measured soil depth, inclination and geology map of the area as input

data. Also, DEM at 90 m spatial-resolution, linear regression-based and GIS techniques were applied to construct soil moisture maps at field capacity, wilting point, effective porosity and percolation capacity followed the methodology suggested by Saxton and Rawls (2006). The constructed soil profile depth and soil moisture maps were then aggregated to 450x450 $m^2$ pixels. Natural breaks method by Jenks (1967) in ArcGIS converted continuous aggregated soil maps into discrete pixels values. Discrete soil-depth profile map and soil moisture maps were overlain in ArcGIS to create SLCs. Soil profile depth was set to three layers, topsoil layer for decay of organic matter was set to 0.4 m, plant rooting soil layer depth to 1.4 m and deep soil layer. Soil moisture parameter values were assumed to have physical meaning and be uniform with soil depth.

We used monthly averaged reference evapotranspiration ($ET_o$), rainfall and mean temperature maps constructed in Chapter 3 to construct spatially distributed daily variables. These maps were aggregated to 450 m spatial-resolution. Monthly $ET_o$ values were divided by the number of days to calculate average daily $ET_o$ (mm $day^{-1}$) and daily temperature (°C $day^{-1}$) was assumed to be uniform within the respective month. Spatially distributed daily rainfall data were constructed using two datasets: (i) monthly rainfall data from Tanzania Meteorological Agency (TMA) and (ii) daily rainfall data from Pangani-NRM-version-2.0. The rainfall gauge network is shown in Table 4.1. Missing data were described relative to start-end-date of each station. Quality control of TMA dataset was as in Chapter 3.

Table 4.1 Rainfall gauge network. Daily rainfall records from stations marked * were obtained from Pangani-NRM-version-2.0 database which consolidated records collected from Tanzania Ministry of Water and Livestock Development, TMA, Pangani basin district and regional offices and institutions. Values in parentheses are relative to the period 1964–2010.

| Station number | Gauge name | Gauge ID | Elevation (m a.s.l.) | Latitude | Longitude | Record length | %missing |
|---|---|---|---|---|---|---|---|
| 1 | Suji mission * | 9437004 | 1371 | -4.317 | 37.850 | 1923−2008 | 18 (32) |
| 2 | Hassan sisal estate * | 9437001 | 914 | -4.333 | 37.850 | 1933−2007 | 21 (29) |
| 3 | Gonja estate * | 9438011 | 584 | -4.300 | 38.033 | 1937−1988 | 10 (50) |
| 4 | Kalimawe | 9438040 | 488 | -4.417 | 38.083 | 1963−2010 | 40 (41) |
| 5 | Ndungu sisal estate | 9438051 | 533 | -4.367 | 38.050 | 1966−2002 | 16 (34) |
| 6 | Tia dam | 9437010 | 1676 | -4.233 | 37.950 | 1962−2010 | 32 (31) |

Daily rainfall records of the Pangani-NRM-version-2.0 dataset were aggregated to monthly sums and compared with the TMA dataset. Monthly values of the former dataset were assumed to be missing if they passed for outliers during quality control of the latter dataset. A daily station rainfall dataset was then created using station 1, its missing data were filled by stations 2 and 3. Spatially distributed daily rainfall, R (mm $day^{-1}$), was then calculated as

$$R_{(i,m,y)} = D_{(i,m,y)} \frac{A_{(m,y)}}{S_{(m,y)}} rf \quad (4.1)$$

where D (mm) is daily station rainfall dataset, A (mm) is monthly average rainfall maps values estimated as in Chapter 3, S (mm) is monthly station rainfall, rf (-) is the monthly rainfall factor which accounts for spatial variability of rainfall, and i is day in month m of year y. This y value is for the period 1964–2010 (see Chapter 3 for the period). Eq. (4.1) eliminates the effects of the lines of best fit (least squares), construct respective monthly rainfall for each year, and distribute the latter into daily rainfall events.

Daily rainfall was calculated for the period 1964–1983, the period in which available riverflow records coincide with the available rainfall data. Therefore, such period was used for both calibration and validation. Monthly rainfall factors were calculated in ArcGIS as ratios between monthly rainfall stations records (TMA dataset cleaned for outliers) and monthly rainfall maps values at stations' location for the interval 1964–1983. We used monthly rainfall factors for the stations located within the Mkomazi river basin (see Tab. 4.1). Maximum rainfall factors were then used for the period November–April and minimum values for the period May–October.

The HYPE model was applied to simulate hydrological response for the Saseni river catchment, with a size of approximately 177 $km^2$. Availability of riverflow data was the main reason to select the Saseni river catchment (see Fig. 2.1 for the location). The observed runoff records at the outlet of the Saseni river (river-gauge 1DB2A) thus explained the model performance. Three simple yet effective statistical assessments and graphical representation were applied to describe the quality of the model simulation results: (i) the model efficiency ($R^2$), criterion suggested by Nash and Sutcliffe (1970), (ii) the percentage error by volume change ($\Delta V\%$) between observed and simulated total runoff (relative bias), and (iii) the index of volumetric fit (IVF). The model efficiency $R^2$ indicates the ability of the model to explain the variance of the observed riverflow. A value of ($R^2 = 1$) indicates a perfect model. The IVF is the ratio between observed and estimated total riverflow and indicates the ability of the model to preserve the total volume. IVF values close to one are desirable. In addition, the sensitivity of the model to the variation in rainfall, evapotranspiration and soil moisture was analysed for the calibration period by increments of systematic errors of ±5%, ±10%, ±20%, ±30% and ±50% in input data. The model was run by varying one input at a time over these increments while keeping the rest of input at their optimized values.

During calibration, the main focus was to optimise the $R^2$. This was done using manual calibration for the period 1978–1983. For the calibration period, riverflow records were complete without missing data for at least five years. Inputs data were not calibrated. We calibrated the model parameters controlling shape, magnitude and timing of the flood hydrograph. The model contains many parameters, some of the parameters were at default model values and some were reasonably fixed based on literature. Only those that have been fixed or optimized are listed in Table 4.2. Note that riverflow records were available only for the period 1964–1983 and the period 1978–1983 was used to calibrate the model. Therefore, the model was validated for the period 1964–1977. Hydrological response was then simulated for the period 1964–1983 using the calibrated parameters, and the implicitly simulated soil moisture availability values were drawn in ArcGIS to create soil moisture availability maps averaged for the period 1964–1983. To create soil moisture availability maps for other periods

between 1984 and 2010, spatially distributed daily rainfall had to be created (Eq. (4.1)), preceded by computed monthly rainfall factors (rf).

Table 4.2. List of calibrated model parameters. Parameters marked * were fixed (not optimized).

| Parameter | Description |
|---|---|
| ttmp* | threshold temperature for snow melt and evapotranspiration (-) |
| lp* | limit for potential evapotranspiration (-) |
| epotdist | coefficient in exponential function for potential evapotranspiration's depth dependency (-) |
| rivvel* | celerity of flood in watercourse (ms-1) |
| rrcs1 | recession coefficient for uppermost soil layer (-) |
| rrcs2 | recession coefficient for lowest soil layer soil layer (-) |
| rrcs3 | recession coefficient for slope dependence (-) |
| trrcs | recession coefficient for tile drains (-) |
| srrate | rate for surface runoff (-) |
| macro1 | rate for macropore flow (-) |
| macro2* | threshold for macropore flow (mm) |
| macro3 | threshold soil water for macropore flow and surface runoff (-) |

Table 4.3. Monthly rainfall (mm).

| Month/Year | 1964 | 1965 | 1966 | 1967 | 1968 | 1969 | 1970 | 1971 | 1972 | 1973 | 1974 | 1975 | 1976 | 1977 | 1978 | 1979 | 1980 | 1981 | 1982 | 1983 |
|---|---|---|---|---|---|---|---|---|---|---|---|---|---|---|---|---|---|---|---|---|
| January | 41 | 87 | 59 | 19 | 10 | 101 | 186 | 120 | 13 | 79 | 54 | 22 | 8 | 132 | 194 | 175 | 6 | 57 | 6 | 21 |
| February | 98 | 6 | 265 | 24 | 77 | 63 | 38 | 43 | 74 | 88 | 45 | 8 | 59 | 69 | 48 | 137 | 17 | 61 | 17 | 51 |
| March | 143 | 150 | 176 | 12 | 220 | 119 | 267 | 64 | 96 | 102 | 53 | 40 | 22 | 309 | 403 | 91 | 93 | 135 | 113 | 133 |
| April | 79 | 18 | 32 | 215 | 93 | 63 | 39 | 22 | 27 | 74 | 186 | 59 | 26 | 74 | 178 | 223 | 185 | 96 | 186 | 26 |
| May | 8 | 74 | 34 | 95 | 24 | 2 | 35 | 24 | 77 | 58 | 39 | 59 | 44 | 48 | 45 | 165 | 69 | 41 | 69 | 103 |
| June | 0 | 0 | 0 | 90 | 16 | 0 | 0 | 11 | 0 | 7 | 9 | 0 | 22 | 13 | 18 | 24 | 0 | 5 | 21 | 18 |
| July | 0 | 3 | 0 | 45 | 15 | 0 | 0 | 0 | 0 | 0 | 14 | 7 | 4 | 0 | 0 | 31 | 0 | 2 | 8 | 1 |
| August | 0 | 8 | 9 | 2 | 13 | 28 | 0 | 0 | 0 | 0 | 3 | 0 | 0 | 41 | 6 | 3 | 10 | 4 | 8 | 2 |
| September | 0 | 4 | 0 | 45 | 19 | 60 | 0 | 0 | 69 | 0 | 4 | 5 | 26 | 28 | 1 | 10 | 13 | 6 | 43 | 13 |
| October | 28 | 34 | 0 | 31 | 6 | 5 | 5 | 0 | 23 | 6 | 4 | 79 | 0 | 96 | 10 | 13 | 0 | 51 | 148 | 0 |
| November | 25 | 113 | 51 | 85 | 65 | 92 | 42 | 110 | 82 | 113 | 61 | 36 | 78 | 90 | 390 | 83 | 78 | 112 | 436 | 137 |
| December | 286 | 276 | 62 | 15 | 82 | 70 | 73 | 154 | 33 | 84 | 82 | 28 | 131 | 147 | 311 | 119 | 97 | 183 | 97 | 269 |

Table 4.4. Monthly rainfall factors, rf (-).

| Month/Year | 1964 | 1965 | 1966 | 1967 | 1968 | 1969 | 1970 | 1971 | 1972 | 1973 | 1974 | 1975 | 1976 | 1977 | 1978 | 1979 | 1980 | 1981 | 1982 | 1983 |
|---|---|---|---|---|---|---|---|---|---|---|---|---|---|---|---|---|---|---|---|---|
| January | 1.474 | 0.443 | 1.144 | 0.130 | 0.013 | 2.535 | 2.258 | 0.955 | 3.898 | 1.318 | 0.585 | 0.754 | 2.486 | 2.364 | 3.759 | 3.570 | 2.987 | 0.473 | 0.330 | 1.787 |
| February | 2.293 | 0.026 | 3.471 | 1.337 | 0.699 | 2.556 | 2.168 | 0.660 | 1.152 | 1.086 | 0.613 | 0.126 | 2.536 | 1.156 | 0.590 | 3.720 | 1.604 | 0.339 | 0.202 | 1.872 |
| March | 1.865 | 0.640 | 0.977 | 0.776 | 2.081 | 1.404 | 3.504 | 0.605 | 0.952 | 0.563 | 0.407 | 0.990 | 3.878 | 2.341 | 3.049 | 2.051 | 0.878 | 0.039 | 2.611 | 0.593 |
| April | 0.991 | 0.531 | 0.497 | 1.643 | 2.613 | 1.656 | 0.908 | 3.801 | 0.546 | 0.968 | 1.167 | 0.576 | 3.673 | 0.204 | 0.864 | 1.196 | 2.254 | 1.471 | 1.260 | 0.546 |
| May | 0.028 | 0.636 | 0.659 | 1.074 | 0.604 | 0.024 | 0.168 | 0.195 | 1.804 | 0.677 | 0.157 | 0.488 | 0.498 | 0.331 | 0.385 | 1.853 | 0.354 | 0.392 | 0.513 | 0.918 |
| June | 0 | 0 | 0 | 0.128 | 2.385 | 0 | 0 | 0.270 | 0 | 0.103 | 0.256 | 0 | 0.087 | 0.199 | 0.829 | 0.813 | 0 | 0.052 | 0.425 | 0.282 |
| July | 0 | 0.299 | 0 | 2.056 | 0.582 | 0 | 0 | 0 | 0 | 0 | 1.145 | 0.605 | 0.147 | 0 | 0.039 | 0.548 | 0 | 0.070 | 0.794 | 0.047 |
| August | 0 | 0.698 | 0.462 | 0.220 | 0.145 | 1.050 | 0 | 0 | 0 | 0 | 0.284 | 0 | 0 | 0.933 | 0.273 | 0.247 | 1.464 | 0.383 | 0.479 | 0.016 |
| September | 0 | 0.225 | 0 | 2.970 | 0.102 | 0.264 | 0 | 0 | 1.317 | 0 | 0.069 | 0.317 | 1.696 | 0.673 | 0.020 | 0.363 | 0.802 | 0.077 | 0.077 | 0.704 |
| October | 0.207 | 0.908 | 0 | 0.580 | 0.163 | 0.100 | 0.052 | 0 | 0.679 | 0 | 0.085 | 0.397 | 0 | 0.822 | 0.199 | 0.043 | 0 | 0.999 | 1.454 | 0 |
| November | 0.255 | 1.056 | 0.662 | 1.414 | 1.369 | 0.902 | 1.073 | 0.539 | 1.307 | 1.020 | 1.205 | 1.255 | 0.266 | 2.350 | 1.219 | 0.915 | 1.534 | 0.715 | 2.876 | 0.635 |
| December | 1.947 | 2.553 | 1.071 | 0.102 | 1.563 | 0.745 | 1.989 | 1.769 | 3.937 | 1.628 | 3.347 | 1.476 | 1.310 | 2.386 | 3.971 | 1.709 | 2.768 | 3.165 | 1.856 | 1.622 |

## Results

The values of monthly rainfall ranged from zero during the dry season June–September to about 450 mm during the rainy season (Tab. 4.3). More statistical details of temporal rainfall variability of individual stations are given in Chapter 3. From the created monthly rainfall factors, a factor of zero indirectly indicates a dry month (Tab. 4.4). The plot of the simulated hydrograph superimposed on the observed hydrograph showed that the HYPE model captured the peaks, time to peaks and low flows (Fig. 4.4). However, some peaks and low flows were overestimated and others were underestimated. The overestimated flood-events were in February (1966), April (1968, 1980), and December (1971, 1974), whereas flood-events in January (1972, 1973, 1980), February (1969), March (1969, 1976, 1982), April (1966, 1971, 1976), May (1964, 1967, 1976) and December (1968, 1972) were underestimated.

Summarized model results showed that for the calibration period, the model produced a runoff hydrograph with $R^2$, $\Delta V$ and IVF values of 0.85, -10.69% and 1.12, respectively, while for calibration period values of 0.68, -7.93% and 1.09 resulted. The plot of the sensitivity of the model to the variation in the input data showed that the systematic errors of ±10% in rainfall, evapotranspiration and soil moisture could be accommodated by the model without reduction of the model performance (Fig. 4.5).

The constructed monthly soil moisture availability maps, with monthly values drawn relative to the total annual simulated soil moisture availability (Figure 4.6) and absolute values (Figure 4.7). Note that the HYPE model simulates average soil moisture in mm. The constructed maps show substantial differences in soil moistures availability between dry and wet seasons, with higher soil moisture for the rainy season than for the dry season. However, this was as expected. For the rainy season, in December–May, soil moisture availability for each month was in excess of 9%, and maximum was in April with above 11% of soil moisture availability. For the dry season, in July–October, soil moisture availability ranged from 5 to 7.7%. In June and November, soil moisture availability was moderate, between dry and wet seasons. Nevertheless, November was drier than June. In addition to rainfall which is the main source of water into the catchment, soil moisture availability was also influenced by soil depth. From the maps, soil moisture availability was higher on mountain valleys depending on the orientation of slopes. Most of the mountains valleys (windward-side) had high soil depths and thus higher soil moistures availability than leeward-side slopes. Likewise, soil moisture availability was high on the slopes and flood-plains close to the Saseni river. Soil depth profile map and soil textures maps are shown in Figures 4.8 and 4.9.

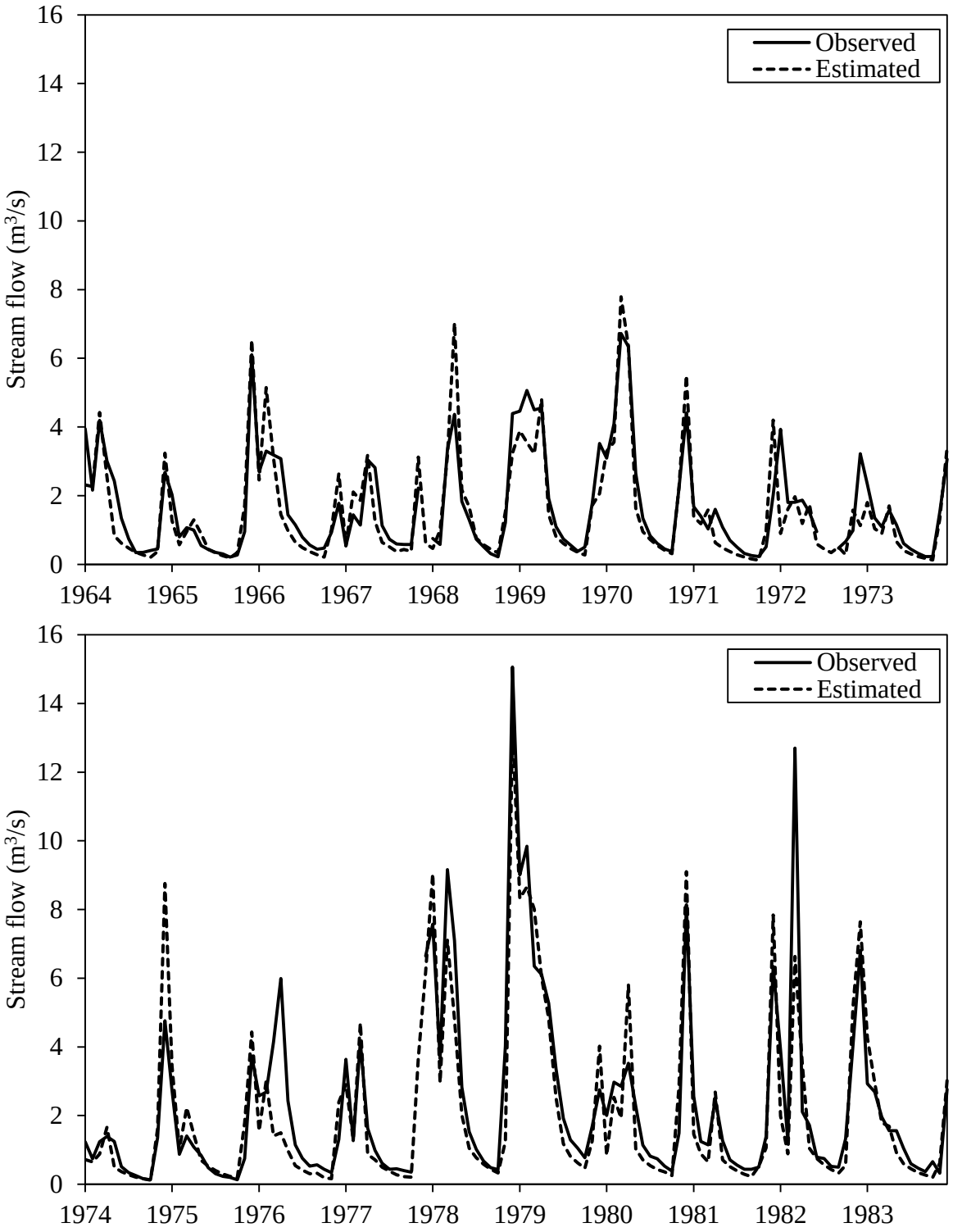


Figure 4.4. Time series plot of the HYPE model performance for the Saseni river for the period 1964–1983.

Table 4.5. Optimized model parameters values using manual calibration procedure. Parameters marked * were fixed (not optimized). For description of parameter: see Table 4.2.

| Parameter | Range | Optimized |
|---|---|---|
| ttmp* | 0 ─ 0.5 | 0.1 |
| lp* | 0.5 ─ 1 | 0.9 |
| epotdist | 0 ─ 5 | 0.01 |
| rivvel* | 0.1 ─ 1.5 | 1.0 |
| rrcs1 | 0 ─ 1 | 0.0085 |
| rrcs2 | 0 ─ 1 | 0.009 |
| rrcs3 | 0 ─ 1 | 0.0009 |
| trrcs | 0 ─ 1 | 0.008 |
| srrate | 0 ─ 1 | 0.3 |
| macro1 | 0 ─ 1 | 0.5 |
| macro2* | 5 ─ 30 | 10 |
| macro3 | 0 ─ 1 | 0.5 |

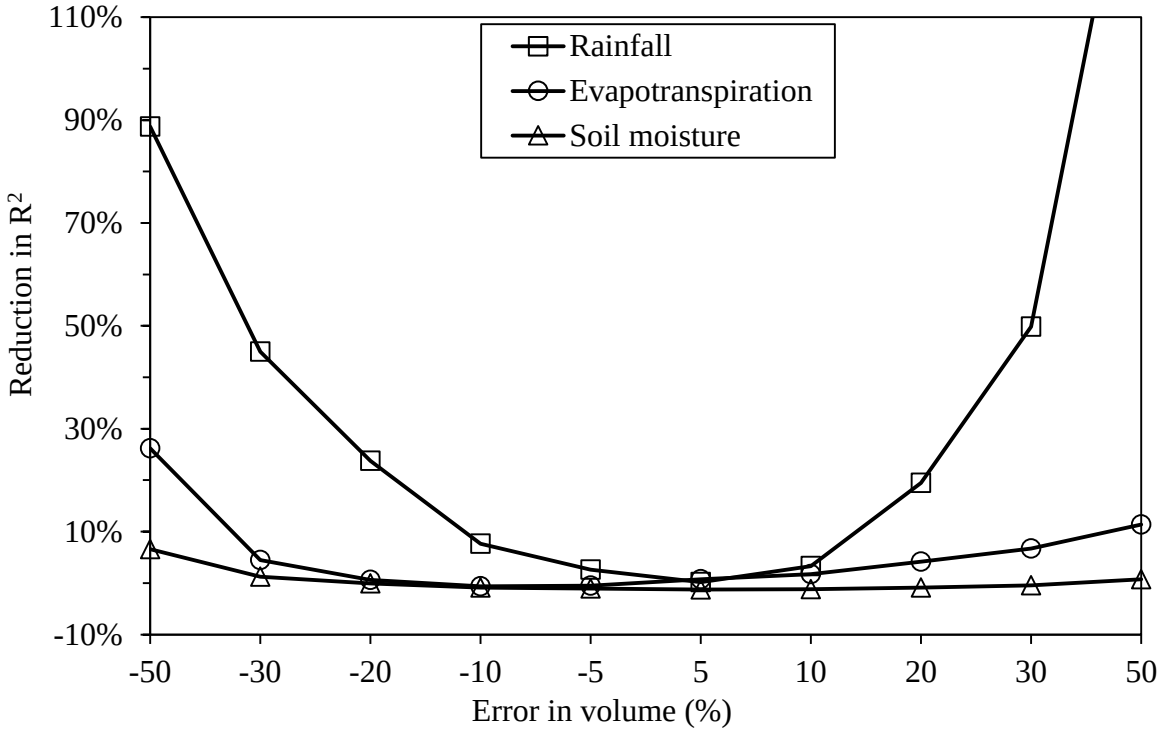


Figure 4.5. Reduction in the model performance for the calibration period using the optimized parameters at different levels of the assumed systematic errors in input data.

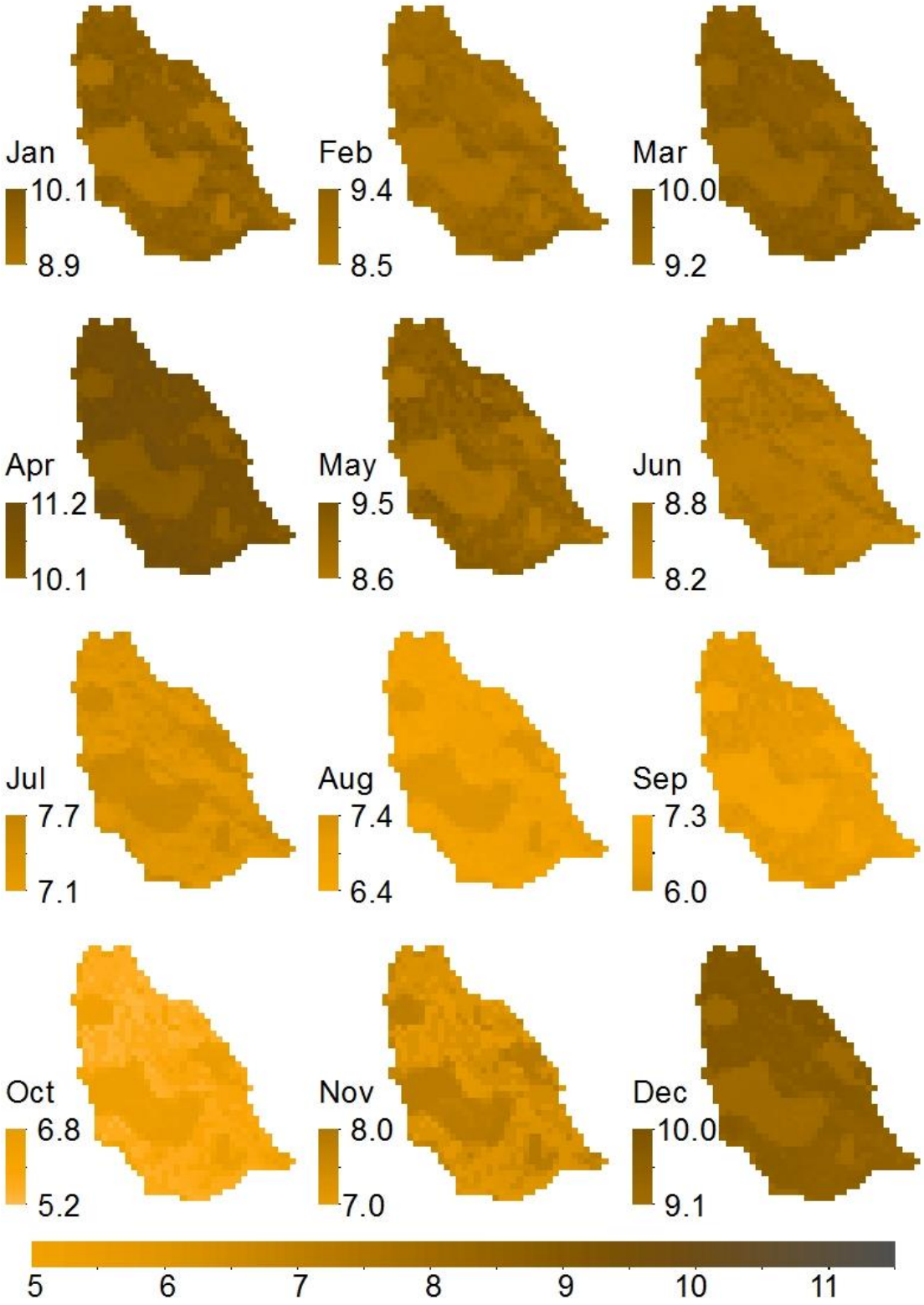

Figure 4.6. Monthly soil moisture availability (%) relative to annual soil moisture availability simulated for the period 1964–1983 for the Saseni catchment.

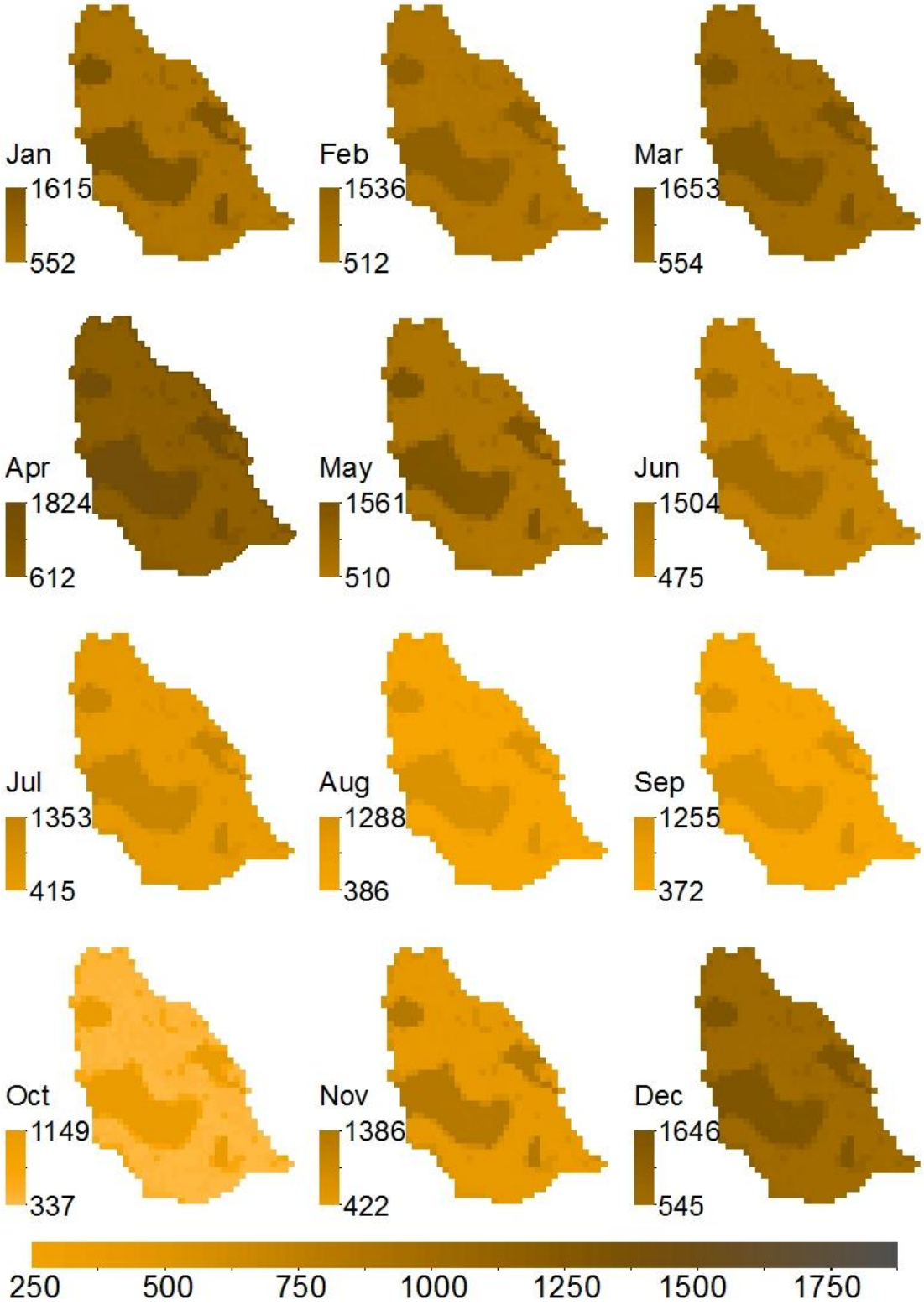

Figure 4.7. Simulated monthly soil moisture availability (mm) for the period 1964–1983 for the Saseni catchment.

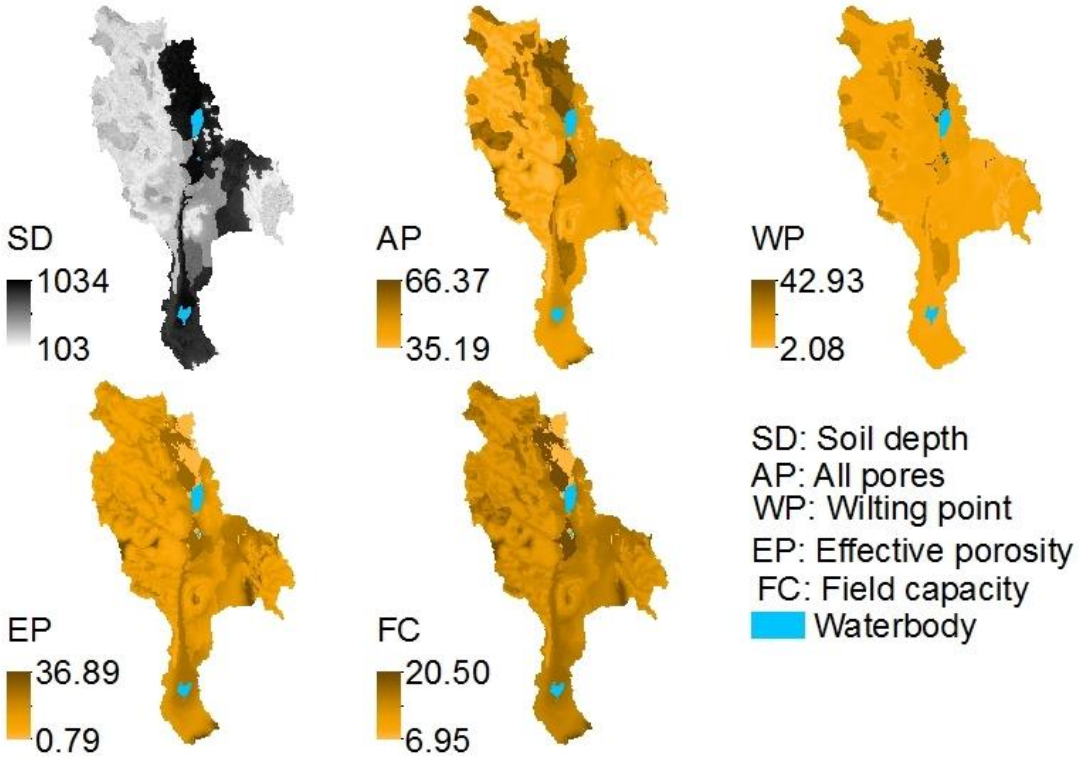


Figure 4.8. Soil depths profile (cm) and soil textures (**%**) constructed at 90x90 $m^2$ for the southern Mkomazi river basin.

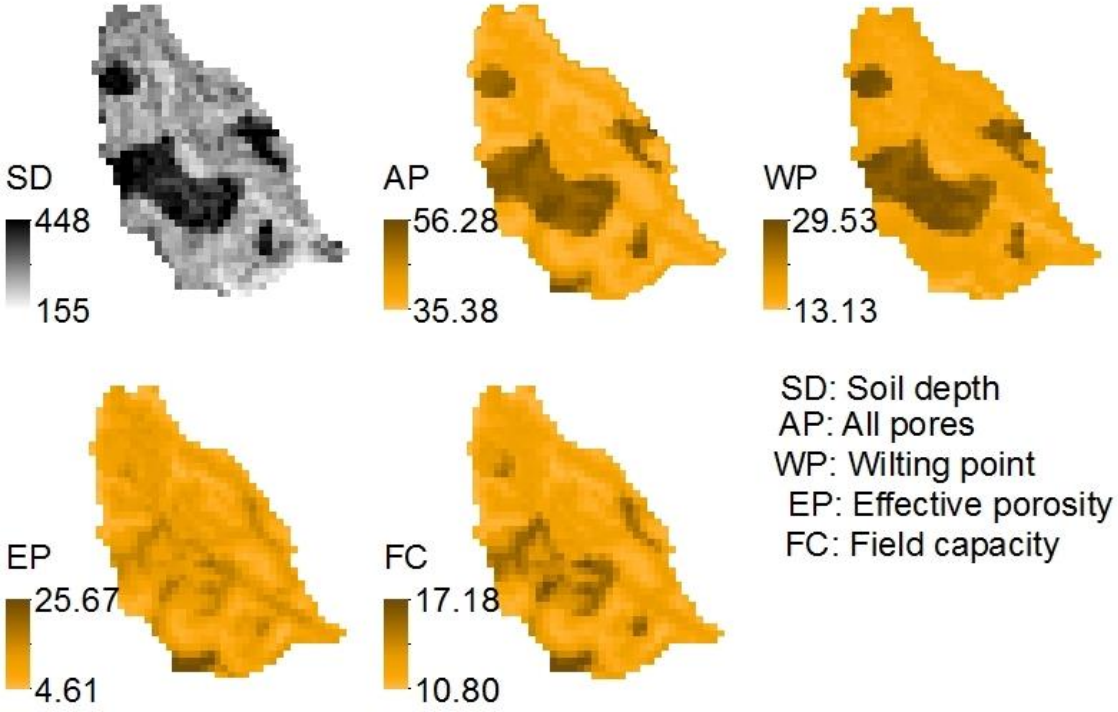


Figure 4.9. Soil depths profile (cm) and soil textures (%) extracted for the Saseni river catchment and resampled to a 450x450 $m^2$.

## Discussion

The model captured the pattern of the observed riverflow hydrograph both for calibration and validation periods, such as the peak flow, the time to peak, and the low flow. According to the model and the observed data, the Saseni river showed great annual runoff variation, ranging from almost zero to more than 10 $m^3$ water per second when dry seasons change to wet seasons. Runoff during wet seasons was characterised by marked inter-annual variability which poses a production risk for downstream agricultural irrigation schemes.

Our study reveals the potential use of semi-distributed hydrological models in rainfall-runoff modelling. Such simulations are important for understanding hydrological processes of a river basin. Model input data and parameters were constructed by means of regression-based and GIS techniques. The calibration of the model was based on visual comparison of the observed and simulated monthly runoff to optimize $R^2$ efficiency (Nash and Sutcliffe, 1970), in which better performance was obtained for the calibration period than for validation as expected. The calculated index of volumetric fit, IVF, was approximately the same both for calibration and validation periods, and close to one. The IVF close to one and the percentage error by volume change, $\Delta V$, of -10% suggested that the total volume maintained, and it can be assumed that the water balance achieved (available soil moisture is equal to water enters the catchment minus water leaves the catchment), although some peak flows were overestimated and others underestimated.

The model was calibrated manually. Although successfully, the approach was still subjective, contrasting to an automatic calibration which can eliminate human subjectivity (Boyle et al., 2000), and reduces the need for expertise with a particular model (Sorooshian and Gupta, 1995). Manual calibration is dependent on familiarity with the model structure and the study catchment, and thus different results will be obtained by different modellers (Wheater, 2002). Donnelly et al. (2009) managed to calibrate the HYPE model manually when predicting hydrological responses for multi-basins in Europe. Lidén and Harlin (2000) reported that three calibration procedures (manual, automatic and Monte Carlo) yielded a similar model performance when they calibrated the HBV-96 model for catchments in Tanzania, Bolivia, Zimbabwe and Turkey. Note that parts of the HYPE model are based on the HBV-96 model. Automatic calibration is often very successfully when used in conjunction with manual methods. In other words, an automatic method has not yet developed to the point that it can entirely replace manual methods, due to the difficulty of constructing objective functions and optimization algorithms (Beven, 2001).

In addition to the estimated parameters, the performance of hydrological models is influenced by the quality of input data, particularly rainfall, evapotranspiration and soil moisture. In the present study, the input data sensitivity based on $R^2$ efficiency (Nash and Sutcliffe 1970) reveals that rainfall appeared to be the most influential variable controlling the peak flows. The performance of the model was completely reduced when the systematic errors of ±50% applied, and the efficiency $R^2$ decreased rapidly between the errors of ±10% and ±50%.

However, it was also shown that inadequacies of ±10% in rainfall, evapotranspiration and soil moisture could be accommodated without loss of the model performance.

Obled et al. (1994) used two different rainfall datasets in terms of spatial coverages densities, when they analysed the sensitivity of the TOPMODEL to spatial rainfall patterns for a well monitored mountainous region – the Réal Collobrier catchment – in France. The first dataset was an arithmetic mean of only 5 rain-gauges but well distributed across the catchment, whereas a spline-surface fitting method of 21 rain-gauges created the second dataset. There was no significant improvement in simulation, based on $R^2$ efficiency (Nash and Sutcliffe, 1970), when the model was provided with a better description of spatially varying rainfall pattern (second dataset). They reported that this was because the dynamics of the response were already reproduced well enough with the first dataset, which indirectly explains an advantage of conceptual semi-distributed models in terms of data demand. However, in addition, the conclusion was that in simulation of hydrological response of a catchment, spatially distributed rainfall pattern must be taken into account because it improves an estimate of a basin rainfall volume, and also hydrological models sometime respond to a rainfall event which a catchment ignores or dampens. In this latter issue, the model produced a few secondary peaks when it was provided with the second dataset.

For the systematic errors of -50% in evapotranspiration, the $R^2$ efficiency (Nash and Sutcliffe, 1970) was reduced by 30%, while only 10% of this $R^2$ efficiency was reduced for the error of +50%. A low evapotranspiration rate means that the soil was kept at wet conditions, because the HYPE model assumes the initial soil moisture content to be a sum of the product of soil depth and soil textures at wilting point and field capacity. Therefore, even low rainfall could produce runoff. In contrast, a high evapotranspiration rate could dry up the soil, below the wilting point, but incoming rainfall must fill all soil pores prior to the formation of runoff. It can be assumed that the structure of the model, on these complex dynamics of moisture transfer in the hydrologic cycle from the soil to the atmosphere, was less sensitive to evapotranspiration. However, less sensitivity of the model to the variations in evapotranspiration can also be due to the assumption that daily evapotranspiration rates were the same for each day within the perspective month, and due to the subjectivity of the manual calibration method when tuning the parameters controlling the removal of water from the soil. In general, the model was insensitive to inadequacies in soil moisture, only 10% of this $R^2$ efficiency was reduced for the error of -50%, which is the same reduction for the error of +50% in evapotranspiration, thus this suggested that inadequacies in soil moisture and evapotranspiration was compensating each other.

Hydrographs in arid and semi-arid catchments are characterized by flashy peaks with steep rising and falling limbs and times of rise and baseflow are often short (Pilgrim et al., 1988). The Saseni river catchment has the characteristics of a medium wet to dry basin, based on its hydrograph. A wet basin characteristic is shown by the less steep falling limbs of the hydrograph for the period May–July, whereas the steep rising limbs for the period November–December are the characteristic for arid catchment's hydrographs. These characteristics were also pronounced when the systematic errors in soil moisture were introduced. Addition (+) errors in soil moisture during rainy season kept the evapotranspiration at their potential rates

and the soil wetness enabled the contribution of the subsurface flow to the runoff formation, which is a common situation in wet basins. On the other hand, steep rising limbs for the period November–December are the characteristic of dry catchment hydrographs because runoff formation after a prolonged dry condition is mainly due to infiltration excess, particularly in elevated areas with sparse vegetation (Horton, 1933).

Soil moisture depth profile and the soil textures play a key role in influencing the soil water availability. The plant rooting soil layer depth for the present hydrological simulation was obtained after several trials and errors. Thin soil layers resulted in an insignificant difference in soil moistures between dry and rainy seasons, associated with high baseflow during the dry season. In contrast, thick soil layers dried up the runoff during the dry season.

High soil moisture values indirectly indicate the locations of high soil depth, and these locations are mostly on mountain valleys (windward-side) and valleys close to the river. The DEM pixel size of 450 m spatial resolution was obtained after several trials and errors. Smaller pixel size exceeded the soil class combination limit specified in the model, whereas larger pixels smoothed several parts of topography which distorted watershed characteristics such as slope, altitude and area which were important for the reliability of the model results.

## Conclusion

The ability of the HYPE in simulating hydrological response of a river basin has been assessed, in which based on manual calibration procedure and $R^2$ efficiency by Nash and Sutcliffe, the model simulated closely monthly hydrological response of the Saseni river catchment, a sub-catchment of the Mkomazi river basin in north-eastern Tanzania. The model captured the observed hydrograph, maintained the total volume and achieved the water balance. The constructed soil moisture availability maps can be useful for environment studies in the area.

The sensitivity analysis indicated that some input data were more sensitive than others. Rainfall had been the most sensitive parameter that influenced the total runoff followed by evapotranspiration and soil moisture. The sensitivity analysis also indicated that to some extent inadequacies in rainfall, evapotranspiration and soil moisture can be accommodated with the HYPE model without loss of the model performance.

It should be emphasized that it was not the aim of this study to explicitly validate the HYPE model for the Mkomazi river basin, but rather to use the model to explain the hydrological process responses and describe the vertical soil moisture availability in the area. However, because the model had the capability to explain the dynamics of the hydrological response for the Saseni catchment, with an ability to accommodate inadequacies in input data without loss of model performance, the HYPE can be applied for environment-related studies in the area.

# Chapter 5

# Modelling the Hydrological Response to Climate Change: a case study Mkomazi river basin in Tanzania

## Abstract

Implications of 21st century climate change on the hydrology of the Mkomazi river basin were assessed using a multimodel ensemble approach, in which downscaled and bias corrected output from seven General Circulation Models (GCMs) was used to drive the basin hydrology model. Downscaled climate ensembles concentrated for the period 2046–2065 were used as forcing to the Hydrological Predictions for Environment (HYPE) model. Ensembles of downscaled precipitation and temperature, and simulated riverflows were assessed through comparison with current simulations for the baseline period 1964–1983. All seven GCMs were forced under Special Report on Emissions Scenarios (SRES) A2.

All seven GCMs predict a warming in the Mkomazi river basin at Saseni catchment, but the amount of warming varied between the models. The predicted increases in the mean monthly maximum (minimum) temperatures, averaged over the seven ensembles, ranged from 1.72 to 2.11 °C (1.64 to 2.03 °C) and from 1.82 to 2.04 °C in mean temperature. Relative precipitation changes varied more between the models, and modest in the ensemble mean with increases of 3% in annual precipitation. An analysis of seasonal precipitation patterns showed an increase in November–April precipitation and a reduction in May–October precipitation. The mean ensemble runoff changes were mostly the result of precipitation changes, the annual riverflow predicted to increase by 7%, and by 5% (4%) for maximum (minimum) monthly riverflow. There were insignificant relative changes in soil moisture availability. However, soil moisture availability followed precipitation changes patterns predicted by the ensemble mean.

**Keywords:** A2 emission scenario, HYPE model, hydrological modelling, Mkomazi river basin, soil moisture.

## Introduction

The importance of water for humans and ecosystems accentuate the necessity of understanding how undesired effects of a changing climate could affect the variability of sub-regional hydrological responses. Changes in climate systems are shown by increases in global mean surface air temperature (Brohan et al., 2006; Hansen et al., 2006; Trenberth et al., 2007b) and vanishing glaciers (Thompson et al., 2002; Kaser et al., 2004). There is evidence that this has been caused by continuing increases emissions of greenhouse gases in the atmosphere, mostly due to human activities such as burning of fossil fuels (Glantz, 1992; Solomon et al., 2007). Increasing emissions of such gases in the atmosphere appear relatively uniform globally, but its feedbacks on climatic variables are unequally distributed (Hulme et al., 2001; Conway et al., 2007; Zorita et al., 2008; Shongwe et al., 2011). For example, Christensen et al. (2007) noted that the African continent is very likely to be warmer than the global annual mean warming, with drier subtropical regions warming stronger than the moister tropics. In addition, according to them, annual precipitation is likely to decrease over much of Mediterranean Africa and northern Sahara as well as to decrease in winter

precipitation over western-southern Africa, while annual mean precipitation is likely to increase in East Africa.

Climate change under enhanced greenhouse gases is likely to have potential implications both for human population and ecological processes in East Africa region. Previous studies showed that both extreme weather events of flood and drought (Behera et al., 1999; Hastenrath et al., 2007) brought disaster on the livelihoods of the people in the region. Precipitation is the main source of water for the terrestrial water cycle, and changes in precipitation patterns affect water availability and runoff directly, whereas changes in temperature, radiation and humidity have an effect on evapotranspiration. The latter removes water from surface (Jackson et al., 2001; Daly and Porporato, 2005) and thus has influence on soil moisture availability, which has in turn implications on crop productivity, particularly for rain-fed agriculture. Soil moisture availability and variability has been among the top challenges facing rain-fed agriculture in the East African region (Gowing et al., 2003; Mongi et al., 2010). To develop appropriate measures to adapt land uses to future climate change and its effects on soil water, it is necessary to downscale continent-wide climate change predictions to the landscape or catchment scale where most of these measures apply. Hydrological modelling at the catchment scale can make relevant contributions to foster downscaled predictions of soil water availability derived from global circulation models (GCMs.)

GCMs are governed by the fundamental laws of physics which describe the conservation of mass, energy and momentum. This solid physical basis gives a strong reason to believe that the models are a useful tool for exploring the behaviour of the climate system and its response to changes in external forcing such as increases in greenhouse gases. GCMs demonstrate significant skill for modelling the present climate and predict how the global climate may change in the future at continental spatial scales (Minville et al., 2008). Unfortunately large discrepancies exist between GCM datasets (Varis et al., 2004), especially for precipitation (Dai, 2006) the meteorological variable of utmost importance in hydrological processes. Because of the variance amongst GCMs ensembles, multimodel ensemble of GCMs has been combined to obtain reliable predictions (Murphy et al., 2004; Räisänen, 2007; Knutti et al., 2010).

Despite the progress in recent years in the modelling of hydrological response to the global climate change, the coarse-resolution of global circulation models is unable to represent local sub-grid scale features such as topography (Schulze, 1997; Wilby and Wigley, 1997; Fowler et al., 2007), which is a significant factor influencing hydrological responses in mountainous catchments. The gap between GCM resolution and regional or local-grid scales is narrowed by using downscaling techniques (Salathé, 2003; Varis et al., 2004; Diaz-Nieto and Wilby, 2005). Dynamical downscaling nests regional climate models (RCM) using initial conditions, observed lateral meteorological conditions derived from GCMs and surface boundary conditions to produce higher-resolution regional climate variables (Hostetler, 1994; von Storch et al., 2000; Cocke and LaRow, 2000; Hay et al., 2002; Samuelsson et al., 2003; Rummukainen, 2010). Computational demands has limited the application of dynamical downscaling techniques in some area, the need to downscale the results from RCM to individual catchment scales for impacts studies thus still remains (Wilby and Wigley, 1997;

Xu, 1999; Wood et al., 2004; Xu et al., 2005). Statistical downscaling has been developed as an alternative to dynamic downscaling to link the GCMs or RCMs with catchment-scale hydrological models, some examples include the studies by Müller-Wohlfeil et al. (2000), Wilby et al. (2000) and PWBO/IUCN (2010). Statistical downscaling techniques are computationally inexpensive. However, a drawback of statistical downscaling techniques is the assumption that predictor-predictand relationships remain unchanged in the future.

Hydrological modelling responses to climate change is now abounded at catchment-scale (Elshamy and Wheater, 2009; Sperna et al., 2010; Gosling et al., 2011). For example, Chiew et al. (2010) downscaled rainfall to assess the modelled runoff using the SIMHYD model (Chiew and McMahon, 2002) and compared – using rainfall and streamflow catchment data – the modelled changes in the future rainfall-runoff characteristics of unimpaired catchments in Australia; Todd et al. (2011) used a soil moisture balance model (SMBD) calibrated by Mileham et al. (2008) and a downscaled regional climate model to simulate hydrological responses to climate change in the Mitamo river basin in Uganda. Goulden et al. (2009) noted that adaptation and mitigation to climate change and accelerated development will normally be conducted at a river basin scale which requires the knowledge of hydrological responses to future climate change scenarios.

The present study aimed to simulate the hydrological responses in the Mkomazi river basin to global climate change from seven GCMs ensembles by PWBO/IUCN (2010). All seven GCMs were forced under an assumed SRES A2 scenario (Nakićenović et al., 2000), concentrated in the middle of the 21$^{st}$ century on the period 2046–2065. The SRES scenarios comprise six plausible global greenhouse gas emissions scenarios. With respect to temperature increases from warmest to coolest such scenarios are A1F, A2, A1B, B2, A1T and B1. The A2 scenario which corresponds to relatively unconstrained growth in greenhouse gases emissions was chosen for this study because it is the most widely simulated over many GCMs, and represents a plausible range of conditions over the 21$^{st}$ century. Also, in the middle of 21$^{st}$ century global climate changes are similar across most greenhouse gases emissions scenarios. SRES scenarios were replaced by Representative Concentration Pathways (RCPs) in the IPCC 5$^{th}$ assessment report (www.ipcc.ch/report/ar5/). Predictions based on RCPs were not yet available at the beginning of our study. The hydrological responses were simulated using the HYPE model (Lindström et al., 2010).

## Methods

*Input data and model setup*

To enable the simulation and assessment of the hydrological response to climate change in the Mkomazi river basin in particular for the Saseni catchment (river-gauge 1DB2A), past-present hydrological response was first validated (see Chapter 4). The simulated hydrological response (past-present or baseline conditions) suggested that the HYPE model adequately represented the hydrological response of the Saseni catchment across a range of both wet and dry period's climate conditions, such that it can be used to assess an impact of future climate scenarios.

The seven GCMs ensembles which produce the climate scenario used to assess the hydrological response to climate change of the Saseni catchment are summarized in Table 5.1. All seven GCMs were statistical downscaled and bias corrected, and simulates closely the climate (precipitation, minimum and maximum temperature) of the Saseni catchment for the control period 1960–2000 (present). Details of predictors, downscaled approach and bias correction are described by PWBO/IUCN (2010). Tables 5.2, 5.3 and 5.4 summarize the predicted changes in precipitation, and maximum and minimum temperatures, respectively. Precipitation changes were calculated as the ratio of the future change to control period whereas temperatures as an absolute changes. As such, daily precipitation for the period 2046–2065 (future) is calculated by multiplying baseline daily precipitation (mm $day^{-1}$) calculated in Chapter 4 with the respective monthly precipitation changes in Table 5.2.

Table 5.1. The seven GCMs used to downscale the climate for the 1960–2000 and 2046–2065

| GCM | IPCC Model I.D. | Modelling Group | Country |
|---|---|---|---|
| GCM1 | CGCM3.1 | Canadian Centre for Climate Modelling and Analysis | Canada |
| GCM2 | CNRM-CM3 | Centre National de Recherches Météorologiques | France |
| GCM3 | ECHAM5/MPI-OM | Max Planck Institute for Meteorology | Germany |
| GCM4 | GFDL-CM2.1 | Geophysical Fluid Dynamics Laboratory | USA |
| GCM5 | ECHO-G | Meteorological Research Institute of KMA, and Model and Data group | Germany/Korea |
| GCM6 | MRI-CGCM2.3.2 | Meteorological Research Institute | Japan |
| GCM7 | IPSL-CM4 | Institute Pierre Simon Laplace | France |

The predicted monthly reference evapotranspiration, $ET_{of}$ (mm $day^{-1}$), under climate variability for the period 2046–2065 in the Saseni catchment was calculated in ArcGIS using the Hargreaves and Samani (HS; 1985) method, which is defined as

$$ET_{of} = 0.0023 * 0.408 R_a (T_{fmean} + 17.8)\sqrt{T_{fmax} - T_{fmin}} \quad (5.1)$$

where $R_a$ is extraterrestrial radiation (MJ $m^{-2}$ $day^{-1}$), $T_{fmean}$ is the predicted future monthly mean temperature (°C), and $T_{fmax}$ ($T_{fmin}$) are the predicted future monthly maximum (minimum) temperatures (°C). Extra-terrestrial radiation ($R_a$) was modelled as in Chapter 3.

The predicted future monthly maximum temperatures, $T_{fmax}$ (°C), for the period 2046–2065 were calculated in ArcGIS as

$$T_{fmax} = T_b + c_f \quad (5.2)$$

where $T_b$ (°C) and $c_f$ (°C) are respectively, baseline monthly averaged maximum temperature maps values as in Chapter 3 and ensemble mean values in Table 5.3. Similarly, minimum baseline conditions and the ensemble mean values in Table 5.4 were used to calculate future monthly minimum temperatures ($T_{fmin}$). Future monthly mean temperatures, $T_{fmean}$ (°C), were then calculated by arithmetic means of maximum and minimum temperatures as

$$T_{fmean} = 0.5(T_{fmax} + T_{fmin}) \quad (5.3)$$

The constructed monthly averaged reference evapotranspiration maps ($ET_{of}$) for the future climate were divided by number of days to calculate averaged daily $ET_{of}$ (mm $day^{-1}$), and daily temperature (°C $day^{-1}$) was assumed to be uniform within the respective month, and then all climate variables were aggregated to 450x450 $m^2$, the same assumption and spatial-resolution used in the baseline conditions. Also, we used the optimized HYPE model parameters, soil moistures holding capacities and soil depth values as in Chapter 4 to assess the hydrological response of the ensemble mean for the period 2046–2065, through comparison with baseline hydrological response conditions for the period 1964–1983.

Table 5.2. The seven GCMs predicted mean fractional change in rainfall for each month in the Saseni catchment (1DB2A) for the period 2046–2065 relative to 1960–2000. Data were taken from PWBO/IUCN (2010).

| Month | GCM1 | GCM2 | GCM3 | GCM4 | GCM5 | GCM6 | GCM7 | GCM mean |
|---|---|---|---|---|---|---|---|---|
| January | 1.20 | 1.16 | 1.13 | 1.02 | 0.98 | 1.29 | 0.98 | 1.11 |
| February | 0.99 | 0.98 | 1.02 | 1.20 | 0.92 | 1.14 | 1.01 | 1.04 |
| March | 1.26 | 0.93 | 1.07 | 1.04 | 0.85 | 1.06 | 1.09 | 1.04 |
| April | 1.14 | 0.84 | 0.92 | 0.93 | 1.06 | 0.87 | 1.28 | 1.01 |
| May | 0.66 | 1.17 | 0.83 | 1.02 | 0.79 | 0.77 | 0.91 | 0.88 |
| June | 0.78 | 0.79 | 0.57 | 0.79 | 0.51 | 0.61 | 0.99 | 0.72 |
| July | 0.57 | 0.60 | 1.22 | 0.80 | 0.86 | 0.59 | 0.30 | 0.71 |
| August | 1.87 | 0.62 | 0.54 | 0.50 | 0.47 | 1.25 | 0.78 | 0.86 |
| September | 0.63 | 0.95 | 0.72 | 0.51 | 0.84 | 0.54 | 0.37 | 0.65 |
| October | 0.67 | 1.08 | 1.19 | 0.79 | 0.91 | 0.97 | 1.14 | 0.96 |
| November | 1.27 | 1.29 | 1.05 | 1.07 | 1.25 | 1.14 | 0.87 | 1.13 |
| December | 1.32 | 1.03 | 0.92 | 1.24 | 1.04 | 1.06 | 0.87 | 1.07 |

Table 5.3. The seven GCMs predicted mean absolute change in maximum temperature (°C) for each month in the Saseni catchment (1DB2A) for the period 2046–2065 relative to 1960–2000. Data were taken from PWBO/IUCN (2010).

| Month | GCM1 | GCM2 | GCM3 | GCM4 | GCM5 | GCM6 | GCM7 | GCM mean |
|---|---|---|---|---|---|---|---|---|
| January | 1.57 | 2.05 | 1.57 | 1.93 | 1.79 | 0.94 | 2.21 | 1.72 |
| February | 1.54 | 2.10 | 1.59 | 1.60 | 2.20 | 0.93 | 2.42 | 1.77 |
| March | 1.71 | 2.25 | 1.39 | 1.79 | 1.80 | 1.20 | 2.63 | 1.82 |
| April | 1.96 | 2.02 | 1.61 | 2.15 | 1.57 | 1.75 | 2.43 | 1.93 |
| May | 2.03 | 1.97 | 1.85 | 2.10 | 1.63 | 1.66 | 2.13 | 1.91 |
| June | 2.08 | 1.93 | 1.99 | 2.16 | 1.86 | 1.51 | 2.44 | 2.00 |
| July | 2.19 | 2.11 | 2.16 | 2.19 | 1.82 | 1.69 | 2.40 | 2.08 |
| August | 2.17 | 2.47 | 2.10 | 2.26 | 1.78 | 1.66 | 2.27 | 2.10 |
| September | 2.21 | 2.64 | 2.03 | 2.24 | 1.58 | 1.81 | 2.27 | 2.11 |
| October | 2.43 | 2.42 | 1.92 | 2.37 | 1.69 | 1.74 | 2.20 | 2.11 |
| November | 2.03 | 2.17 | 2.11 | 2.17 | 1.71 | 1.50 | 2.27 | 1.99 |
| December | 1.80 | 1.91 | 1.86 | 1.69 | 1.48 | 1.35 | 2.06 | 1.74 |

Table 5.4. The seven GCMs predicted mean absolute change in minimum temperature (°C) for each month in the Saseni catchment (1DB2A) for the period 2046–2065. Data were taken from PWBO/IUCN (2010).

| Month | GCM1 | GCM2 | GCM3 | GCM4 | GCM5 | GCM6 | GCM7 | GCM mean |
|---|---|---|---|---|---|---|---|---|
| January | 2.00 | 2.30 | 1.78 | 1.89 | 1.80 | 1.41 | 2.29 | 1.92 |
| February | 1.97 | 2.34 | 1.82 | 1.88 | 1.84 | 1.43 | 2.33 | 1.94 |
| March | 2.03 | 2.36 | 1.77 | 1.93 | 1.80 | 1.48 | 2.42 | 1.97 |
| April | 1.84 | 2.13 | 1.82 | 2.08 | 1.66 | 1.64 | 2.40 | 1.94 |
| May | 1.71 | 1.87 | 1.38 | 2.14 | 1.56 | 1.27 | 2.14 | 1.72 |
| June | 1.81 | 1.64 | 1.82 | 2.02 | 1.17 | 1.06 | 1.96 | 1.64 |
| July | 2.12 | 2.01 | 2.09 | 2.03 | 1.57 | 1.52 | 2.06 | 1.91 |
| August | 2.16 | 2.38 | 2.01 | 2.04 | 1.60 | 1.61 | 2.09 | 1.98 |
| September | 2.03 | 2.67 | 1.89 | 1.85 | 1.69 | 1.64 | 2.04 | 1.97 |
| October | 2.23 | 2.22 | 1.96 | 2.00 | 1.76 | 1.33 | 2.25 | 1.96 |
| November | 2.26 | 2.34 | 1.98 | 1.97 | 1.76 | 1.56 | 2.37 | 2.03 |
| December | 2.09 | 2.22 | 1.86 | 1.87 | 1.78 | 1.50 | 2.32 | 1.95 |

## Results

The ensemble mean predicted the increase of 1 to 13% in monthly precipitation for the period November–April and the decrease of 4 to 35% in May–October, and thus the wettest and driest weather conditions in the Saseni catchment for the period 2046–2065 are predicted to be in November and September, respectively (Fig. 5.1). Comparison relative to the baseline conditions in Chapter 4 showed that the annual precipitation predicted to increase by 3% in the ensemble mean, and by 26% in the ensemble highest, but it was predicted to decrease by 18% in the ensemble lowest (Tab. 5.5). Also, relative to this baseline conditions, the ensemble mean predicted the increase (decrease) in November–April (May–October) precipitation of 3%. The calculated mean monthly precipitation for the future conditions ranged between 30 mm (May–October) and 200 mm (November, December and April), with great differences in precipitation regimes between November–April and May–October periods (Fig. 5.5).

Averaged over the seven ensembles, the predicted increases in monthly maximum (minimum) temperature for the Saseni catchment ranged from 1.72 to 2.11 °C (1.64 to 2.03 °C), and of 1.94 °C (1.91 °C) annual warming (Figs. 5.2 & 5.3). The projected mean monthly temperature ranged from 13 °C in June–September to 29 °C in November, February and March (Fig. 5.6). Maximum and minimum temperatures ranged from 35.9 °C (February) to 21.2 °C (July–August) and from 4.5 °C (September) to 23 °C (November), respectively (Figs. 5.7 & 5.8). The predicted increases in monthly $ET_{of}$ relative to the baseline conditions was below 10% (Fig. 5.9), with higher changes for the dry season than rainy season.

The simulated hydrographs under the climate variability showed similar hydrograph patterns as that simulated in baseline conditions based on shape, timing of the peak, falling limbs and base-flow, particularly in the ensemble mean (Fig. 5.4). Riverflow is predicted to increase (in the ensemble mean) relative to the baseline conditions, except in May when it decreases by 2% (Tab. 5.6). The predicted increase in monthly riverflows ranged from 2% (April) to 21% (November). Also, the annual riverflow predicted to increase by 7%, and by 5% and 4% for maximum and minimum monthly riverflow, respectively (Tab.5.6). In baseline conditions, maximum riverflow was in December and minimum in September.

The predicted soil moisture availability changes relative to the baseline conditions, was substantially low, between -1 and +1% (Fig. 5.11). However, it followed changes in precipitation's patterns predicted by the ensemble mean, thus high (low) soil moisture availability is for the wet (dry) seasons, and soil moisture availability decreases in May.

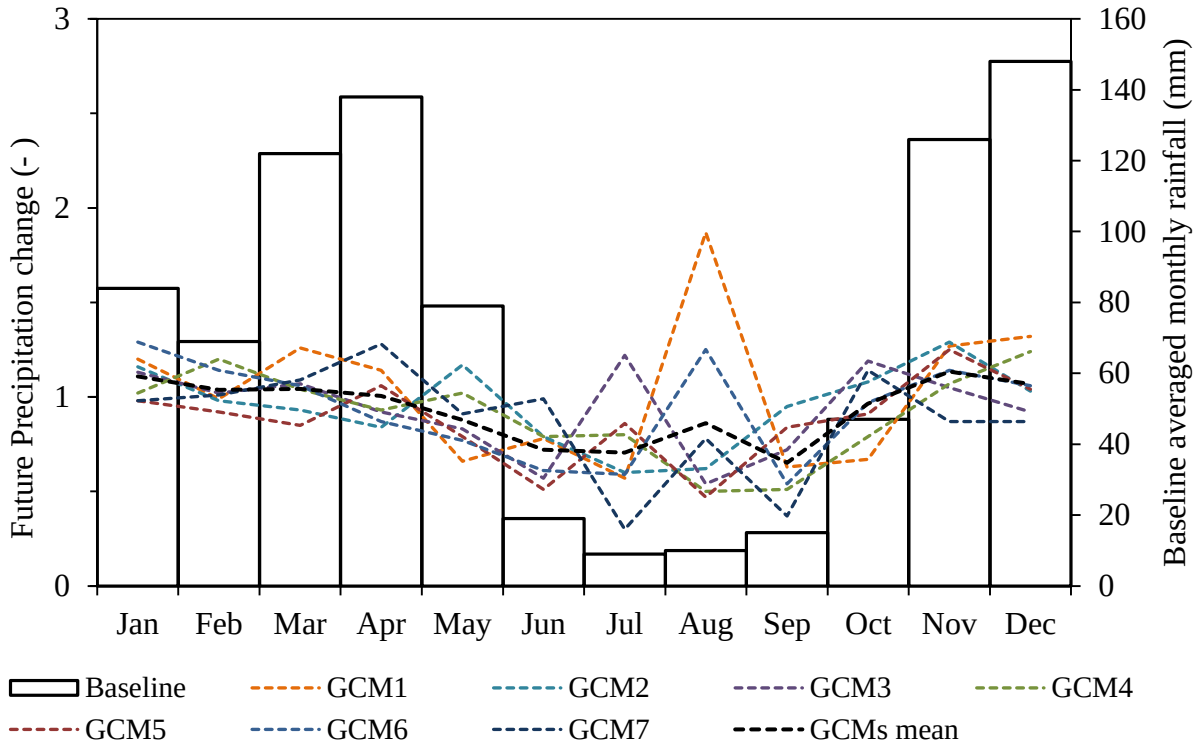


Figure 5.1. Predicted changes in monthly precipitation for the period 2046–2065 relative to the period 1960–2000 (data source: PWBO/IUCN, 2010) superimposed with Saseni catchment's (1DB2A) averaged-area monthly rainfall for the period 1964–2010.

Table 5.5. Impact of climate change on seasons' precipitation for the Saseni catchment (1DB2A) for the period 2046–2065, values in parentheses are relative to ensemble mean precipitation.

| Period | Baseline conditions (%) | GCM-highest (%) | GCM-lowest (%) | GCM-mean (%) |
|---|---|---|---|---|
| Annual mean precipitation change relative to baseline conditions | | +26 | −18 | +3 |
| May−October | +20 | +19 (+24) | +15 (+31) | +17 |
| November−April | +80 | +81 (+76) | +85 (+69) | +83 |

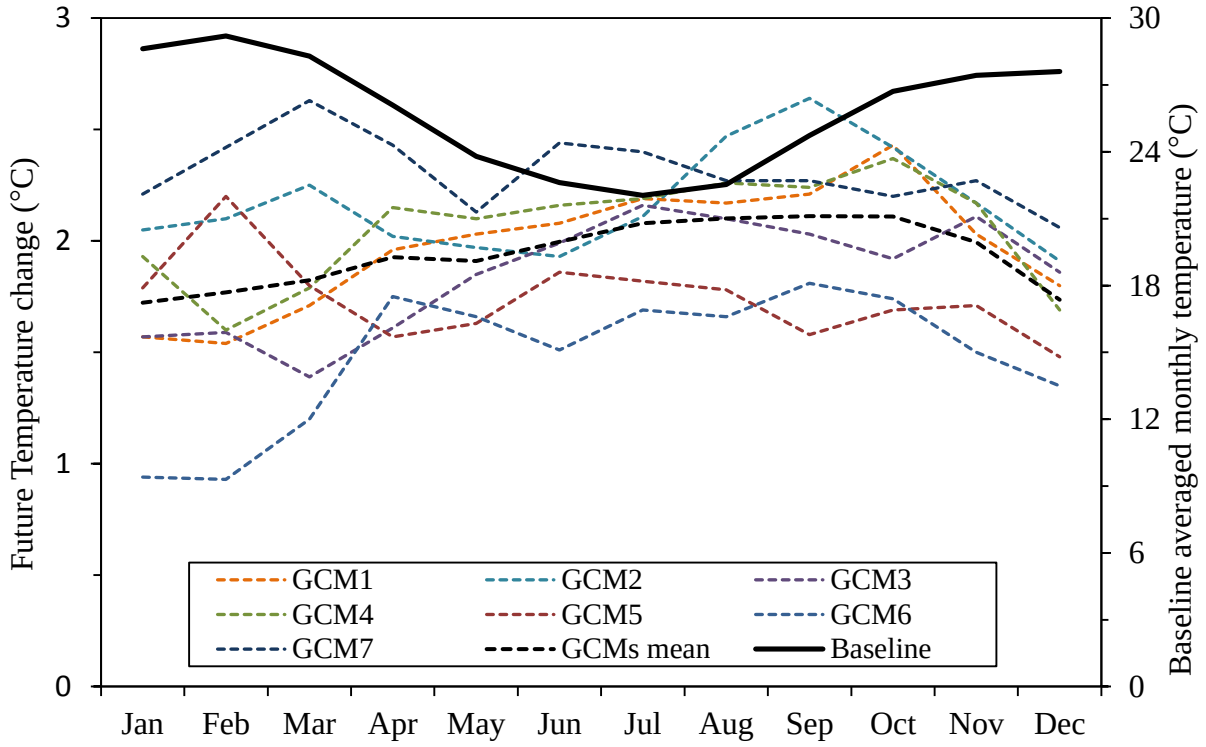


Figure 5.2. Predicted change in monthly maximum temperature for the period 2046–2065 (data taken from PWBO/IUCN, 2010) superimposed with Saseni catchment's (1DB2A) averaged-area monthly maximum temperature for the period 1964–2010.

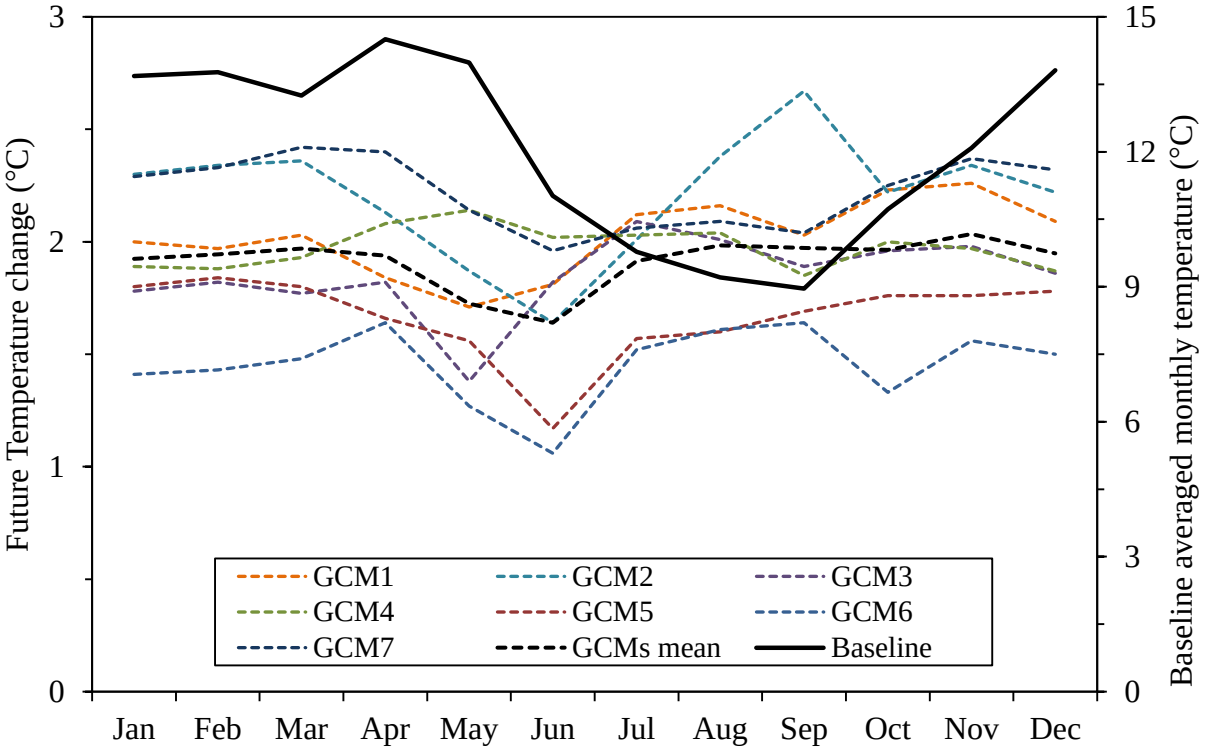


Figure 5.3. Predicted change in monthly minimum temperature for the period 2046–2065 (data taken from PWBO/IUCN, 2010) superimposed with Saseni catchment's (1DB2A) averaged-area monthly minimum temperature for the period 1964–2010.

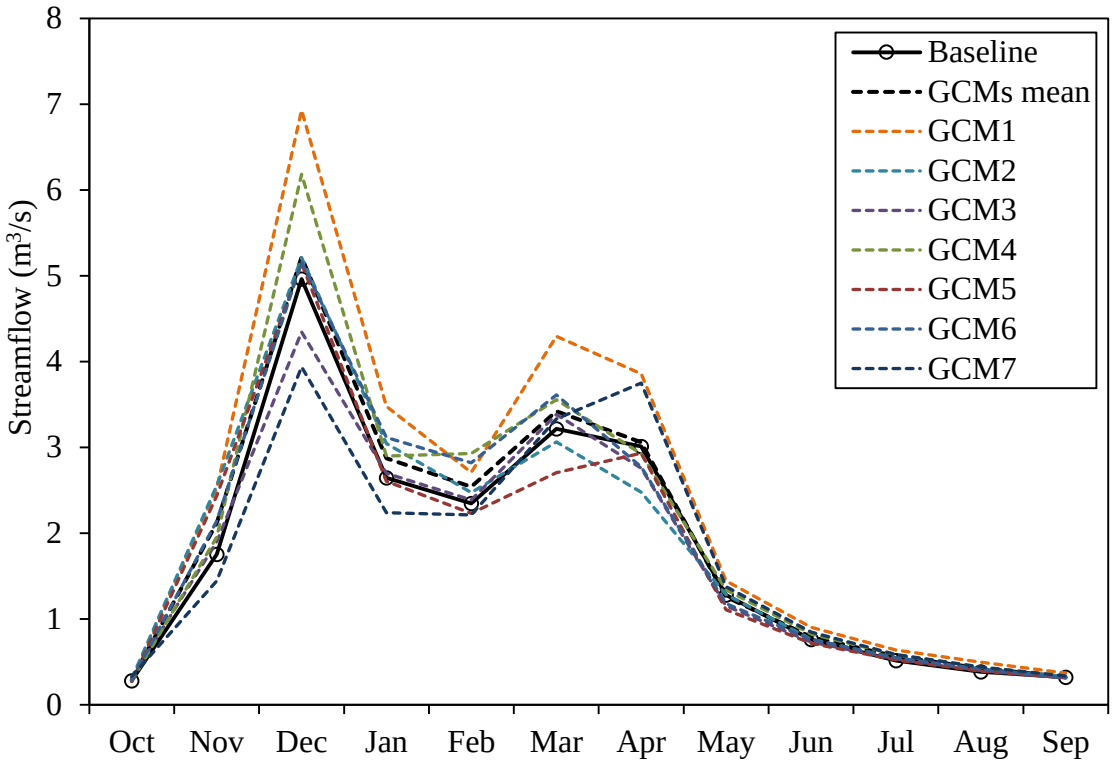


Figure 5.4. Monthly averaged hydrographs for simulated baseline conditions (period 1964–1983) and simulated effects of climate change for the period 2046–2065 on the Saseni catchment.

Table 5.6. Predicted impact of climate change (%) on riverflow for the Saseni catchment (1DB2A) for the period 2046–2065.

| Month | GCM1 | GCM2 | GCM3 | GCM4 | GCM5 | GCM6 | GCM7 | GCM mean |
|---|---|---|---|---|---|---|---|---|
| January | +32 | +15 | +2 | +10 | −1 | +18 | −15 | +9 |
| February | +15 | +5 | +2 | +25 | −5 | +20 | −6 | +8 |
| March | +34 | −5 | +5 | +11 | −16 | +12 | +4 | +6 |
| April | +28 | −18 | −8 | −3 | −3 | −8 | +25 | +2 |
| May | +13 | 0 | −10 | +5 | −14 | −8 | +8 | −2 |
| June | +19 | 0 | −4 | +8 | −6 | 0 | +11 | +4 |
| July | +24 | +5 | +3 | +13 | 1 | +6 | +14 | +9 |
| August | +29 | +5 | +4 | +13 | 2 | +8 | +15 | +10 |
| September | +16 | +4 | −3 | +4 | −2 | −2 | +5 | +2 |
| October | +4 | +9 | +13 | −2 | −4 | +3 | +18 | +4 |
| November | +44 | +46 | +8 | +12 | 39 | +22 | −18 | +21 |
| December | +40 | +5 | −12 | +25 | 4 | +4 | −21 | +5 |
| Annual flow | +30 | +5 | −3 | +13 | 0 | +8 | −3 | +7 |
| Minimum monthly flow | +4 | +9 | +10 | −2 | −4 | +3 | +18 | +4 |
| Maximum monthly flow | +40 | +5 | −12 | +25 | +4 | +4 | −21 | +5 |

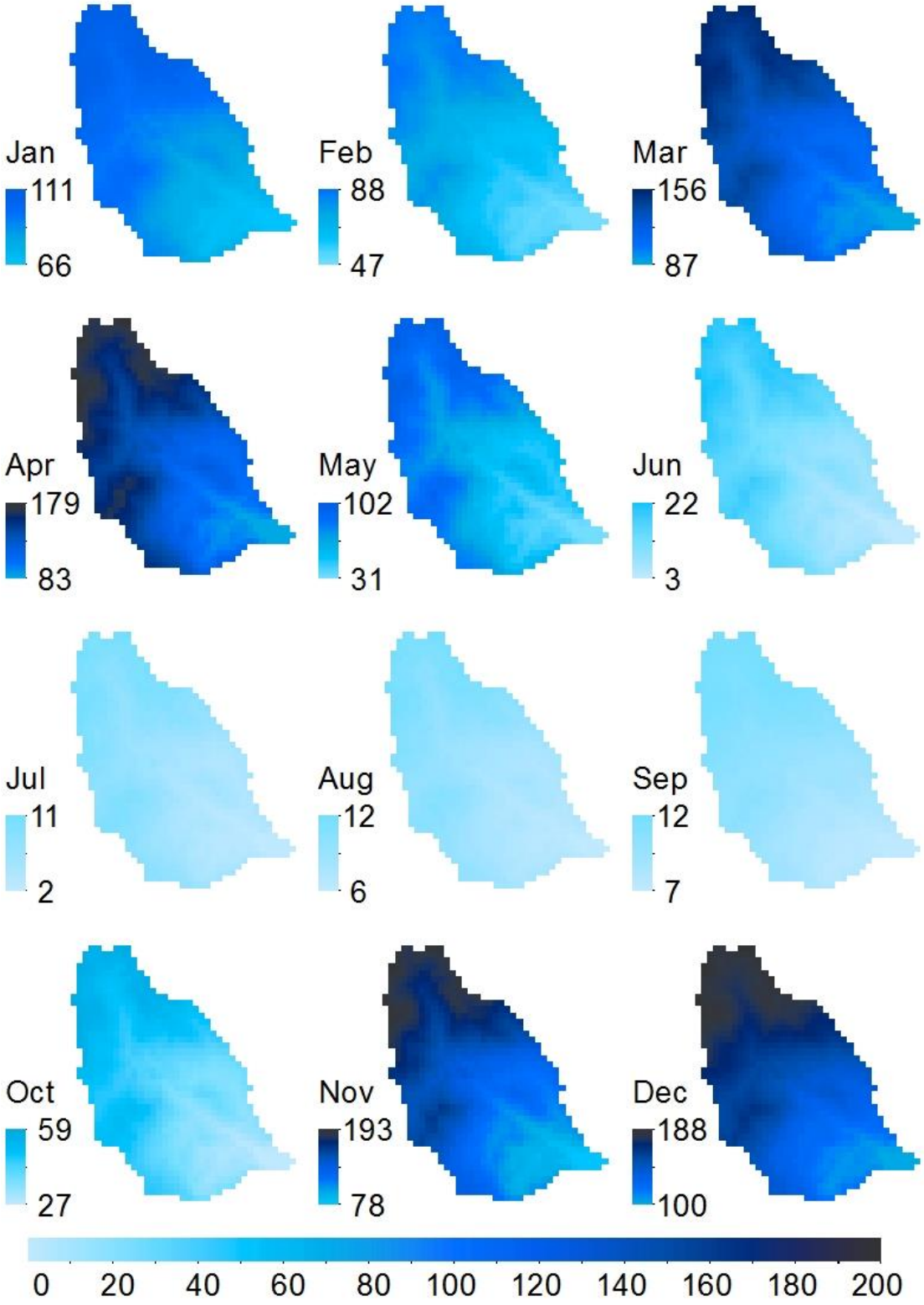


Figure 5.5. Monthly average precipitation (mm) calculated under the effects of climate change for the period 2046–2065 for the Saseni catchment.

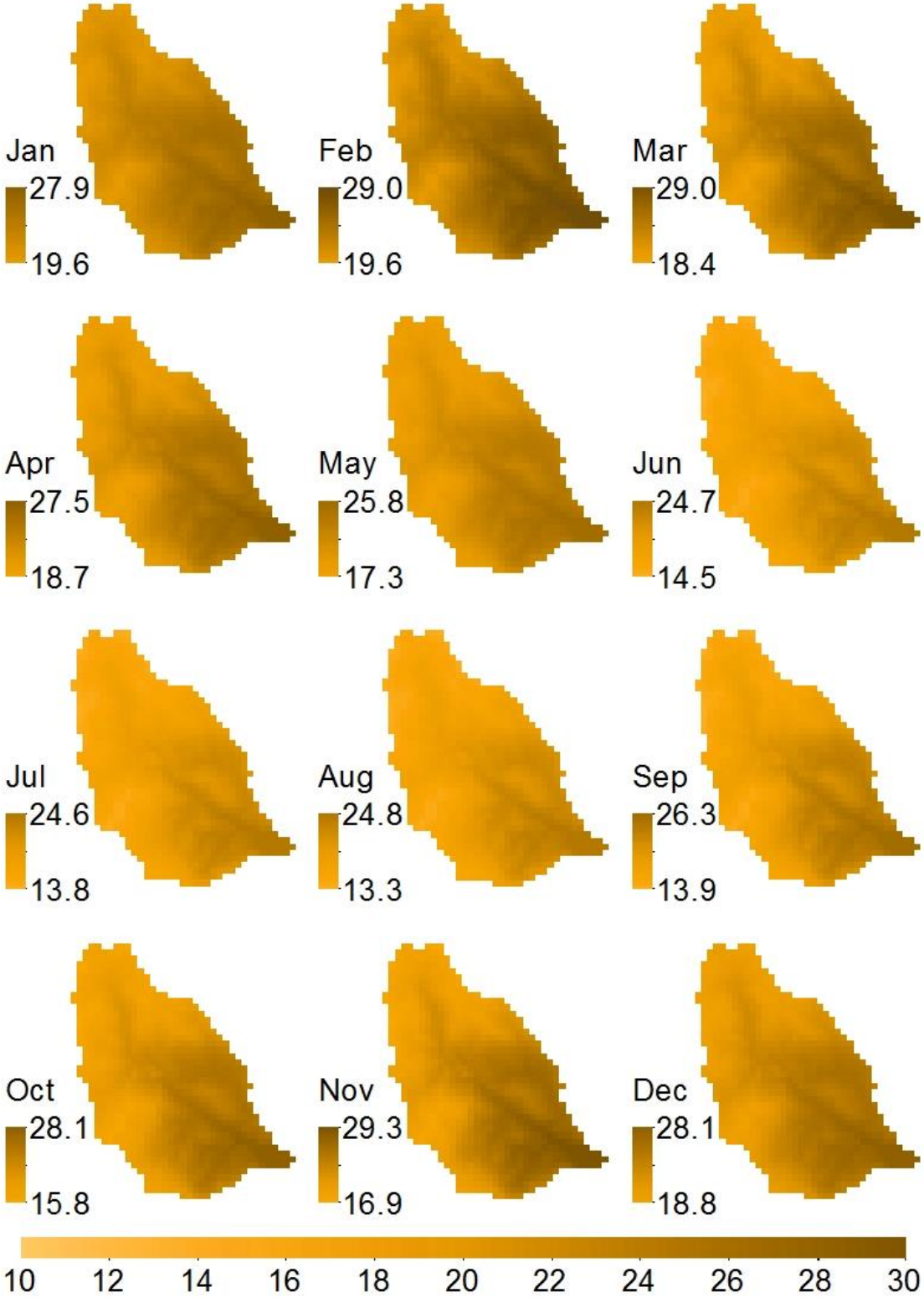


Figure 5.6. Monthly average mean temperature (°C) calculated under the effects of climate change for the period 2046–2065 for the Saseni catchment.

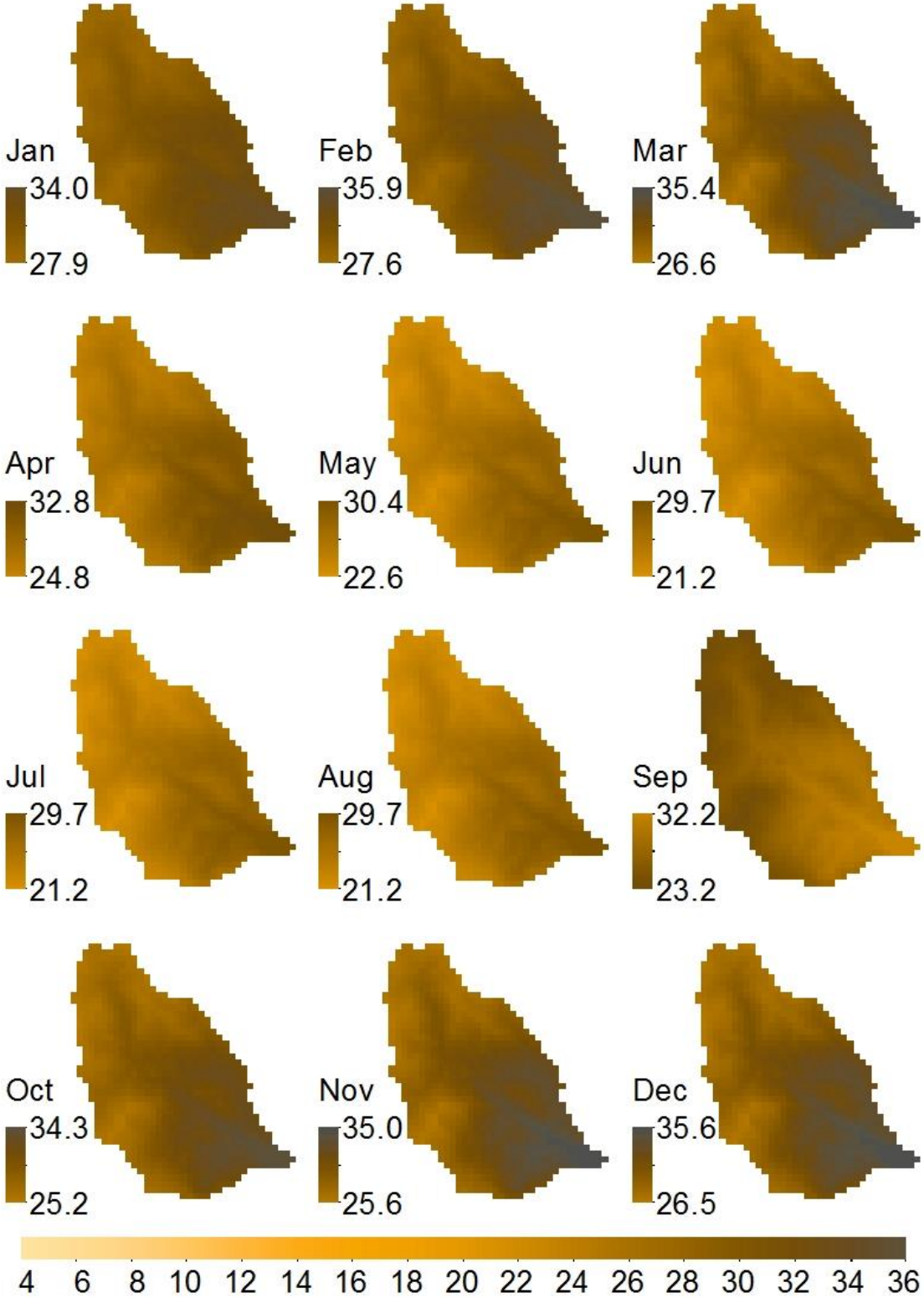


Figure 5.7. Monthly average maximum temperature (°C) calculated under the effects of climate change for the period 2046–2065 for the Saseni catchment.

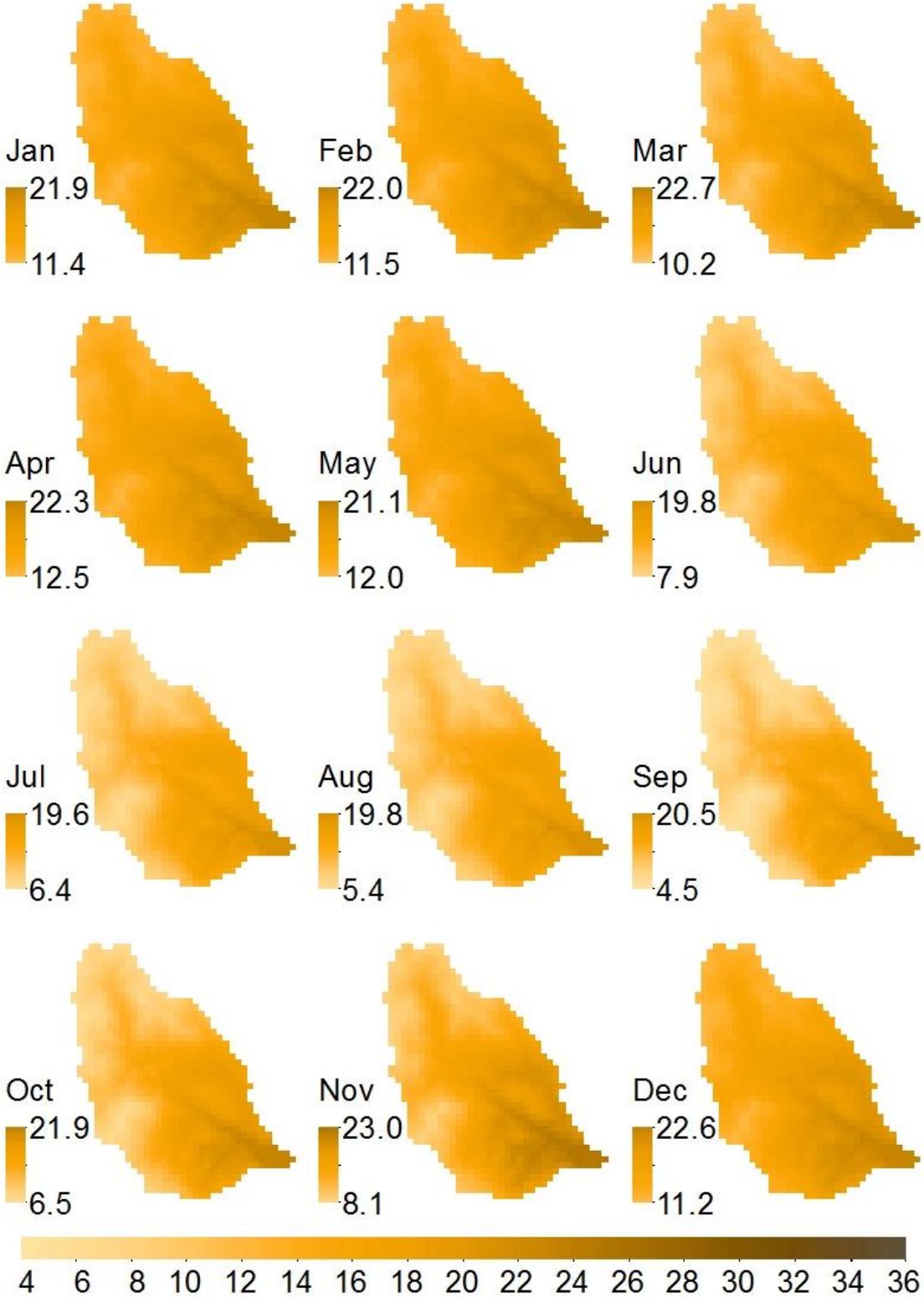


Figure 5.8. Monthly average minimum temperature (°C) calculated under the effects of climate change for the period 2046–2065 for the Saseni catchment.

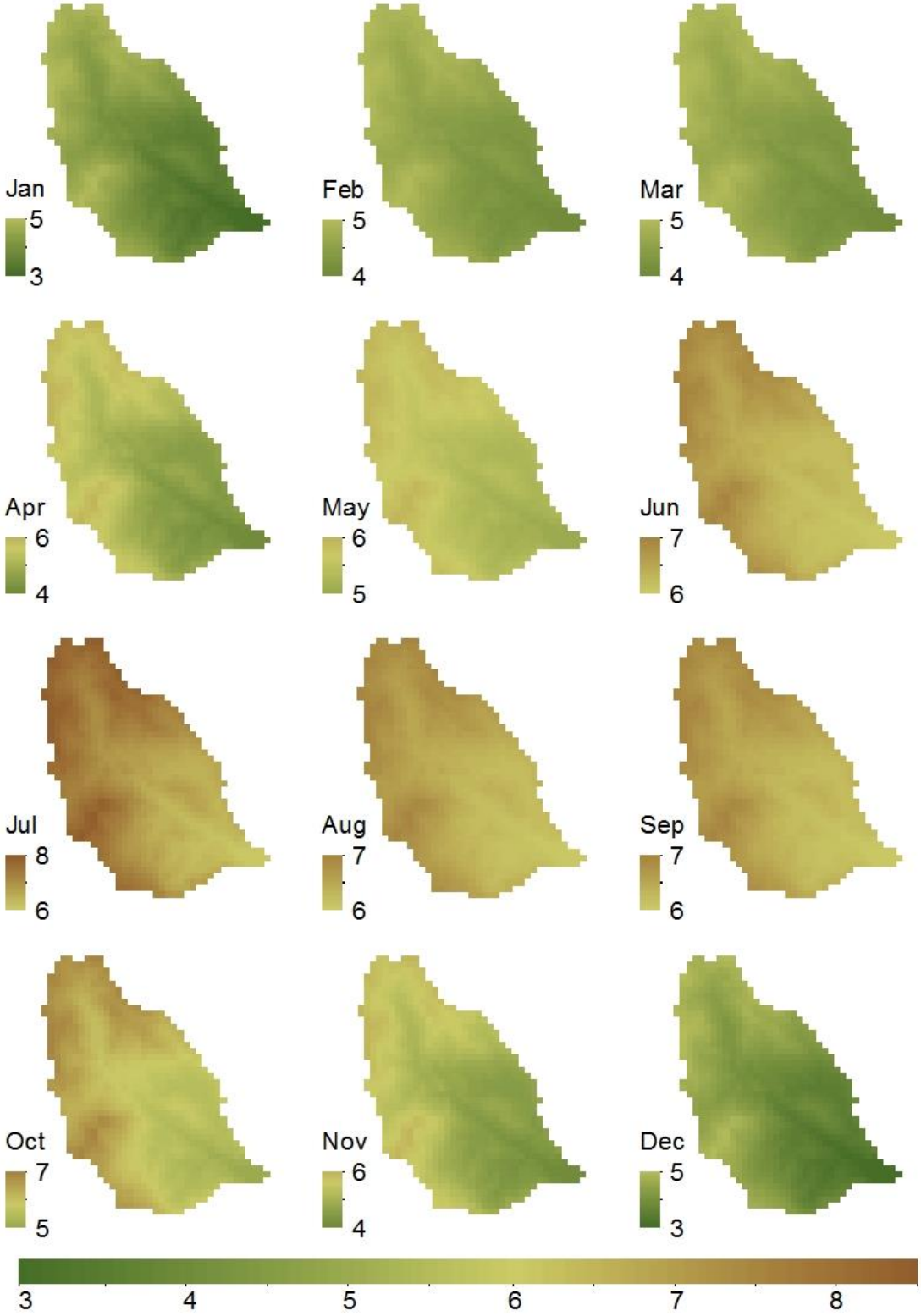

Figure 5.9. Predicted increases in monthly evapotranspiration (%) in the Saseni catchment for the period 2046–2065 relative to the baseline conditions.

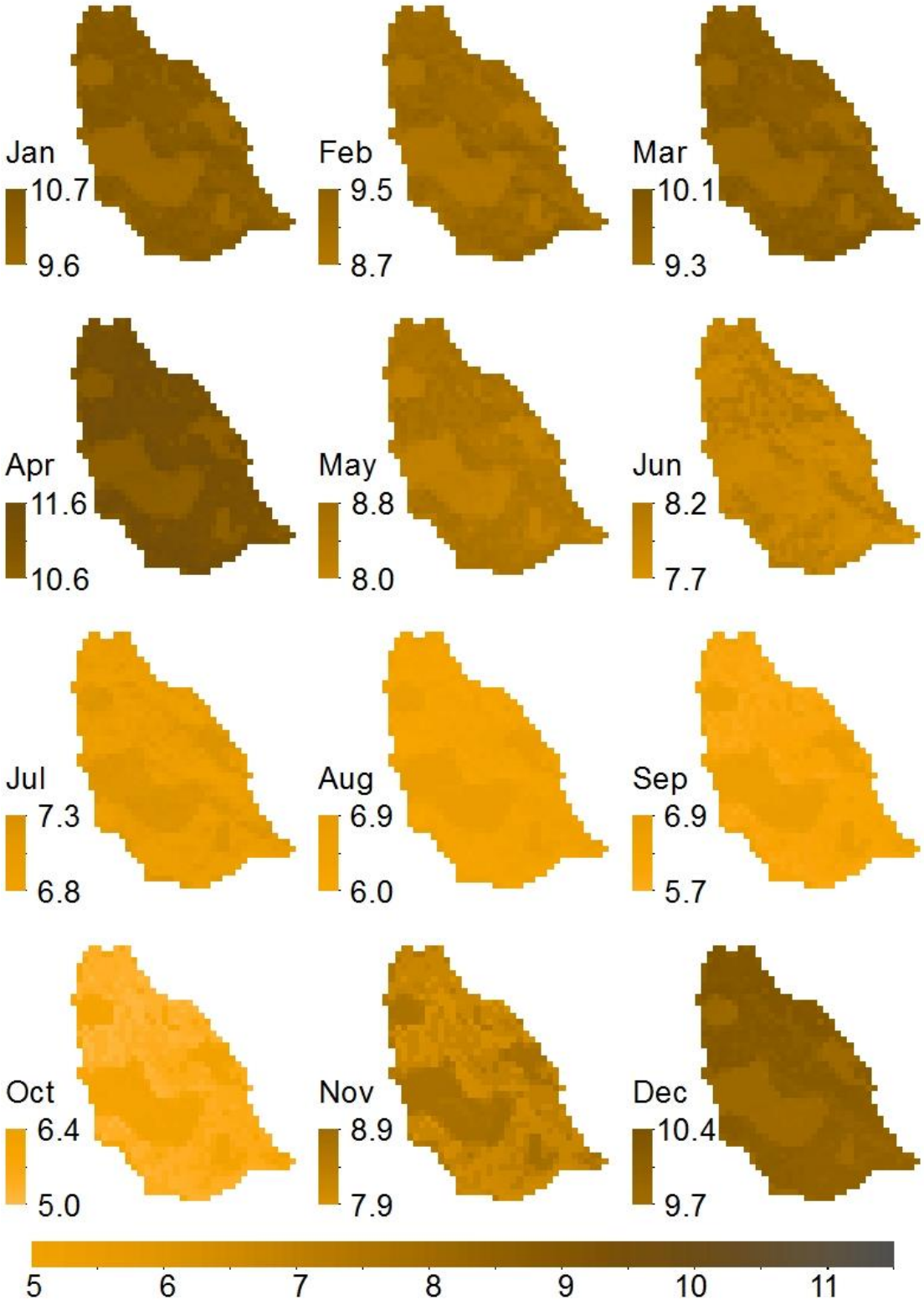

Figure 5.10. Monthly soil moisture availability (%) relative to annual soil moisture availability simulated for the period 2045–2065 for the Saseni catchment.

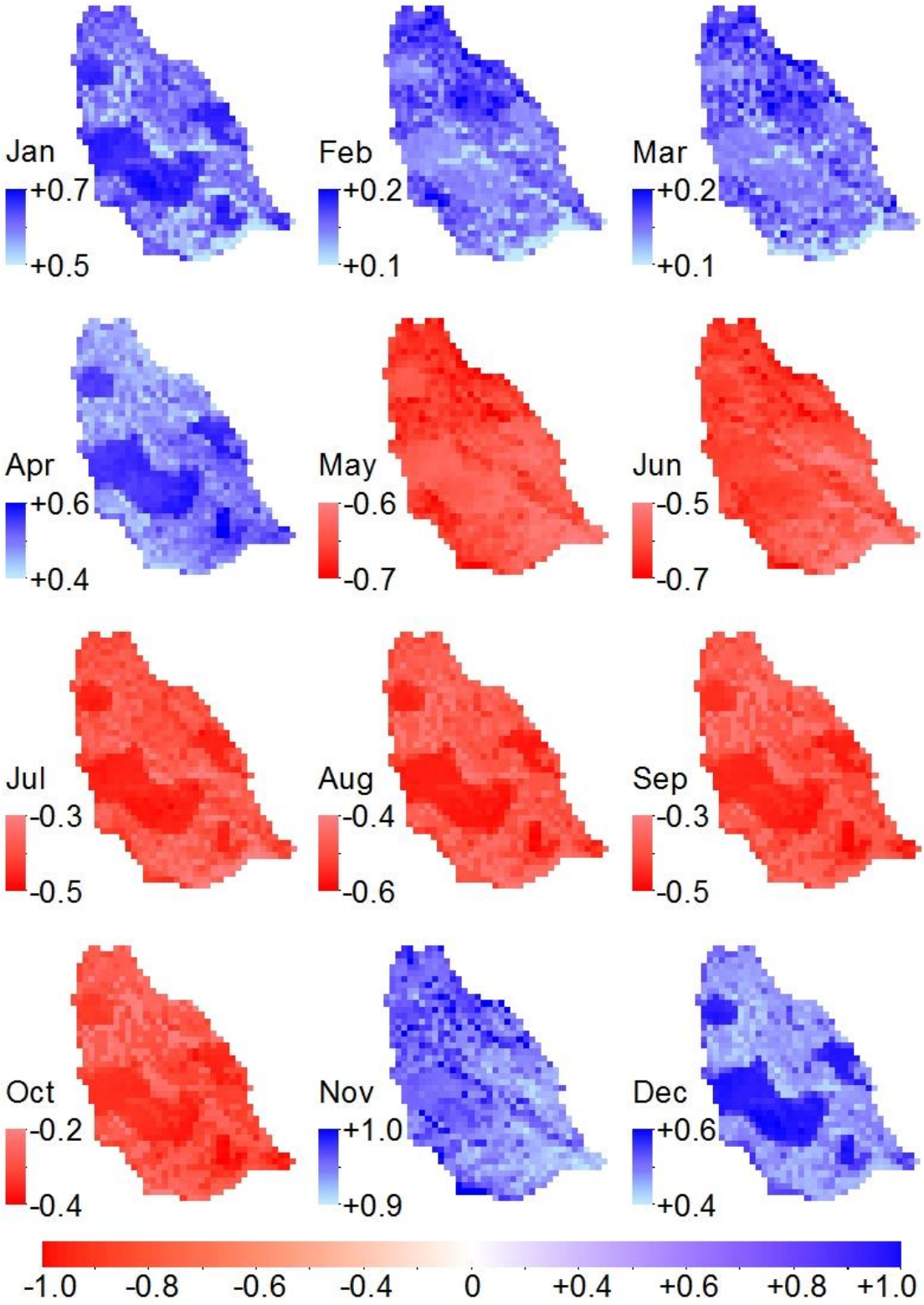


Figure 5.11. Predicted increases (blue) and decreases (red) in monthly soil moisture availability (%) in the Saseni catchment for the period 2045–2065 relative to the baseline conditions.

## Discussion

Monthly averaged changes in precipitation had a strong seasonal signal, with the increases in precipitation predicted for the period November–April and decreases for May–October. Although the ensemble mean predicted modest changes in precipitation, there is considerable variation in the changes predicted by the individual ensembles on a monthly basis. Note that the Saseni catchment climate is largely influenced by the climate systems of the East African region, with long-rains season mainly in March–May and short-rains season in October–December (Hastenrath et al., 1993; Mutai and Ward, 2000; Camberlin and Philippon, 2002). Therefore, although precipitation reductions in May and October are somewhat lower in comparison to the relative changes in June–September, their effects might shorten the long-rains season and lengthen the dry period before the onset of the short-rains.

Baseline simulation usually acts as a proxy for the real world system under baseline climate conditions (Nijssen et al., 2001). The HYPE model was forced with the observed temperatures and precipitation, and the observed and modelled hydrographs were compared (Chapter 4). The model captured well the hydrograph of the Saseni river catchment. As such, all changes in hydrological fluxes in the present study were calculated relative to the baseline simulation (see Chapter 4) rather than the historic observations. This allowed avoiding the effects of model bias (Todd et al., 2011). There is a large spread in the predicted hydrographs from most of the individual ensembles, particularly for the period November–April. Nevertheless, some general hydrograph patterns are apparent. The ensemble mean predicted modest increases in the annual and monthly maximum and minimum riverflows. Tropical river basin runoffs, if not regulated, generally do not show a change in the seasonal hydrographs other than a general wetting or drying, depending on whether changes in temperature and resulting increases in evapotranspiration are sufficient to offset the increases in precipitation (Nijssen et al., 2001).

The ensemble mean predicted warming for both maximum and minimum temperatures. The predicted minimum temperature is higher than the predicted maximum temperature for the period December–March, whereas the predicted maximum temperature is higher than the predicted minimum temperature for the period April–November. Higher increases in minimum temperature than in maximum temperature might intensify night's temperature, which in turn might increase a day temperature.

## Conclusion

Climate predictions from the ensemble mean of the seven GCMs, which were forced under the SRES A2 scenario, were used to assess the hydrological response in the Saseni river catchment in north-eastern Tanzania under global climate change. These GCMs were statistical downscaled and bias corrected, concentrated in the middle of 21$^{st}$ century for the period 2046–2065. All seven GCMs predicted a warming in the Saseni catchment, in which ensemble mean predicted higher warming in dry season. The ensemble mean predicted

modest changes in monthly precipitation, reference evapotranspiration and soil moisture availability. The ensemble mean also predicted modest increases in annual precipitation.

The hydrological responses were simulated using the HYPE model, which successful simulated the baseline hydrological response for the Saseni catchment. The predicted increases in the future annual riverflow and the maximum and minimum monthly riverflows were modest relative to the baseline hydrological conditions.

The hydrological response is driven by combined effects of temperature and precipitation changes and their seasonality. In the present study, hydrological simulation used a baseline model setup and parameters values which allowed avoiding the effects of model bias. The range of runoff changes across individual ensembles was quite large as expected. It is however likely that the spread in individual hydrological response reflects the effects of using the ensemble mean temperature across the individual GCMs ensembles. Nevertheless, there remains considerable variability in response associated with different GCMs and hydrological model, such that uncertainty in our predictions of the future mean river discharge and soil moisture availability is a topic of practical importance that deserve future attention.

# Chapter 6

# General Conclusions

## Introduction

This study is part of the Clim-A-Net, the North-South Network on Climate Proofing of Vulnerability Regions project at the University of Oldenburg in collaboration with University of Dar es Salaam (Tanzania) and Nelson Mandela Metropolitan University in Port Elizabeth (South Africa). The project aimed to facilitate an exchange of opinions between scientists, society and politicians, concerning global climate impacts and adaptation strategies. For the Tanzanian part, the Clim-A-Net project focused on the Pangani river basin. Particularly in the southern Mkomazi river basin which is among five major sub-catchments of the Pangani river basin in the north-eastern part of the country.

The main objective of this study was to simulate the hydrological response for the southern Mkomazi river basin to climate change. However, only hydrological responses for the Saseni river catchment, which is a sub-catchment of the southern Mkomazi river basin, have been simulated. The main reason for this was the availability of data, particularly riverflow data.

To assess the hydrological response of the Saseni catchment to global climate change, the hydrological response for the past-present or baseline conditions of the Saseni catchment was first simulated (Chapter 4). It was necessary to construct spatially distributed data for rainfall, temperature, solar radiation and reference evapotranspiration, which were input to the hydrological model. The modelling and construction of climate maps were accomplished for the southern Mkomazi river basin (Chapter 3). Hydrological response under the influence of global climate change in the middle of the 21$^{st}$ century for the Saseni catchment was then simulated (chapter 5). The baseline hydrological conditions (Chapter 4) and the predicted future hydrological conditions (Chapter 5) were compared and relative changes for the Saseni river catchment were then predicted or assessed.

## Conclusion

Computation capability enables constructions of climatic variables maps and hydrological modelling at local-scale or fine spatial-resolution. These climatic maps can be constructed using regression-based analysis, digital elevation models (DEM) and geographic information systems (GIS) techniques. This methodology was used to construct climate maps for the southern Mkomazi river basin, which were drawn on a monthly basis for rainfall, reference evapotranspiration, air temperature and solar radiation. In addition to this methodology, soil depth profile and soil moisture maps were constructed using in situ measurements of observation plots, in which soil moisture maps at field capacity, wilting point, effective porosity and percolation capacity were constructed.

Both rainfall- and temperature-elevation relationships showed a linear correlation form. However, this was not statistical significant for some months of the year. Particularly for rainfall in which the linear form was greater for the long-rains season than for the short-rains season. It is common in many elevated parts of the Earth for temperature-elevation linear

relationship to be stronger than for rainfall linear relationship with elevation, due to the lower spatiotemporal variability of temperature. However, based on the coefficients of determination ($R^2$), the linear correlation between temperature and elevation was very high. One of the reasons is the low number of temperature stations used to model maximum and minimum air temperature. These temperature stations were located in two contrasting altitudes, which support the linear form strongly. The constructed monthly temperature maps are useful for water resources studies, but when air temperature data across mountains ranges became available, air temperature models deserve improvements.

The rainfall distribution form for the southern Mkomazi river basin has not yet been achieved, particularly for the short-rains season, based on the coefficients of determination ($R^2$) shown by the rainfall-elevation models. This was pronounced when the station at the ridge was not included into rainfall-elevation relationship. The linear correlation form for the short-rains season was improved significantly for the windward side. In contrast, there were no significant changes in $R^2$ with or without the station at the ridge for the long-rains season. These findings widen a research window of spatiotemporally rainfall variability in this remote area of the equatorial East African region. In general, rainfall increases with elevation. However, this study has shown indirectly that elevation is not the only variable affecting rainfall distribution in the southern Mkomazi river basin, particularly for the short-rains season. The constructed rainfall maps are useful for water resources applications, and when meteorological data e.g. wind speed and direction became available, understanding of their effects may improve the rainfall models.

This study has demonstrated the distributed hydrological modelling approach, which enabled discretization of the terrain using DEM and simulated hydrological response for the Saseni river catchment successfully. For the baseline conditions, the HYPE model captured closely patterns of the observed riverflow hydrograph. Both for the calibration and validation periods, it was a suitable candidate model to assess hydrological response sensitivity to global climate changes for the Saseni catchment. The ensemble mean predicted modestly increases in the future annual riverflow, and the maximum and minimum monthly riverflows. There were insignificant relative changes, predicted by the ensemble mean, in soil moisture availability. However, soil moisture availability followed changes in precipitation's patterns predicted by the ensemble mean, which showed increases in soil moisture availability for the period November–April and decreases in May–October.

In addition to the shortcoming outlined for the mapped rainfall and temperature, modest changes predicted for the Saseni catchment for the period 2046–2065 can be due to:

- Spatiotemporally reference evapotranspiration ($ET_o$). Although the modelled monthly $ET_o$ values included effects of slopes and aspects, which are important factors affecting evapotranspiration in complex terrain, $ET_o$ values were assumed to be uniform throughout the respective month during the hydrological simulation. Clouds are common in mountains areas, and they have significant influence on solar radiations, which in turn has effects on $ET_o$ values. However, due to lack of sunshine hour data, clear sky conditions were assumed. In hydrological simulations, an error in input data propagates in a model

and influences the final result. This was pronounced during the sensitivity analysis of the model to the variation in the input data including evapotranspiration. Therefore, the constructed $ET_o$ maps are useful on a monthly basis, rather than for daily approximations.

- Soil depth profile. Soil observation plots were limited to one meter depth or below depending on the soil texture. Generally, this was due to the timeframe associated with limited resources. However, there were very few plots with more than one meter depth, mainly on mountains valleys and slopes close to the river. It was necessary – during hydrological simulation – to estimate the second soil layer depth, due to lack of the actual plant rooting depth. In other words, different second soil layers depth was obtained during hydrological simulation for the baseline conditions. Thin soil layers resulted into insignificantly changes in soil moisture availability between wet and dry seasons, whereas thick soil layers dried up the Saseni river during the dry season. Note that the second soil layer depth was obtained using manual calibration, and the same model parameters and soil depth layers were used to assess the effects of climate change on hydrology of the saseni catchment. Therefore, in addition to soil depths, these changes for the Saseni river catchment can be due to the manual calibration.

- Although manual calibration is often used in hydrological modelling, the method is subjective and it is impossible to know if an optimum obtained set of parameter is the only one that exists. Therefore, manual calibration should be used together with an automatic calibration, which can eliminate human subjectivity.

- Soil land-use classification (SLC). Land-use data, which is also termed land cover, was not available. However, based on our field observations, the Saseni catchment land cover was assumed to be uniform in the model, the only variations being soil textures. In hydrological modelling – particularly distributed hydrological modelling – land cover is usually an important input data in determining transpiration, interception-evaporation, stemflow, through-fall, uptake by roots, and infiltration and saturation excesses flows. Availability of present conditions land-use data and how it can change in the future could have strengthened hydrological modelling for the Saseni catchment.

Although climate variables for the southern Mkomatzi river basin were mapped successfully, hydrological response was simulated only for the Saseni catchment, in which hydrological responses changes were modest. Therefore, in addition to some parts of the southern Mkomazi river basin which have not yet been modelled, uncertainty in this study still remains a significant subject that merits future attention.

# Chapter 7

# Hydrological Sensitivity of the Mkomazi River Basin (Tanzania) to Climate Change: a Synthesis

## Introduction

The ability to simulate the earth climate at global scale has increased significantly. For example, the use of physically-based soil-vegetation-atmosphere-transfer (SVAT) schemes and flow routing models in general circulation models (GCMs). This enables simulations of vertical water flow and streamflow at each region of the earth (Dolman et al., 2001; Varis et al., 2004). In addition to advances in GCMs ability to simulate globe climate, many tools for recording climatic data have been developed e.g. (i) the moderate-resolution imaging spectroradiometer (MODIS), which estimates land-cover and vegetation indices since 2000, (ii) the European centre for medium range weather forecasts (ECMWF) reanalysis (also termed ERA-interim reanalysis), which estimates temperature, humidity and wind speed since 1979, and (iii) the satellite-based rainfall estimates (RFE) distributed by national oceanic and atmospheric administration (NOAA) since 1998.

Climatological data derived from these tools are usefully in areas of data scarcity. However, biases in satellite observations and coarse-resolution of global circulation models are unable to capture local sub-grid scale features as topography (Schulze, 1997; Wilby and Wigley, 1997), which is a significant factor influencing hydrological responses in mountainous catchments. In these catchments, rainfall characteristics e.g. orographic lifting, temperature patterns e.g. lapse rates, and topographic effects on solar radiation e.g. aspect are usually averaged out, either over- or under-estimated.

For hydrological modelling under global climate change, particularly at a local scale, GCMs predictions are usually downscaled. Downscaling procedure can either be dynamical (Hay et al., 2002; Samuelsson et al., 2003; Rummukainen, 2010) or statistical (Müller-Wohlfeil et al., 2000; PWBO/IUCN, 2010). Satellite observations are usually ‘trained’ or ‘bias corrected’ using gauge-station observations (PWBO/IUCN, 2010). Mountains hydrological and ecological systems are sensitive to climate variability (Beniston, 2003; Diaz et al., 2003), and an error in an estimate of climatological variables propagates in a hydrologic model and influence a final result. For that reason, it is important that errors and uncertainties in climatological data should be minimized. At a local scale, this can be achieved by increasing a network of climatological data.

The hydrology system of the southern Mkomazi river basin (in the Pangani river basin) merits attention, and has been explored in this thesis. The objectives of this study were (i) mapping monthly rainfall, air temperature, and evapotranspiration, (ii) modelling hydrological response (rainfall–runoff) for the past-present or baseline conditions, and (iii) modelling hydrological response to climate change concentrated for the period 2045–2065. Although the objectives had been achieved successfully, there are some essentials which lacked when mapping the climate variables and during the hydrological modelling. The drawbacks, which had to be done if data were available or which have to be done when data become available, are addressed in this synthesis.

## Methods

*Data*

The present study used two datasets. The first dataset (hereafter dataset1) includes: (i) monthly averages from 23 stations provided by Tanzania Meteorological Agency (TMA), and (ii) daily rainfall, temperature and riverflow from Pangani-NRM-version-2.0. The Pangani-NRM-version-2.0 consolidates climatological records collected from Tanzania Ministry of Water and Livestock Development, TMA, Pangani river basin district and regional offices and institutions. Daily riverflow records contained in the Pangani-NRM-version-2.0 is hereafter riverflow1.

Few meteorological stations, which were well distributed across the southern Mkomazi river basin, were used to construct the second dataset (hereafter dataset2). Dataset2 comprises daily records including: (i) rainfall, (ii) maximum and minimum temperatures, (iii) relative humidity, (iv) number of sunshine hour, and (v) incoming solar radiation. Most of the rainfall stations in dataset2 were called Type-B stations, in which accumulated rainfall was measured once a day. There were Type-A stations, where, in addition to accumulated daily precipitation, the three-hour observations of a weather code were available. The code is a measure of rainfall intensity, which was used to define the wind speed and wind direction during the precipitation event.

Observed riverflow records (hereafter riverflow2) were available (i) at the outlet of the Saseni (1DB2A) and Yangoma (1DB23) rivers, (ii) at the inlet and outlet of the Kalimawe dam, and (iii) at the outlet of the southern Mkomazi river (1DB6A) catchment (see Fig. 2.1 for the river-gauge locations).

Daily data in dataset2 and riverflow2 were recorded in recent years.

Spatiotemporally consistency of daily rainfall records (dataset2) were analysed followed the procedure similar to that described by Feng et al. (2004), in which (i) records were compared with predefined high extreme values such that in the absence of any reported storm event in the southern Mkomazi river basin, daily rainfall values above 100 mm were removed, (ii) the same rainfall values – in the integer part – for ten consecutive days in a month, they passed for outliers, and (iii) zero rainfall values – monthly sums – during the rainy season were outliers, if the monthly mean rainfall of the other stations was greater than 100 mm. Minimum and maximum temperatures (dataset2) were compared to ensure that minimum temperatures do not exceed maximum temperatures. Dataset1 was cleaned for outliers followed the traditional statistical method and a predefined standard deviation limit of 50% Z-score to pass for outlier. This was done for the period 1964–2010 (same as in Chapter 3).

Two land-cover maps for the southern Mkomazi basin were available: (i) for the naturalized period (see Chapter 2 for the naturalized flow) (hereafter landmap1), and (ii) for the current development (hereafter landmap2).

*Spatial interpolation of rainfall*

Usually wind speed and wind direction varied considerably during rainfall events. Therefore, the weather code from the Type-A stations was used to estimate average daily wind speed and direction. For the Type-B stations, wind speed and direction were assumed to be the same as at the nearest Type-A station. It was then assumed that the wind direction did not vary by more than 90° interval during the actual precipitation event.

Elevation data, digital elevation models at 90 m (www2.jpl.nasa.gov/srtm/) spatial-resolution, was resampled to a 450x450 $m^2$ gird mesh.

Precipitation events were divided into eight classes according to wind direction (i.e. N, NE, E, SE, S, SW, W, and NW). For wind speed, classes were selected after several statistical tests, and the best classification were obtained. For each class and station, the mean precipitation for the whole period of dataset2 was computed.

A distinction was made between the windward (ascending) and the leeward (descending) side of a mountain. As air starts to ascend some distance ahead of a mountain range, both the upwind and the downwind slope are important for the distribution of precipitation amounts (Smith, 1979; Smith and Barstad, 2004). The importance of upwind barriers or topographical effect is also emphasized in the studies by Bader and Roach (1977), Durran and Klemp (1982), Kuligowski and Barros (1999) and Roe (2005). There are two possible effects: (i) the gradual decrease in moisture content as the air passes over one or several mountain ranges, or (ii) the blocking of air by a nearby upwind barrier. Variables representing the ascent and descent of the air mass were selected on a theoretical and empirical basis. Only those that were assumed important for the distribution of precipitation amounts at a specific location under a specific wind conditions are listed in Table 7.1.

Table 7.1. Variables selected for statistical analysis if rainfall

| Variable | Description |
|---|---|
| V | Wind speed |
| SL.U1 (SL.U2) | Upwind slope ascending air (descending air) |
| SL.U1.V (SL.U2.V) | Upwind slope ascending air (descending air) multiplied by wind speed |
| SL.D1 (SL.D2) | Downwind slope ascending air (descending air) |
| SL.D1.V (SL.D2.V) | Downwind slope ascending air (descending air) multiplied by wind speed |
| ELV.450 | Elevation of 450x450 $m^2$ around rainfall station |
| ELV.R | Elevation of radius R $m^2$ around rainfall station |
| V.MRF | Wind speed multiplied by a mountain ranges factor |
| SL.D1.V.BRF | Downwind slope ascending air multiplied by windspeed and barrier factor |
| V = $V_E$ | Wind direction (equals $V_E$ for easterly winds) |
| V = $V_W$ | Wind direction (equals $V_W$ for westerly winds) |

Many approaches were tested to determine the upwind and downwind slope. The slope was then calculated as the difference in elevation between a radius (R) of few meters grid around the station and the weighted mean of a number of upwind or downwind pixels. This radius was selected such that a 450x450 $m^2$ was in the centre. The correlation between upwind slope and daily mean precipitation increased up to a certain upwind grids in the wind direction. On the other hand, the estimated slope depends on the elevation of the station grid.

The stepwise linear regression equation was used to select an optimal set of variables (topographical and wind effects) influencing the distribution of precipitation. The independent variables were added one at a time such that each variable raised the dimension of the equation by one. The independent variable, which provided the increases in the explained variance in precipitation, was stored at every dimension. It was decided to use variables that explained greater than 5% of the variance. The regression equation was then constructed, and daily rainfall was then modelled for the whole period of the dataset2 (hereafter dailyrainfall2). Also, monthly average rainfall maps (hereafter monthlyrainfall2) were constructed.

The regression equation variance explained by wind speed and direction both for ascending- and descending-air were used to adjust 'monthlyrainfall1' maps. Monthly rainfall1 maps are monthly rainfall maps, which were constructed for the period 1964–2010 using dataset1 assuming that rainfall distribution is influenced by orography and altitude only. In other words, monthlyrainfall1 are the same maps as in Chapter 3. Therefore, distributed 'dailyrainfall1' was also adjusted accordingly for the period 1964–1983. Dailyrainfal1 was calculated using monthly rainfall maps, and dataset1 monthly and daily stations rainfall records (see Chapter 4 for the method).

*Spatial interpolation of temperature and evapotranspiration*

Monthly maximum and minimum temperature ($T_{max1}$ and $T_{min1}$) were modelled by means of regression-based, DEM and GIS techniques using dataset1 and respective temperature maps were constructed.

Monthly maximum and minimum temperature ($T_{max2}$ and $T_{min2}$) were then calculated using dataset2. These were temperature values at stations' location of dataset2. Monthly maximum and minimum temperature variables 'X.MAX' and 'X.MIN' were introduced. Such that on a monthly basis $T_{max1}$ and $T_{min1}$ point or pixel temperature values at stations' location of dataset2 were equal to $T_{max2}$ and $T_{min2}$. These variables X.MAX and X.MIN were calculated for the whole record length of dataset2, and were averaged such that on a monthly basis 12 values were obtained for each station. The obtained relationships between the variables X.MAX and X.MIN with elevation were used to adjust $T_{max1}$ and $T_{min1}$ maps, respectively. As such, monthly maximum and minimum temperature maps ($T_{max}$ and $T_{min}$) for the southern Mkomazi river basin were then constructed. Monthly mean temperature maps ($T_{mean}$) were drawn by arithmetic mean of $T_{max}$ and $T_{min}$.

Global solar radiation ($R_{s1}$) was first modelled in ArcGIS followed the methodology described by Fu and Rich (2002). Monthly extraterrestrial radiations ($R_{a1}$) were then computed as a function of $R_{s1}$ (similar as Eq. 7.1), and respective maps constructed. Monthly extraterrestrial radiations ($R_{a2}$) were then calculated using dataset2. These were values at stations' location of dataset2, which were calculated as

$$R_{a2} = R_s/(a_s + b_s\frac{n}{N}) \quad (7.1)$$

where $R_s$ is incoming solar radiation, $a_s$ = 0.25 and $b_s$ = 0.50 (Allen et al., 1998), and N is maximum possible number of sunshine hour n.

Monthly extraterrestrial radiation variable 'X.RA' was then introduced, such that on a monthly basis $R_{a1}$ point or pixel radiation values at stations' location of dataset2 were equal to $R_{a2}$. This variable X.RA was calculated for the whole record length of dataset2, and was averaged such that on a monthly basis 12 values were obtained for each station. The obtained relationship between the variable X.RA with elevation was used to adjust $R_{a1}$ maps. As such, monthly extraterrestrial radiation maps ($R_a$) for the southern Mkomazi river basin were then constructed.

Monthly reference evapotranspiration were then calculated using Hargreaves and Samani equation, $ET_{o(HS)}$, which is defined as

$$ET_{o(HS)} = 0.0023 * 0.408R_a\,(T_{mean} + 17.8)\sqrt{T_{max} - T_{min}} \quad (7.2)$$

At this point, the constructed monthly reference evapotranspiration maps ($ET_{o(HS)}$) were not yet ready for applications in hydrological modelling. According to Hargreaves and Samani (1985) the coefficient 0.0023 (Eq. (7.2)) was obtained after fitted ($R_s/R_a$) versus ($T_{max} - T_{min}$). Therefore, the variable 'X.ETO' was introduced, which adjusted the coefficient 0.0023. Such that on a day or monthly basis $ET_{o(HS)}$ point or pixel evapotranspiration values at stations' location of dataset2 equal to evapotranspiration computed using Penman-Monteith equation, $ET_{o(PM)}$, in which according to Allen et al. (1998) it is defined as

$$ET_{o(PM)} = \frac{0.408\Delta(R_n - G) + \gamma\frac{900}{T_{mean1} + 273}U_2(e_1 - e_2)}{\Delta + \gamma(1 + 0.34U_2)} \quad (7.3)$$

where $\Delta$ is slope vapour pressure curve (kPa °C$^{-1}$), $R_n$ is net radiation at the crop surface (MJ m$^{-2}$ day$^{-1}$), G is soil heat flux density (MJ m$^{-2}$ day$^{-1}$), $\gamma$ is psychrometric constant (kPa °C$^{-1}$), $T_{mean1}$ is mean daily air temperature at 2 m height (°C), $U_2$ is wind speed at 2 m height (m s$^{-1}$), $e_1$ is saturation vapour pressure (kPa), and $e_2$ is actual vapour pressure (kPa). The coefficients in Eq. (7.3) were determined according to the procedure described by Allen et al. (1998) using dataset2 records. The variable X.ETO was calculated for the whole record length of dataset2, and was averaged such that on a monthly basis 12 values were obtained and 365 values were obtained on a daily basis. The obtained relationship between variable X.ETO with elevation (on a monthly basis) was used to adjust $ET_{o(HS)}$ maps using Eq. (7.2), and monthly reference evapotranspiration maps $ET_o$ for the southern Mkomazi basin were then constructed. Similarly, the obtained relationship between variable X.ETO with elevation (on a daily basis)

was used to construct daily $ET_o$ evapotranspiration maps (hereafter $ET_{oDaily1}$). In other words, if not averaged, $ET_{oDaily2}$ were constructed for the whole period of the dataset2.

*Hydrological modelling*

A flow network connecting sub-basins (450x450 $m^2$ pixels) from upstream to the outlet of the southern Mkomazi river basin was constructed followed the methodology described by Jenson and Domingue (1988). The distributed soil textures maps were constructed by means of regression-based analysis and the methodology described by Saxton and Rawls (2006), DEM, ArcGIS techniques and in situ measurements of observations plots (Petzold and Kleyer, [in prep.]) covering the most important soil features. These soil texture maps include: (i) soil moisture at field capacity, (ii) wilting point, (iii) effective porosity, and (iv) percolation capacity. Also, regression-based, DEM, ArcGIS techniques and these in situ measurements of observations plots were used to construct soil depth profiles. Soil depth was set to three layers, in which the thicknesses of the first and second soil layers were set according to the most dominant plant using landmap1. Hydrological response units (HRU) were constructed followed the methodology described by Flügel (1995). Soil textures and landmap1 were overlaid to construct HRU or soil-landuse-classification (SLC). Each SLC were assumed to be homogeneous with respect to soil, vegetation cover, slope, aspect, altitude, evapotranspiration and precipitation (hereafter SLC1). Similarly, soil textures and landmap2 were overlaid to construct SLC2.

The HYPE model was first calibrated manually using the parameters in Table 4.2 and 4.6. This was done for each catchment (Saseni and Yangoma), and the model performance efficiency or objective function $R^2$ (Nash and Sutcliffe, 1970) for the validation period was recorded. The model was then calibrated using an automatic procedure described by Lindström (1997). Furthermore, a Monte Carlo simulation (MCS) procedure for calibration and parameter analysis was applied. The MCS generated values randomly from uniform distributions within the parameter range given in Table 4.2 and 4.6. Each Monte Carlo simulation was set to 1000 runs. The parameter set which gave $R^2 \geq 0$ value over the calibration period was stored. Results from automatic and MCS calibrations were compared with those from manual calibration.

The sensitivity of the model to the variation in rainfall, evapotranspiration and soil moisture was analysed for the calibration period by increments of systematic errors in input data (same as in Chapter 4). In addition, parameter interdependence and sensitivity analysis using the results from the Monte Carlo simulation was done. This was achieved by (i) plotting frequency histograms for the parameter values using generalized likelihood uncertainty estimation (GLUE) methodology (Beven and Binley, 1992), and (ii) plotting the best model performance obtained over the full range of values for the individual parameter. The objective function $R^2$ (Nash and Sutcliffe, 1970) was used as the likelihood measure, consequently a dimensionless weight function $(R^2)^{-N}$, where N is number of parameter, was used. The resulting overlaid graphical plots showed where the good model performance was larger at an

interval of the parameter range, and the model performance sensitivity to the individual parameter.

The best obtained set or sets of parameters, which best simulated hydrological responses both for the Saseni and Yangoma catchments, were then used to simulate hydrological responses for other ungauged catchments. As such, the southern Mkomazi river basin was then hydrological modelled (hereafter baseline2). Note that baseline2 used (i) $ET_{oDaily2}$, (ii) dailyrainfall2, (iii) SLC2, and (iv) riverflow2.

The best obtained parameter set, which simulated baseline2, was then used to simulate the hydrological response for the southern Mkomazi river basin (hereafter baseline1) using (i) $ET_{oDaily1}$, (ii) dailyrainfall1, (iii) SLC1, and (iv) riverflow1. Baseline1 was then compared with baseline2.

The SRES A2 scenario (Nakićenović et al., 2000) and the ensemble mean of the seven global circulation models (GCMs) were used to simulate hydrological response under global climate change. These GCMs were statistical downscaled by PWBO/IUCN (2010) for the southern Mkomazi river basin for the period 2046–2065. Hydrological response was first simulated using landmap1 (hereafter future1), and then using landmap2 (hereafter future2). Baseline1 and future1 were then compared, similarly, baseline2 and future2 were compared.

*Outlook*

Type-B rainfall stations were read every day at 9 AM similar to the official meteorological stations in Tanzania, whereas Type-A were read automatically. Dataset2 spanned at least two years. The rainfall distribution regression equation included most of the variables listed in Table 7.1. The regression variance explained that rainfall increases with elevation for the long rains season. Wind speed and direction, particularly northeasterly and southwesterly winds, had significant influence on rainfall distribution for the short-rains season. The constructed monthly rainfall maps showed that the mountainous areas receive more rainfall than the valleys, whereas during the short-rains season (in November–December) the valleys receive rainfall amounts similar as on mountains. Monthly temperature maps showed that temperature decreases with elevation. The constructed evapotranspiration maps ($ET_o$) showed seasonal trend, with higher $ET_o$ values for the rainy season than for the dry season. Also, with lower $ET_o$ values in higher altitudes than lower altitudes. However, some slopes had greater $ET_o$ values than in plains for some months, due to seasonal variations in the position of the Sun.

All three calibration methods – manual, automatic, Monte Carlo simulation – produced a similar model performance quality, in terms of the objective function $R^2$ (Nash and Sutcliffe, 1970) and graphical plots of simulated and observed hydrographs. However, automatic and Monte Carlo methods had more than one optimum set of parameters. The parameter set frequency histograms overlaid with individual parameter showed that some parameters curves had strong variations across the full parameter range, whereas others had uniformly distributed curves over the full parameter range. The former indicated that good results were obtained for a certain range of parameter combinations intervals, whereas the latter is defined

as equifinality (Beven, 1993). The optimum sets of parameters showed transferability, such that hydrological responses for ungauged catchments of the southern Mkomazi river basin were simulated.

There were significant differences between baseline1 and baseline2 in terms of their hydrological responses. Likewise, it was the case between baseline1 and future1, and between baseline2 and future2. The trend analysis indicated hydrological response that might arise due to land-use changes and their effects due to global climate change, concentrated in the middle of 21$^{st}$ century for the period 2046–2065.

# Appendix

## List of Tables

## List of Figures

# References


Abbott, M. B., Bathurst, J. C., Cunge, J. A., O'connell, P. E., & Rasmussen, J. (1986). An introduction to the European Hydrological System—Systeme Hydrologique Europeen,"SHE", 2: Structure of a physically-based, distributed modelling system. *Journal of hydrology*, *87*(1), 61-77.

Adams, W.M., Potkanski, T., & Sutton, J.E.G. (994). Indigenous farmer-managed irrigation in Sonjo, Tanzania. The Geographical Journal, 160(1): 17-32.

Aguado, E., & Burt, J. E. (2001). *Understanding weather and climate.* 2nd ed. Prentice Hall, Upper Saddle River, New Jersey, USA, 505 pp.

Anderson, G. D. (1963). Soils of Tanganyika. *Ministry of Agriculture Bulletin No. 16*

Allen, R. G., Pereira, L. S., Raes, D., & Smith, M. (1998). FAO Irrigation and drainage paper No. 56. *Rome: Food and Agriculture Organization of the United Nations*, 26-40.

Alexandratos, N. (1999). World food and agriculture: outlook for the medium and longer term. *Proceedings of the National Academy of Sciences*, *96*(11), 5908-5914.

Andersson, L., Rosberg, J., Pers, B. C., Olsson, J., & Arheimer, B. (2005). Estimating catchment nutrient flow with the HBV-NP model: sensitivity to input data. *AMBIO: A Journal of the Human Environment*, *34*(7), 521-532.

Arheimer, B., Löwgren, M., Pers, B. C., & Rosberg, J. (2005). Integrated catchment modeling for nutrient reduction: scenarios showing impacts, potential, and cost of measures. *AMBIO: A Journal of the Human Environment*, *34*(7), 513-520.

Atkinson, P. M. (1997). Geographical information science. *Progress in Physical Geography* 21: 573–582.

Atkinson, S. E., Woods, R. A., & Sivapalan, M. (2002). Climate and landscape controls on water balance model complexity over changing timescales. *Water Resources Research*, *38*(12), 50-1.

Auer, I., Böhm, R., Jurković, A., Orlik, A., Potzmann, R., Schöner, W., ... & Mercalli, L. (2005). A new instrumental precipitation dataset for the greater alpine region for the period 1800–2002. *International Journal of Climatology*, *25*(2), 139-166.

Bader, M. J., & Roach, W. T. (1977). Orographic rainfall in warm sectors of depressions. *Quarterly Journal of the Royal Meteorological Society*, *103*(436), 269-280.

Bagnall, P. S. (1963). The geology of the north Pare mountains. *Bulletin of the Geological Survey of Tangayika*, *10*, 7-16.

Barros, A. P., & Lettenmaier, D. P. (1993). Dynamic modeling of the spatial distribution of precipitation in remote mountainous areas. *Monthly weather review*, *121*(4), 1195-1214.

Barry, R.G. (1992). *Mountain Weather and Climate.* 2nd edn, Routledge, London

Basist, A., Bell, G. D., & Meentemeyer, V. (1994). Statistical relationships between topography and precipitation patterns. *Journal of climate*, *7*(9), 1305-1315.

Bautista, F., Bautista, D., & Delgado-Carranza, C. (2009). Calibration of the equations of Hargreaves and Thornthwaite to estimate the potential evapotranspiration in semi-arid and subhumid tropical climates for regional applications *Atmósfera*, 22 (4), 331–348

Becker, A. (1992). Criteria for a hydrologically sound structuring of large scale land surface process models. In: O'Kane, J.O.P. (Ed.), Advances in Theoretical Hydrology. Elsevier, Amsterdam, pp. 97–111.

Becker, A., & Braun, P. (1999). Disaggregation, aggregation and spatial scaling in hydrological modelling. *Journal of Hydrology*, *217*(3), 239-252.

Begert, M., Schlegel, T., & Kirchhofer, W. (2005). Homogeneous temperature and precipitation series of Switzerland from 1864 to 2000. *International Journal of Climatology*, *25*(1), 65-80.

Behera, S. K., Krishnan, R., & Yamagata, T. (1999). Unusual ocean-atmosphere conditions in the tropical Indian Ocean during 1994. *Geophysical Research Letters*, *26*(19), 3001-3004.

Behera, S. K., Luo, J. J., Masson, S., Delecluse, P., Gualdi, S., Navarra, A., & Yamagata, T. (2005). Paramount impact of the Indian Ocean dipole on the East Africa short rains: a CGCM study. *J Clim* 18:4514–4530

Beniston, M. (2003). Climatic change in mountain regions: a review of possible impacts. In *Climate Variability and Change in High Elevation Regions: Past, Present & Future* (pp. 5-31). Springer Netherlands.

Bergström, S. (1976). Development and application of a conceptual runoff model for Scandinavian catchments. SMHI Reports RHO, No. 7, Norrköping.

Bergström, S. (1991). Principles and confidence in hydrological modelling. *Nord. Hydrol.*, *22*(2), 123-136.

Bergström, S., & Graham, L. (1998). On the scale problem in hydrological modelling. *Journal of Hydrology*, *211*(1), 253-265.

Beven, K. J., & Kirkby, M. J. (1979). A physically based, variable contributing area model of basin hydrology/Un modèle à base physique de zone d'appel variable de l'hydrologie du bassin versant. *Hydrological Sciences Journal*, *24*(1), 43-69.

Beven, K. J., Kirkby, M. J., Schofield, N., & Tagg, A. F. (1984). Testing a physically-based flood forecasting model (TOPMODEL) for three UK catchments. *Journal of Hydrology*, *69*(1), 119-143.

Beven, K., Calver, A., & Morris, E. M. (1987). The Institute of Hydrology Distributed Model (IHDM). *Rep. 98, Institute of Hydrology, Wallingford.*

Beven, K. (1989). Changing ideas in hydrology—the case of physically-based models. *Journal of hydrology*, *105*(1), 157-172.

Beven, K., & Binley, A. (1992). The future of distributed models: model calibration and uncertainty prediction. *Hydrological processes*, *6*(3), 279-298.

Beven, K. (1993). Prophecy, reality and uncertainty in distributed hydrological modelling. *Advances in Water resources*, *16*(1), 41-51.

Beven, K. J. (2001). *Rainfall-runoff modelling: the primer*. John Wiley & Sons.

Binley, A., & Beven, K. (2003). Vadose zone flow model uncertainty as conditioned on geophysical data. *Groundwater*, *41*(2), 119-127

Birkett, C., Murtugudde, R., & Allan, T. (1999). Indian Ocean climate event brings floods to East Africa's lakes and the Sudd Marsh. *Geophys. Res. Lett.*, 26, 1031–1034.

Bjørndalen, J. E. (1992). Tanzania's vanishing rain forests—assessment of nature conservation values, biodiversity and importance for water catchment. *Agriculture, Ecosystems & Environment*, *40*(1), 313-334.

Black, E., Slingo, J., & Sperber, K. R. (2003). An observational study of the relationship between excessively strong short rains in coastal East Africa and Indian Ocean SST. *Mon. Wea. Rev.*, 131, 74–94.

Blaney, H.F., & Criddle, W.D. (1950). Determining Water Requirements in Irrigated Areas from Climatological and Irrigation Data, USDA SCSTP-96. U.S. Department of Agriculture, Washington, DC.

Blöschl, G., & Sivapalan, M. (1995). Scale issues in hydrological modelling: a review. *Hydrological processes*, *9*(3-4), 251-290.

Boyle, D. P., Gupta, H. V., & Sorooshian, S. (2000). Toward improved calibration of hydrologic models: Combining the strengths of manual and automatic methods. *Water Resources Research*, *36*(12), 3663-3674.

Brady, N. C. (1990). *The Nature and Properties of Soils*. New York: Macmillian. 621 pp.

Brohan, P., Kennedy, J. J., Harris, I., Tett, S. F., & Jones, P. D. (2006). Uncertainty estimates in regional and global observed temperature changes: A new data set from 1850. *Journal of Geophysical Research: Atmospheres (1984–2012)*, *111*(D12).

Brunetti, M., Maugeri, M., Monti, F., & Nanni, T. (2006). Temperature and precipitation variability in Italy in the last two centuries from homogenised instrumental time series. *International Journal of Climatology*, *26*(3), 345-381.

Buytaert, W., Celleri, R., Willems, P., De Beivre, B., & Wyseure, G. (2006). Spatial and temporal rainfall variability in mountainous areas: A case study from the south Ecuadorian Andes. *Journal of Hydrology* 329, 413–421

Burrough, P. A., & McDonnell, R. A. (1998). *Principles of Geographical Information Systems*, Oxford University Press, New York, USA.

Camberlin, P., & Philippon, N. (2002). The East African March-May rainy season: Associated atmospheric dynamics and predictability over the 1968-97 period. *Journal of Climate*, *15*(9), 1002-1019.

Carvalho, F. P. (2006). Agriculture, pesticides, food security and food safety. *environmental science & policy*, *9*(7), 685-692.

Cassman, K. G. (1999). Ecological intensification of cereal production systems: Yield potential, soil quality, and precision agriculture. *Proceedings of the National Academy of Sciences*, *96*(11), 5952-5959.

Chapman, L., & Thornes, J. E. (2003). The use of geographical information systems in climatology and meteorology. *Progress in physical geography*, *27*(3), 313-330.

Chiew, F. H., & McMahon, T. A. (2002). Modelling the impacts of climate change on Australian streamflow. *Hydrological Processes*, *16*(6), 1235-1245.

Chiew, F. H. S., Kirono, D. G. C., Kent, D. M., Frost, A. J., Charles, S. P., Timbal, B., ... & Fu, G. (2010). Comparison of runoff modelled using rainfall from different downscaling methods for historical and future climates. *Journal of Hydrology*, *387*(1), 10-23.

Christensen, J. H., Hewitson, B., Busuioc, A., Chen, A., Gao, X., Held, I., Jones, R., Kolli, R. K., Kwon, W. T., Laprise, R., Magaña R. V., Mearns, L., Menéndez, C. G., Räisänen, J., Rinke, A., Sarr, A., & Whetton, P. (2007). Regional Climate Projections. In: *Climate Change 2007: The Physical Science Basis.* Contribution of Working Group I to the Fourth Assessment Report of the Intergovernmental Panel on Climate Change

[Solomon, S., Qin, D., Manning, M., Chen, Z., Marquis, M., Averyt, K. B., Tignor, M., & Miller, H. L. (eds.)]. Cambridge University Press, Cambridge, United Kingdom and New York, NY, USA.

Clark, C. O., Webster, P. J., & Cole, J. E. (2003). Interdecadal variability of the relationship between the Indian Ocean zonal mode and East African coastal rainfall anomalies. *Journal of Climate*, *16*(3), 548-554.

Clarke, R. T. (1973). A review of some mathematical models used in hydrology, with observations on their calibration and use. *Journal of hydrology*, *19*(1), 1-20.

Cocke, S., & LaRow, T. E. (2000). Seasonal predictions using a regional spectral model embedded within a coupled ocean-atmosphere model. *Monthly Weather Review*, *128*(3), 689-708.

Collier, C. G. (1975). A representation of the effects of topography on surface rainfall within moving baroclinic disturbances. *Quarterly Journal of the Royal Meteorological Society*, *101*(429), 407-422.

Conte, C. A. (1999). The forest becomes desert: Forest use and environmental change in Tanzania's West Usambara mountains. *Land Degradation & Development*, *10*(4), 291-309.

Conway, D., Hanson, C. E., Doherty, R., & Persechino, A. (2007). GCM simulations of the Indian Ocean dipole influence on East African rainfall: Present and future. *Geophysical research letters*, *34*(3).

Dai, A. (2006). Precipitation characteristics in eighteen coupled climate models. *Journal of Climate*, *19*(18), 4605-4630.

Daly, C., Neilson, R. P., & Phillips, D. L. (1994). A statistical-topographic model for mapping climatological precipitation over mountainous terrain. *Journal of applied meteorology*, *33*(2), 140-158.

Daly, E., & Porporato, A. (2005). A review of soil moisture dynamics: from rainfall infiltration to ecosystem response. *Environmental engineering science*, *22*(1), 9-24.

de Fraiture, C., Wichelns, D., Rockström, J., Kemp-Benedict, E., Eriyagama, N., Gordon, L. J., Hanjra, M. A., Hoogeveen, J., Huber-Lee, A., & Karlberg, L. (2007). Looking ahead to 2050: scenarios of alternative investment approaches. In: Molden, D. (Ed.), Comprehensive Assessment of Water Management in Agriculture, Water for Food, Water for Life: A Comprehensive Assessment of Water Management in Agriculture. International Water Management Institute, London: Earthscan, Colombo, pp. 91–145 (Chapter 3)

Diaz, H. F., Grosjean, M., & Graumlich, L. (2003). *Climate variability and change in high elevation regions: past, present and future* (pp. 1-4). Springer Netherlands.

Diaz-Nieto, J., & Wilby, R. L. (2005). A comparison of statistical downscaling and climate change factor methods: impacts on low flows in the River Thames, United Kingdom. *Climatic Change*, *69*(2-3), 245-268.

Dingman, S. L. (1994). *Physical hydrology* (Vol. 575). Englewood Cliffs, NJ: Prentice Hall.

Dingman, S. L., Seely-Reynolds, D. M., & Reynolds, R. C. (1988). Application of kriging to estimating mean annual precipitation in a region of orographic influence. *Water Resources Bulletin* 24: 329–339.

Diodato, N. (2005). The influence of topographic co-variables on the spatial variability of

precipitation over small regions of complex terrain. *International Journal of Climatology* 25: 351–363.

Dolman, A. J., Hall, A. J., Kavvas, M. L., Oki, T. & Pomeroy, J. W. (Eds.). (2001). *Soil-Vegetation-Atmosphere Transfer Schemes and Large-Scale Hydrological Models.* IAHS Publ. No 270, 372pp.

Donnelly, C., Dahne, J., Lindström, G., Rosberg, J., Strömqvist, J., Pers, C., & Arheimer, B. (2009). An evaluation of multi-basin hydrological modelling for predictions in ungauged basins. *IAHS publication*, *333*, 112

Draper, N. R., & Smith, H. (1998). Fitting a straight line by least squares. Applied Regression Analysis, Third Edition.

Drogue, G., Humbert, J., Deraisme, J., Mahr, N., & Freslon, N. (2002). A statistical-topographic model using an omnidirectional parametrization of the relief for mapping orographic rainfall. *International Journal of Climatology* 22: 599–613.

Droogers, P., & Allen, R. G. (2002). Estimating reference evapotranspiration under inaccurate data conditions. *Irrigation and drainage systems*, *16*(1), 33-45.

Droogers, P., & Aerts, J. (2005). Adaptation strategies to climate change and climate variability: a comparative study between seven contrasting river basins. *Physics and Chemistry of the Earth, Parts A/B/C*, *30*(6), 339-346

Dunne, T., Moore, T., & Taylor, C. H. (1975). Recognition and prediction of runoff-producing zones in humid regions. *Hydrological Sciences Bulletin*, *20*(3), 305-327.

Durran, D. R., & Klemp, J. B. (1982). The effects of moisture on trapped mountain lee waves. *Journal of the Atmospheric Sciences*, *39*(11), 2490-2506.

Eagleson, P. S. (1978). Climate, soil, and vegetation: 1. Introduction to water balance dynamics. *Water Resources Research*, *14*(5), 705-712.

Egger, K. (1980). Soil Erosion Control and Afforestation in the West Usambaras (Phase I). Immediate report on findings of the feasibility study teams, Tanga Integrated Rural Development Project TIRDEP

Eischeid, J. K., Bruce Baker, C., Karl, T. R., & Diaz, H. F. (1995). The quality control of long-term climatological data using objective data analysis. *Journal of Applied Meteorology*, *34*(12), 2787-2795.

Elshamy, M. E., & Wheater, H. S. (2009). Performance assessment of a GCM land surface scheme using a fine-scale calibrated hydrological model: an evaluation of MOSES for the Nile Basin. *Hydrological processes*, *23*(11), 1548-1564.

Fahey, B., & Jackson, R. (1997). Hydrological impacts of converting native forests and grasslands to pine plantations, South Island, New Zealand. *Agricultural and Forest Meteorology*, *84*(1), 69-82.

Falkenmark, M. & Rockström, J. (2004). *Balancing Water for Humans and Nature. The new approach in ecohydrology* . Earthscan, London

Falkenmark, M., Berntell, A., Jägerskog, A., Lundqvist, J., Matz, M. & Tropp, H. (2007). On the verge of a new water scarcity: a call for good governance and human ingenuity. SIWI Policy Brief (Sweden: Stockholm International Water Institute).

Falkenmark, M., & Molden, D. (2008). Wake up to realities of river basin closure. *Water Resources Development*, *24*(2), 201-215.

Farmer, D., Sivapalan, M., & Jothityangkoon, C. (2003). Climate, soil, and vegetation

controls upon the variability of water balance in temperate and semiarid landscapes: Downward approach to water balance analysis. *Water Resources Research*, *39*(2).
Feng, S., Hu, Q., & Qian, W. (2004). Quality control of daily meteorological data in China, 1951–2000: a new dataset. *International Journal of Climatology*, *24*(7), 853-870.
Fischer, A. S., Terray, P., Guilyardi, E., Gualdi, S., & Delecluse, P. (2005). Two independent triggers for the Indian Ocean dipole/zonal mode in a coupled GCM. *Journal of climate*, *18*(17), 3428-3449.
Fleuret, P. (1985). The social organization of water control in the Taita Hills, Kenya. *American Ethnologist*, *12*(1): 103-118.
Flügel, W. A. (1995). Delineating hydrological response units by geographical information system analyses for regional hydrological modelling using PRMS/MMS in the drainage basin of the River Bröl, Germany. *Hydrological Processes*, *9*(3-4), 423-436.
Food and Agriculture Organization (FAO). (2002). World Agriculture: Towards 2015/2030: Summary Report, Rome.
Fowler, H. J., Blenkinsop, S., & Tebaldi, C. (2007). Linking climate change modelling to impacts studies: recent advances in downscaling techniques for hydrological modelling. *International Journal of Climatology*, *27*(12), 1547-1578.
Freeze, R. A., & Harlan, R. L. (1969). Blueprint for a physically-based, digitally-simulated hydrologic response model. *Journal of Hydrology*, *9*(3), 237-258.
Fu, P., & Rich, P. M. (2002). A geometric solar radiation model with applications in agriculture and forestry. *Computers and electronics in agriculture*, *37*(1), 25-35.
Gilland, B. (2002). World population and food supply: Can food production keep pace with population growth in the next half-century?. *Food Policy*, *27*(1), 47-63.
Glantz, M. H. (1992). Global warming and environmental change in sub-Saharan Africa. *Global Environmental Change*, *2*(3), 183-204.
Gleick, P. H. (2003). Global freshwater resources: soft-path solutions for the 21st century. *Science*, *302*(5650), 1524-1528.
Gonzalez-Rouco, J. F., Jimenez, J. L., Quesada, V., & Valero, F. (2001). Quality control and homogeneity of precipitation data in the southwest of Europe. *J Climate* 14(5):964–978
Goodale, C. L., Aber, J. D. , & Ollinger, S. V. (1998). Mapping monthly precipitation, temperature, and solar radiation for Ireland with polynomial regression and a digital elevation model. *Climate Research* 10:35–49
Goovaerts, P. (1997). *Geostatistics for natural resources evaluation*. Oxford University Press.
Goovaerts, P. (2000). Geostatistical approaches for incorporating elevation into the spatial interpolation of rainfall. *Journal of Hydrology* 228, 113–129.
Gosling, S. N., Taylor, R. G., Arnell, N. W., & Todd, M. C. (2011). A comparative analysis of projected impacts of climate change on river runoff from global and catchment-scale hydrological models. *Hydrology and Earth System Sciences*, *15*(1), 279-294.
Goulden, M., Conway, D., & Persechino, A. (2009). Adaptation to climate change in international river basins in Africa: a review/Adaptation au changement climatique dans les bassins fluviaux internationaux en Afrique: une revue. *Hydrological Sciences Journal*, *54*(5), 805-828.
Gowing, J. W., Young, M. D. B., Hatibu, N., Mahoo, H. F., Rwehumbiza, F., & Mzirai, O. B.

(2003). Developing improved dryland cropping systems for maize in semi-arid Tanzania. Part II. Use of a model to extrapolate and add value to experimental results. *Experimental Agriculture*, *39*(03), 293-306.

Gómez, J. D., Etchevers, J. D., Monterroso, A. I., Gay, C., Campo, J., & Martínez, M. (2008). Spatial estimation of mean temperature and precipitation in areas of scarce meteorological information. *Atmósfera*, *21*(1), 35-56.

Grayson, R. B., Moore, I. D., & McMahon, T. A. (1992). Physically based hydrologic modeling: 1. A terrain-based model for investigative purposes. *Water Resources Research*, *28*(10), 2639-2658.

Green, W. A., & Ampt, G. A. (1911). Studies on soil physics: 1. The flow of air and water through soils. *Journal of Agricultural Science*, **4**, 1–24.

Grove, A. (1993). Water use by the Chagga on Kilimanjaro. African Affairs 92: 431-448

Guan, H., Wilson, J. L., & Makhnin, O. (2005). Geostatistical mapping of mountain precipitation incorporating autosearched effects of terrain and climatic characteristics. *Journal of Hydrometeorology* 6:1018–1031.

Hansen, J., Sato, M., Ruedy, R., Lo, K., Lea, D. W., & Medina-Elizade, M. (2006). Global temperature change. *Proceedings of the National Academy of Sciences*, *103*(39), 14288-14293.

Hargreaves, G.H., & Samani, Z.A. (1985). Reference crop evapotranspiration from temperature. *Applied Engineering in Agriculture 1*(2), 96-99.

Hargreaves, G.H., & Allen, R. G. (2003). History and evaluation of Hargreaves evapotranspiration equation. *Journal of Irrigation and Drainage Engineering*, *129*(1), 53-63.

Hastenrath, S., Nicklis, A. & Greischar, L. (1993). Atmospheric–hydrospheric mechanisms of climate anomalies in the Western equatorial Indian Ocean. *J. Geophys. Res.*, 98, 219–235.

Hastenrath, S., Polzin, D., & Camberlin, P. (2004). Exploring the predictability of the 'short rains' at the coast of East Africa. *International journal of climatology*, *24*(11), 1333-1343.

Hastenrath, S., Polzin, D., & Mutai, C. (2007). Diagnosing the 2005 drought in equatorial East Africa. *Journal of Climate*, *20*(18), 4628-4637.

Hastenrath, S., Polzin, D., & Mutai, C. (2010). Diagnosing the Droughts and Floods in Equatorial East Africa during Boreal Autumn 2005–08. *Journal of Climate*, *23*(3).

Hay, L., Viger, R. & McCabe, G. (1998). Precipitation interpolation in mountainous regions using multiple linear regression', in *Hydrology, Water Resources and Ecology in Headwaters, Proceedings of the HeadWater '98 Conference,* Merano, Italy, April 1998, IASH Publ. 248, 33 – 38

Hay, L. E., Clark, M. P., Wilby, R. L., Gutowski Jr, W. J., Leavesley, G. H., Pan, Z., ... & Takle, E. S. (2002). Use of regional climate model output for hydrologic simulations. *Journal of Hydrometeorology*, *3*(5), 571-590.

Hanjra, M. A., & Qureshi, M. E. (2010). Global water crisis and future food security in an era of climate change. *Food Policy*, *35*(5), 365-377.

Häntzschel, J., Goldberg, V., & Bernhofer, C. (2005). GIS-based regionalisation of radiation,

temperature and coupling measures in complex terrain for low mountain ranges. *Meteorological Applications*, *12*(1), 33-42.

Hillel, D. (1998). *Environmental soil physics: Fundamentals, applications, and environmental considerations*. Academic press.

Hobbs, P. V., Easter, R. C., & Fraser, A. B. (1973). A theoretical study of the flow of air and fallout of solid precipitation over mountainous terrain: Part II. Microphysics. *Journal of the Atmospheric Sciences*, *30*(5), 813-823.

Hong, Y., Nix, H. A., Hutchinson, M. F., & Booth, T. H. (2005). Spatial interpolation of monthly mean climate data for China. *International Journal of Climatology*, *25*(10), 1369-1379.

Horton, R. E. (1933). The role of infiltration in the hydrologic cycle. *Transactions, American Geophysical Union*, *14*, 446-460.

Hostetler, S. W. (1994). Hydrologic and atmospheric models: the (continuing) problem of discordant scales. *Climatic Change*, *27*(4), 345-350.

Houghton, J. G. (1979). A model for orographic precipitation in the north-central Great Basin. *Monthly Weather Review*. 107: 1462-1475

Hulme, M., Doherty, R., Ngara, T., New, M., & Lister, D. (2001). African climate change: 1900-2100. *Climate research*, *17*(2), 145-168.

Indeje, M., & Semazzi, F. H. M. (2000). Relationships between QBO in the lower stratospheric zonal winds and east African seasonal rainfall. *Meteor. Atmos. Phys.* 73, 227–244.

Isaaks, E. H., & Srivastava, R. M. (1989). *An introduction to applied geostatistics*, Oxford University Press, New York.

IUCN. (2003). Eastern Africa Programme – The Pangani River Basin: A Situation Analysis, xvi + 104pp.

Jackson, R. B., Carpenter, S. R., Dahm, C. N., McKnight, D. M., Naiman, R. J., Postel, S. L., & Running, S. W. (2001). Water in a changing world. *Ecological applications*, *11*(4), 1027-1045.

Janowiak, J. E., (1988). An investigation of interannual rainfall variability in Africa. *J. Climate,* 1, 165–179.

Jenks, G. F. (1967). The data model concept in statistical mapping. *International yearbook of cartography*, *7*(1), 186-190.

Jenson, S. K., & Domingue, J. O. (1988). Extracting topographic structure from digital elevation data for geographic information system analysis. *Photogrammetric engineering and remote sensing*, *54*(11), 1593-1600.

Jiang, Q. (2003). Moist dynamics and orographic precipitation. *Tellus A*, *55*(4), 301-316.

Johansson, L. (2001). Ten million trees later: land use change in the West Usambara Mountains. The Soil Erosion Control and Agroforestry Project in Lushoto District 1981-2000. *Ten million trees later: land use change in the West Usambara Mountains. The Soil Erosion Control and Agroforestry Project in Lushoto District 1981-2000*.

Johnson, N. L., Kotz, S., & Balakrishnan, N. (1995). Continuous Univariate Distributions, vol. 2. *Second Edition*.

Jothityangkoon, C., Sivapalan, M., & Farmer, D. L. (2001). Process controls of water balance

variability in a large semi-arid catchment: downward approach to hydrological model development. *Journal of Hydrology*, *254*(1), 174-198.

Kaoneka, A. R. S., & Solberg, B. (1994). Forestry related land use in the West Usambara mountains, Tanzania. *Agriculture, ecosystems & environment*, *49*(2), 207-215.

Kaser, G., Hardy, D. R., Mölg, T., Bradley, R. S., & Hyera, T. M. (2004). Modern glacier Retreat on Kilimanjaro as evidence of climate change: observations and facts. *International journal of Climatology*, *24*(3), 329-339.

Kashimbiri, N., Chen, Y-F., & Zhou, J-X., (2005). Assessment of Effects of Human Development on the Environment by Using System Dynamic Modeling Technique (SD): A Case Study of the Mkomazi Watershed (Pangani Basin) in Northeastern Tanzania, Human and Ecological Risk Assessment: *An International Journal*, 11:2, 451-467,

Keiser, D. T., & Griffiths, J. F. (1997). Problems associated with homogeneity testing in climate variation studies: A case study of temperature in the northern Great Plains, USA. *International journal of climatology*, *17*(5), 497-510.

Khan, S., & Hanjra, M. A. (2008). Sustainable land and water management policies and practices: a pathway to environmental sustainability in large irrigation systems. *Land Degradation & Development*, *19*(5), 469-487.

Kijazi, A. L., & Reason, C. J. C. (2005). Relationships between intraseasonal rainfall variability of coastal Tanzania and ENSO. *Theoretical and applied climatology*, *82*(3-4), 153-176.

Ki-Moon, B. (2008). The new face of hunger. *Washington Post*, *12*.

Kirkby, M.J. (1993). Network hydrology and geomorphology. In: Beven, K., Kirkby, M.J. (Eds.), Channel Network Hydrology. John Wiley and Sons, Chichester, pp. 1–12.

Kirkby, M., Bracken, L., & Reaney, S. (2002). The influence of land use, soils and topography on the delivery of hillslope runoff to channels in SE Spain. *Earth Surface Processes and Landforms*, *27*(13), 1459-1473.

Klemeš, V. (1983). Conceptualization and scale in hydrology. *Journal of hydrology*, *65*(1), 1-23.

Knutti, R., Furrer, R., Tebaldi, C., Cermak, J., & Meehl, G. A. (2010). Challenges in combining projections from multiple climate models. *Journal of Climate*, *23*(10), 2739-2758.

Kuligowski, R. J., & Barros, A. P. (1999). High-resolution short-term quantitative precipitation forecasting in mountainous regions using a nested model. *Journal of Geophysical Research: Atmospheres (1984–2012)*, *104*(D24), 31553-31564.

Kurukulasuriya, P., Mendelsohn, R., Hassan, R., Benhin, J., Deressa, T., Diop, M., ... & Dinar, A. (2006). Will African agriculture survive climate change?. *The World Bank Economic Review*, *20*(3), 367-388.

Kutílek, M., & Nielsen, D. R. (1994). *Soil hydrology: texbook for students of soil science, agriculture, forestry, geoecology, hydrology, geomorphology and other related disciplines*. Catena Verlag.

Lanzante, J. R. (1996). Resistant, robust and non-parametric techniques for the analysis of climate data: Theory and examples, including applications to historical radiosonde station data. *International Journal of Climatology*, *16*(11), 1197-1226.

Latif, M., Dommenget, D., Dima, M., & Grötzner, A. (1999). The role of Indian Ocean sea surface temperature in forcing east African rainfall anomalies during December-January 1997/98. *Journal of Climate*, *12*(12), 3497-3504.

Legesse, D., Vallet-Coulomb, C., & Gasse, F. (2003). Hydrological response of a catchment to climate and land use changes in Tropical Africa: case study South Central Ethiopia. *Journal of Hydrology*, *275*(1), 67-85

Li, J., & Heap, A.D. (2008). *A Review of Spatial Interpolation Methods for Environmental Scientists*. Geoscience Australia, Record 2008/23, 137 pp.

Lidén, R., & Harlin, J. (2000). Analysis of conceptual rainfall–runoff modelling performance in different climates. *Journal of Hydrology*, *238*(3), 231-247.

Lindström, G. (1997). A simple automatic calibration routine for the HBV model. *Nordic Hydrology 28*, 153-168.

Lindström, G., Johansson, B., Persson, M., Gardelin, M., & Bergström, S. (1997). Development and test of the distributed HBV-96 hydrological model. *Journal of hydrology*, *201*(1), 272-288.

Lindström, G., Rosberg, J., & Arheimer, B. (2005). Parameter precision in the HBV-NP model and impacts on nitrogen scenario simulations in the Rönneå River, Southern Sweden. *AMBIO: A Journal of the Human Environment*, *34*(7), 533-537.

Lindström, G., Pers, C., Rosberg, J., Strömqvist, J., & Arheimer, B. (2010). Development and testing of the HYPE (Hydrological Predictions for the Environment) water quality model for different spatial scales. *Hydrology research*, *41*.

Maeda, E. E. M., Wiberg, D. A., & Pellikka, P. K. E. (2011). Estimating reference evapotranspiration using remote sensing and empirical models in a region with limited ground data availability in Kenya. *Applied Geography* 31: 251–258.

Mair, A., & Fares, A. (2010). Comparison of rainfall interpolation methods in a mountainous region of a tropical island. *Journal of Hydrologic Engineering*, *16*(4), 371-383.

Makurira, H., Mul, M.L., Vyagusa, N.F., Uhlenbrook, S., & Savenije, H.H.G. (2007). Evaluation of community-driven smallholder irrigation in dryland South Pare Mountains, Tanzania: A case study of Manoo micro dam. Physics and Chemistry of the Earth 32(15-18): 1090-1097.

Marchant, R., Mumbi, C., Behera, S., & Yamagata, T. (2007). The Indian Ocean dipole–the unsung driver of climatic variability in East Africa. *African Journal of Ecology*, *45*(1), 4-16.

Mardikis, M. G., Kalivas, D. P., & Kollias, V. J. (2005). Comparison of interpolation methods for the prediction of reference evapotranspiration – An application in Greece. *Water Resources Management* 19: 251–278

Martínez-Cob, A. (1996). Multivariate geostatistical analysis of evapotranspiration and precipitation in mountainous terrain. *Journal of Hydrology*, *174*(1), 19-35.

Marquínez, J., Lastra, J., & García, P. (2003). Estimation models for precipitation in mountainous regions: the use of GIS and multivariate analysis. *Journal of hydrology*, *270*(1), 1-11.

McCuen, R. H. (1989). *Hydrologic analysis and design*, Prentice-Hall, Englewood Cliffs, NJ.

McVicar, T. R., Van Niel, T. G., Li, L., Hutchinson, M. F., Mu, X., & Liu, Z. (2007).

Spatially distributing monthly reference evapotranspiration and pan evaporation considering topographic influences. *Journal of Hydrology*, *338*(3), 196-220.

Merrey, D. J., & Sally, H. (2008). Micro-agricultural water management technologies for food security in southern Africa: part of the solution or a red herring. *Water Policy*, *10*(5), 515-530.

Mileham, L., Taylor, R., Thompson, J., Todd, M., & Tindimugaya, C. (2008). Impact of rainfall distribution on the parameterisation of a soil-moisture balance model of groundwater recharge in equatorial Africa. *Journal of Hydrology*, *359*(1), 46-58.

Minville, M., Brissette, F., & Leconte, R. (2008). Uncertainty of the impact of climate change on the hydrology of a nordic watershed. *Journal of Hydrology*, *358*(1), 70-83

Mitchell, T. D., & Jones, P. D. (2005). An improved method of constructing a database of monthly climate observations and associated high-resolution grids. *International journal of climatology*, *25*(6), 693-712.

Molden, D., Frenken, K., Barker, R., de Fraiture, C., Mati, B., Svendsen, M., Sadoff, C. & Finlayson, M. (2007). Trends in water and agricultural development, in: D. Molden (Ed.) Water for Food, Water for Life: A Comprehensive Assessment of Water Management in Agriculture, pp. 57–89 (London: Earthscan; Colombo: IWMI).

Mongi, H., Majule, A. E., & Lyimo, J. G. (2010). Vulnerability and adaptation of rain fed agriculture to climate change and variability in semi-arid Tanzania. *African Journal of Environmental Science and Technology*, *4*(6).

Monteith, J. L. (1965). Evaporation and environment. In *Symp. Soc. Exp. Biol* (Vol. 19, No. 205-23, p. 4).

Moral, F. J. (2010). Comparison of different geostatistical approaches to map climate variables: application to precipitation. *International Journal of Climatology*, *30*(4), 620-631.

Muhongo, S., & Lenoir, J. L. (1994). Pan-African granulite-facies metamorphism in the Mozambique Belt of Tanzania: U-Pb zircon geochronology. *Journal of the Geological Society*, *151*(2), 343-347.

Mu, Q., Heinsch, F. A., Zhao, M., & Running, S. W. (2007). Development of a global evapotranspiration algorithm based on MODIS and global meteorology data. *Remote Sensing of Environment*, *111*(4), 519-536.

Mul, M.L., Mutiibwa, R.K., Foppen, J.W.A., Uhlenbrook, S., & Savenije, H.H.G. (2007). Identification of groundwater flow systems using geological mapping and chemical spring analysis in South Pare Mountains, Tanzania. *Physics and Chemistry of the Earth*, 32(15-18): 1015-1022.

Murphy, J. M., Sexton, D. M., Barnett, D. N., Jones, G. S., Webb, M. J., Collins, M., & Stainforth, D. A. (2004). Quantification of modelling uncertainties in a large ensemble of climate change simulations. *Nature*, *430*(7001), 768-772.

Murtugudde, R. McCreary, P. P. J, & Busalacchi, A. J. (2000). Oceanic processes associated with anomalous events in the Indian Ocean with relevance to 1997–1998. *J. Geophys. Res.*, 105 (C2), 3295–3306.

Mutai, C. C., Ward, M. N., & Colman, A. W. (1998). Towards the prediction of the East Africa Short Rains based on sea-surface temperature–atmosphere coupling. *International Journal of Climatology* 18: 975–997.

Mutai, C. C., & Ward, M. N. (2000). East African rainfall and the tropical

circulation/convection on intraseasonal to interannual timescales. *Journal of Climate*, *13*(22), 3915-3939.

Mutakyahwa, M. K. D., Ikingura, J. R., & Mruma, A. H. (2003). Geology and geochemistry of bauxite deposits in Lushoto District, Usambara Mountains, Tanzania. *Journal of African Earth Sciences*, *36*(4), 357-369.

Müller-Wohlfeil, D. I., Bürger, G., & Lahmer, W. (2000). Response of a river catchment to climatic change: application of expanded downscaling to Northern Germany. *Climatic Change*, *47*(1-2), 61-89.

Nakićenović, N., Alcamo, J., Davis, G., De Vries, B., Fenhann, J., Gaffin, S., ... & Dadi, Z. (2000). Special report on emissions scenarios, working group III, Intergovernmental Panel on Climate Change (IPCC).

Nash, J., & Sutcliffe, J. V. (1970). River flow forecasting through conceptual models part I–A discussion of principles. *Journal of hydrology*, *10*(3), 282-290.

Neiman, P. J., Ralph, F. M., White, A. B., Kingsmill, D. E., & Persson, P. O. G. (2002). The statistical relationship between upslope flow and rainfall in California's coastal mountains: Observations during CALJET. *Monthly weather review*, *130*(6), 1468-1492.

New, M., Todd, M., Hulme, M., & Jones, P. (2001). Precipitation measurements and trends in the twentieth century. *International Journal of Climatology* 21: 1899–1922.

Newmark, W.D. (1998). Forest area, fragmentation, and loss in the Eastern Arc Mountains: implication for the conservation of biological diversity. Journal of East African Natural History, 87: 1-8.

Nicholson, S. E. (1996). A review of climate dynamics and climate variability in Eastern Africa. *The Limnology, Climatology and Paleoclimatology of the East African Lakes*, T. C. Johnson and E. O. Odada, Eds., Gordon and Breach, 25–56.

Nijssen, B., O'Donnell, G. M., Lettenmaier, D. P., Lohmann, D., & Wood, E. F. (2001). Predicting the discharge of global rivers. *Journal of Climate*, *14*(15), 3307-3323.

Nikolopoulos, E. I., Anagnostou, E. N., Borga, M., Vivoni, E. R., & Papadopoulos, A. (2011). Sensitivity of a mountain basin flash flood to initial wetness condition and rainfall variability. *Journal of Hydrology*, *402*(3), 165-178

Ninyerola, M., Pons, X., & Roure, J. M. (2000). A methodological approach of climatologically modeling air temperature and precipitation through GIS techniques. *International Journal of Climatology* 20(14):1823–1841

Ninyerola, M., Pons, X., & Roure, J. M. (2007). Monthly precipitation mapping of the Iberian Peninsula using spatial interpolation tools implemented in a Geographic Information System. *Theoretical and Applied Climatology*, *89*(3-4), 195-209.

Norbert, J., Moges, S.A. & Kachroo, R.K. (2002). Assessment of mapping of sustainability of rainfed agriculture in Pangani basin using dry spell analysis. In: J.O. Ngana (Editor), Water resources management , the case of the Pangani river basin, Issues and approaches. Dar Es Salaam University Press, Dar Es Salaam, Tanzania.

Noshadi, M., & Sepaskhah, A. R. (2005). Application of geostatistics for potential evapotranspiration estimation. *Iranian Journal of Science and Technology Transaction B-Engineering* 29: 343–355.

Obled, C. H., Wendling, J., & Beven, K. (1994). The sensitivity of hydrological models to

spatial rainfall patterns: an evaluation using observed data. *Journal of hydrology*, *159*(1), 305-333.

Ogallo, L. J. (1988). Relationship between seasonal rainfall in East Africa and the Southern Oscillation. *J. Climatol.*, 8, 31–43.

Osborn, H. B. (1984). Estimating precipitation in mountainous regions. J. Hydr. Eng 110: 1859-1863.

Palamuleni, L. G., Ndomba, P. M., & Annegarn, H. J. (2011). Evaluating land cover change and its impact on hydrological regime in Upper Shire river catchment, Malawi. *Regional Environmental Change*, *11*(4), 845-855

Pardo-Igúzquiza, E. (1998). Comparison of geostatistical methods for estimating the areal average climatological rainfall mean using data of precipitation and topography. *International Journal of Climatology* 18: 1031–1047.

Parry, M., Arnell, N., McMichael, T., Nicholls, R., Martens, P., Kovats, S., ... & Fischer, G. (2001). Millions at risk: defining critical climate threats and targets. *Global environmental change*, *11*(3), 181-183.

PBWO/IUCN. (2006). Hydrology and System Analysis Volume 1 of 2: The Hydrology of the Pangani River Basin. Report 1: Pangani River Basin Flow Assessment Initiative, Moshi, Tanzania.

PBWO/IUCN. (2007). Pangani River System – State of the Basin Report – 2007. PBWO, Moshi, Tanzania and IUCN Eastern Africa Regional Program, Nairobi, Kenya.

PWBO/IUCN. (2010). Climate change modelling for the Pangani Basin to support the IWRM planning process. Pangani River Basin Flow Assessment. Pangani Basin Water Board, Moshi and IUCN Eastern and Southern Africa Regional Programme. V+36 pp

Pereira, L.S., Perrier, A., & Allen, R. G. (1999). Evapotranspiration: concepts and future trends. *Journal of Irrigation and Drainage Engineering-ASCE* 125: 45–51.

Peterson, T. C., & Easterling, D. R. (1994). Creation of homogeneous composite climatological reference series. *International journal of climatology*, *14*(6), 671-679.

Petzold, M., & Kleyer, M. ([in prep]). Modeling sensitivity of land cover to environmental Factors and disturbance in North East Tanzania

Philippon, N., Camberlin, P., & Fauchereau, N. (2002). Empirical predictability study of October–December East African rainfall. *Quarterly Journal of the Royal Meteorological Society*, *128*(585), 2239-2256.

Phillips, D.L., Dolph, J., & Marks, D. (1992) A comparison of geostatistical procedures for spatial analysis of precipitation in mountainous terrain. *Agricultural and Forest Meteorology* 58: 119–141

Pilgrim, D. H., Chapman, T. G., & Doran, D. G. (1988). Problems of rainfall-runoff modelling in arid and semiarid regions. *Hydrological Sciences Journal*, *33*(4), 379-400.

Popkin, B. M. (2006). Technology, transport, globalization and the nutrition transition food policy. *Food Policy*, *31*(6), 554-569.

Postel, S. L., Daily, G. C., Ehrlich, P. R., Gelbard, A. H., Homer-Dixon, T., Fareri, P., ... & Ouharon, A. (1996). Human appropriation of renewable fresh water. *Science.*, *271*(5250), 785-8.

Postel, S. L., & Wolf, A. T. (2001). Dehydrating conflict. *Foreign Policy*,

*126*(September/October), 60-67.
Potkanski, T. & Adams, W.M. (1998). Water scarcity, property regimes and irrigation management in Sonjo, Tanzania. Journal of Development Studies, 34(4): 86-116
Priestley, C. H. B., & Taylor, R. J. (1972). On the assessment of surface heat flux and evaporation using large-scale parameters. *Monthly weather review*, *100*(2), 81-92.
Prudhomme, C., & Reed, D. W. (1999). Mapping extreme rainfall in a mountainous region using geostatistical techniques: a case study in Scotland. *International Journal of Climatology* 19(12): 1337–1356.
Ranhao, S., Baiping, Z., Jing, T. (2008). A multivariate regression model for predicting precipitation in the Daqing Mountains. Mt Res Dev 28:318–325
Räisänen, J. (2007). How reliable are climate models?. *Tellus A*, *59*(1), 2-29
Reek, T., Doty, S. R., & Owen, T. W. (1992). A deterministic approach to the validation of historical daily temperature and precipitation data from the cooperative network. *Bulletin of the American Meteorological Society*, *73*(6), 753-762.
Rhoades, D. A., & Salinger, M. J. (1993). Adjustment of temperature and rainfall records for site changes. *International Journal of climatology*, *13*(8), 899-913.
Rodriguez-Iturbe, I. (2000). Ecohydrology: A hydrologic perspective of climate-soil-vegetation dynamies. *Water Resources Research*, *36*(1), 3-9.
Roe, G. H. (2005). Orographic Precipitation. *Annual Review of Earth and Planetary Sciences*, *33*, 645-671.
Ronda, R. J., Van den Hurk, B. J. J. M., & Holtslag, A. A. M. (2002). Spatial Heterogeneity of the Soil Moisture Content and Its Impact on Surface Flux Densities and Near-Surface Meteorology. *Journal of Hydrometeorology*, *3*(5).
Rosegrant, M. W., & Cline, S. A. (2003). Global food security: challenges and policies. *Science*, *302*(5652), 1917-1919.
Rost, S., Gerten, D., Bondeau, A., Lucht, W., Rohwer, J., & Schaphoff, S. (2008). Agricultural green and blue water consumption and its influence on the global water system. *Water Resources Research*, *44*(9).
Rummukainen, M. (2010). State-of-the-art with Regional Climate Models. *Wiley Interdisciplinary Reviews: Climate Change*, *1*(1), 82-96.
Saji, N. H., Goswami, B. N., Vinayachandran, P. N., & Yamagata, T. (1999). A dipole mode in the tropical Indian Ocean. *Nature*, *401*(6751), 360-363.
Salathé, E. P. (2003). Comparison of various precipitation downscaling methods for the simulation of streamflow in a rainshadow river basin. *International Journal of Climatology*, *23*(8), 887-901.
Samuelsson, P., Bringfelt, B., & Graham, L. (2003). The role of aerodynamic roughness for runoff and snow evaporation in land-surface schemes—comparison of uncoupled and coupled simulations. *Global and Planetary Change*, *38*(1), 93-99.
Saxton, K. E., & Rawls, W. J. (2006). Soil water characteristic estimates by texture and organic matter for hydrologic solutions. *Soil Science Society of America Journal*, *70*(5), 1569-1578.
Schulze, R. E. (1997). Impacts of global climate change in a hydrologically vulnerable region: challenges to South African hydrologists. *Progress in Physical Geography*, *21*(1), 113-136.
Seckler, D., Barker, R., & Amarasinghe, U. (1999). Water scarcity in the twenty-first century. *International Journal of Water Resources Development*, *15*(1-2), 29-42.
Sevruk, B. (1986). Correction of precipitation measurements, summary report. In: Sevruk B

(ed) Correction of precipitation measurements. ETH, Geographisches Institut, Zurich, pp 13–23

Shah, T., Bhatt, S., Shah, R. K., & Talati, J. (2008). Groundwater governance through electricity supply management: Assessing an innovative intervention in Gujarat, western India. *Agricultural Water Management*, *95*(11), 1233-1242.

Shepard, D.L., (1968). A two dimensional interpolation function for irregularly spaced data. Proc. 23rd Nat. Conf., Assoc. Computing Machinery, ACM, Washington, pp. 517–524.

Shiffler, R. E. (1988). Maximum Z scores and outliers. *The American Statistician*, *42*(1), 79-80.

Shongwe, M. E., van Oldenborgh, G. J., van den Hurk, B., & van Aalst, M. (2011). Projected changes in mean and extreme precipitation in Africa under global warming. Part II: East Africa. *Journal of Climate*, *24*(14), 3718-3733

Sinclair, M. R. (1994). A diagnostic model for estimating orographic precipitation. *Journal of applied meteorology*, *33*(10), 1163-1175.

Singh V.P. (1995). Computer models of watershed hydrology, Water Resources Publications, LLC, USA.

Slingo, J., Spencer, H., Hoskins, B., Berrisford, P., & Black, E. (2005). The meteorology of the Western Indian Ocean, and the influence of the East African Highlands. *Philosophical Transactions of the Royal Society A: Mathematical, Physical and Engineering Sciences*, *363*(1826), 25-42.

Smith, R. B. (1979). The influence of mountains on the atmosphere. *Advances in geophysics.*, *21*, 87-230.

Smith, R. B., & Barstad, I. (2004). A linear theory of orographic precipitation. *Journal of the Atmospheric Sciences*, *61*(12), 1377-1391.

Solomon, S., Qin, D., Manning, M., Chen, Z., Marquis, M., Averyt, K. B., Tignor, M., & Miller, H. L. (eds.) (2007). Climate Change 2007: *The Physical Science Basis.* Contribution of Working Group I to the Fourth Assessment Report of the Intergovernmental Panel on Climate Change. Cambridge University Press, Cambridge, United Kingdom and New York, NY, USA, 996 pp.

Sorooshian, S., & Gupta, V. K. (1995). Model calibration. *Computer models of watershed hydrology*, 23-68.

Sperna, W. F. C., van Beek, L. P. H., Kwadijk, J. C. J., & Bierkens, M. F. P. (2010). The ability of a GCM-forced hydrological model to reproduce global discharge variability. *Hydrology and Earth System Sciences*, *14*(8), 1595-1621.

Syvitski, J. P., Morehead, M. D., & Nicholson, M. (1998). HYDROTREND: a climate-driven hydrologic-transport model for predicting discharge and sediment load to lakes or oceans. *Computers & Geosciences*, *24*(1), 51-68.

Thiessen, A. H. (1911). Precipitation Averages for Large Areas. *Monthly Weather Review* 39(7):1082-1084.

Thornthwaite, C. W. (1948). An approach toward a rational classification of climate. *Geographical review*, 55-94.

Tilman, D., Cassman, K. G., Matson, P. A., Naylor, R., & Polasky, S. (2002). Agricultural sustainability and intensive production practices. *Nature*, *418*(6898), 671-677.

Tilman, D., Balzer, C., Hill, J., & Befort, B. L. (2011). Global food demand and the sustainable intensification of agriculture. *Proceedings of the National Academy of Sciences*, *108*(50), 20260-20264.

Todd, M. C., Andersson, L., Ambrosino, C., Hughes, D., Kniveton, D. R., Mileham, L., ... & Wolski, P. (2011). Climate Change Impacts on Hydrology in Africa: Case Studies of River Basin Water Resources. In *African Climate and Climate Change* (pp. 123-153). Springer Netherlands.

Todini, E. (1988). Rainfall-runoff modeling—Past, present and future. *Journal of Hydrology*, *100*(1), 341-352.

Todini, E. (1996). The ARNO rainfall-runoff model. *Journal of Hydrology*, *175*(1), 339-382.

Thompson, L. G., Mosley-Thompson, E., Davis, M. E., Henderson, K. A., Brecher, H. H., Zagorodnov, V. S., ... & Beer, J. (2002). Kilimanjaro ice core records: evidence of Holocene climate change in tropical Africa. *Science*, *298*(5593), 589-593.

Trenberth, K. E., Smith, L., Qian, T., Dai, A., & Fasullo, J. (2007a). Estimates of the global water budget and its annual cycle using observational and model data. *Journal of Hydrometeorology*, *8*(4).

Trenberth, K.E., Jones, P.D., Ambenje, P., Bojariu, R., Easterling, D., Klein, T. A., Parker, D., Rahimzadeh, F., Renwick, J. A., Rusticucci, M., Soden, B., & Zhai, P. (2007b). Observations: Surface and Atmospheric Climate Change. In: *Climate Change 2007: The Physical Science Basis*. Contribution of Working Group I to the Fourth Assessment Report of the Intergovernmental Panel on Climate Change [Solomon, S., Qin, D., Manning, M., Chen, Z., Marquis, M., Averyt, K. B., Tignor, M., & Miller, H. L. (eds.)]. Cambridge University Press, Cambridge, United Kingdom and New York, NY, USA.

Turpie, J., Ngaga, Y. & Karanja, F. (2003). A preliminary economic assessment of water resources of the Pangani river basin, Tanzania: economic value, incentives for sustainable use and mechanisms for financing management., PBWO, Moshi

Um, M. J., Yun, H., Cho, W., & Heo, J. H. (2010). Analysis of Orographic Precipitation on Jeju-Island Using Regional Frequency Analysis and Regression. *Water resources management*, *24*(7), 1461-1487.

United Nations (UN). (2013). World Population Prospects: The 2012 Revision, Volume I: Comprehensive Tables ST/ESA/SER.A/336.

United Republic of Tanzania (URT). (1965). Geological survey of Tanzania, quarter degree sheet 89, Same, Geological division, Dodoma, Tanzania.

United Republic of Tanzania (URT). (1977). Water Master Plan: Kilimanjaro Region, Ministry of Water, Energy and Minerals, Dar es Salaam.

Varis, O., Kajander, T., & Lemmelä, R. (2004). Climate and water: from climate models to water resources management and vice versa. *Climatic Change*, *66*(3), 321-344.

Vicente-Serrano, S. M., Lanjeri, S., & López-Moreno, J. I. (2007). Comparison of different procedures to map reference evapotranspiration using geographical information systems and regression-based techniques. *International Journal of Climatology*, *27*(8), 1103-1118.

Vincent, L. A., & Gullett, D. W. (1999). Canadian historical and homogeneous temperature datasets for climate change analyses. *International Journal of Climatology*, *19*(12), 1375-1388.

von Storch, H., Langenberg, H., & Feser, F. (2000). A spectral nudging technique for dynamical downscaling purposes. *Monthly weather review*, *128*(10), 3664-3673.

Ward, A. D., & Trimble, S. W. (2004). *Environmental Hydrology 2nd Edition*. Lewis Publishers, New York

Webster, P. J., Moore, A. M., Loschnig, J. P., & Leben, R. R. (1999). Coupled ocean-atmosphere dynamics in the Indian Ocean during 1997–98. *Nature,* 401, 356–360.

Weisse, A. K., & Bois, P. (2001). Topographic effects on statistical characteristics of heavy rainfall and mapping in the French Alps. *J. Appl. Meteor.*, 40, 720–740.

Western, A. W., Grayson, R. B., & Blöschl, G. (2002). Scaling of soil moisture: A hydrologic perspective. *Annual Review of Earth and Planetary Sciences*, *30*(1), 149-180.

Western, A. W., Grayson, R. B., & Blöschl, G. (2002). Scaling of soil moisture: A hydrologic perspective. Annual Review of Earth and Planetary Sciences, 30(1), 149-180.

Westerberg, I., Walther, A., Guerrero, J. L., Coello, Z., Halldin, S., Xu, C. Y., ... & Lundin, L. C. (2010). Precipitation data in a mountainous catchment in Honduras: quality assessment and spatiotemporal characteristics. *Theoretical and applied climatology*, *101*(3-4), 381-396.

Wheater, H. S. (2002). Progress in and prospects for fluvial flood modelling. *Philosophical Transactions of the Royal Society of London. Series A: Mathematical, Physical and Engineering Sciences*, *360*(1796), 1409-1431

White, R. E. (2009). *Principles and practice of soil science: the soil as a natural resource*. John Wiley & Sons.

Whiteman, C. D. (2000). *Mountain meteorology: fundamentals and applications* (No. PNNL-12063). Pacific Northwest National Laboratory, Richland, WA (US).

Wilby, R. L., & Wigley, T. M. L. (1997). Downscaling general circulation model output: a review of methods and limitations. *Progress in Physical Geography*, *21*(4), 530-548.

Wilby, R. L., Hay, L. E., Gutowski, W. J., Arritt, R. W., Takle, E. S., Pan, Z., ... & Clark, M. P. (2000). Hydrological responses to dynamically and statistically downscaled climate model output. *Geophysical Research Letters*, *27*(8), 1199-1202.

Wood, A. W., Leung, L. R., Sridhar, V., & Lettenmaier, D. P. (2004). Hydrologic implications of dynamical and statistical approaches to downscaling climate model outputs. *Climatic change*, *62*(1-3), 189-216.

World Bank (2000). Spurring Agricultural and Rural Development. In: Can Africa Claim the 21st Century? Washington, DC.

Xu, C. Y., & Vandewiele, G.L. (1994). Sensitivity of monthly rainfall-runoff models to input errors and data length. *Hydrological Sciences Journal-Journal Des Sciences Hydrologiques* 39(2):157–176

Xu, C. Y. (1999). From GCMs to river flow: a review of downscaling methods and hydrologic modelling approaches. *Progress in Physical Geography*, *23*(2), 229-249.

Xu, C.Y., & Singh, V.P. (2001). Evaluation and generalization of temperature based methods for calculating evaporation. *Hydrological Processes* 15: 305–319.

Xu C. Y., & Singh, V. P. (2002). Cross Comparison of Empirical Equations for Calculating Potential Evapotranspiration with Data from Switzerland. *Water Resources Management* 16: 197–219.

Xu, C. Y., Widén, E., & Halldin, S. (2005). Modelling hydrological consequences of climate

change—progress and challenges. *Advances in Atmospheric Sciences*, *22*(6), 789-797.
Xu, C. Y., Tunemar, L., Chen, Y. D., & Singh, V. P. (2006). Evaluation of seasonal and spatial variations of lumped water balance model sensitivity to precipitation data errors. *Journal of hydrology*, *324*(1), 80-93.
Yawson, D. K., Kongo, V. M., & Kachroo, R. K. (2005). Application of linear and nonlinear techniques in river flow forecasting in the Kilombero River basin, Tanzania. *Hydrological sciences journal*, *50*(5).
Zaslavsky, D., & Sinai, G. (1981). Surface hydrology: I – explanation of phenomena. *Journal of the Hydraulics Division*, *107*(1), 1-16.
Zhang, X., & Srinivasan, R. (2009). GIS-Based Spatial Precipitation Estimation: A Comparison of Geostatistical Approaches1. *JAWRA Journal of the American Water Resources Association*, *45*(4), 894-906.
Zorita, E., Stocker, T. F., & von Storch, H. (2008). How unusual is the recent series of warm years?. *Geophysical Research Letters*, *35*(24).

# Curriculum vitae

## Personal data

Name: Godfrey Augustine Mmbando.
Born: September 04th 1977, Tanzania.

## Academic record

2004–2006: Master of Science in Water Resources Engineering, MSc. (WRE), at the University of Dar es Salaam, Tanzania.
2000–2004: Bachelor of Science in Civil and Transportation Engineering, BSc. (CET), at the University of Dar es Salaam, Tanzania.

## Professional appointments

2008–2010: CARE International in Tanzania: Project Manager, Trans-boundary Water for Biodiversity and Human Health project in the Mara River Basin, Tanzania.
2006–2007: CARE International in Tanzania: Project Engineer, Community Water Supply and Sanitation project in Kinondoni Municipal, Dar es Salaam, Tanzania.

## Publications [in preparation]

Mmbando, G., & Kleyer, M. Mapping Monthly Precipitation, Temperature and Evapotranspiration: a case study Mkomazi river basin (Tanzania).
Mmbando, G., & Kleyer, M. Hydrological modelling: a case study Mkomazi river basin (Tanzania).
Mmbando, G., & Kleyer, M. Hydrological modelling to Climate Change: a case study Mkomazi river basin (Tanzania).

# Acknowledgement

I would like to thank the friendship between Tanzania and Germany (Deutscher Akademisher Austausch Dienst, DAAD), which awarded grant for the Clim-A-Net project. The North-South Network on Climate Proofing of Vulnerable Regions project at the University of Oldenburg in cooperation with University of Dar es Salam and Nelson Mandela Metropolitan University in Port Elizabeth (DAAD grant number 50750590). This friendship awarded a scholarship for my study in Germany.

I am happy to see this doctoral research has come to an end successfully. Thanks to Prof. Dr. Michael Kleyer for his guidance, ideas, and comments. Such that this doctoral research works have been completed successfully and contribute a significant drop, in a scientific-arena pool. Likewise, thanks to Prof. Dr. Gudrun Massmann, her recommendations enabled me to undertake this research work at the University of Oldenburg.

Thanks to Mrs. Brigitte Hülsmann and Mrs. Helga Hosts, staffs of the department of landscape ecology at the University of Oldenburg. , I was never short of office supplies and computer software packages relevant to my study. I also appreciate working with PhD students of this department. It was great to work with Maximilian Petzold.

Many thanks to Clim-A-Net project coordinators: Kilian Köbrich, Malve von Möllendorff and Friederike Walther. My life in Germany was pleasing.

I acknowledge Tanzania Meteorological Agency and Pangani Water Board Office (Tanzania) for providing us with meteorological data.

# Erklärungen

Folgende Erklärungen füge ich gemäß § 10 Abs. 2 der Promotionsordnung (Stand: 12.01.2012) der Fakultät für Mathematik und Naturwissenchaften, Carl von Ossietzky Universität Oldenburg:

- Ich strebe eine Promotion zur Doktor der (Dr. Rer. Nat.) an.
- Ich habe die Dissertation „Hydrological Sensitivity of the Mkomazi Basin (Tanzania) to Climate Change" selbständing verfasst. Es wurden keine anderen als die angegebenen Hilfsmittel verwendet.
- Die Dissertation liegt/lag weder in ihrer Gesamtheit noch in Teilen einer anderen wissenschaftlichen Hochschule zur Begutachtung in einen Promotionsverfahren vor.

Ich bestätige hiermit die Richtigkeit dieser allegemeinen Erklärungen.

.....

Godfrey Mmbando.

# Authors' contribution

This section lists the contributions of all authors to Chapters 3 to 5.

**Chapter 3:** Mmbando, G., & Kleyer, M. Mapping Monthly Precipitation, Temperature and Evapotranspiration: a case study Mkomazi river basin (Tanzania).

MK designed the study; MG designed the methodology for modelling evapotranspiration and rainfall (transition zone), analysed data, prepared graphs and tables, constructed climate maps, and wrote the initial draft of the manuscript. All authors contributed to revisions of the manuscript.

**Chapter 4:** Mmbando, G., & Kleyer, M. Modelling Hydrological Response (rainfall–runoff): a case study Mkomazi river basin (Tanzania).

MK designed the study; MG designed the methodology for hydrological modelling, achieved hydrological modelling, prepared graphs and tables, constructed soil depths profile and moistures maps and wrote the initial draft of the manuscript. All authors contributed to revisions of the manuscript.

**Chapter 5:** Mmbando, G., & Kleyer, M. Modelling Hydrological Response to Climate Change: a case study Mkomazi river basin (Tanzania).

MK designed the study; MG designed the methodology for hydrological modelling, achieved hydrological modelling, prepared graphs and tables, constructed soil moisture availability maps and wrote the initial draft of the manuscript. All authors contributed to revisions of the manuscript.

# Dedication

To my father Augustine Barnabas Mmbando, he passed-away in the beginning of my study.
To my mother Mary John Mmbando, she took care of my children during my absence.
To my children Godson and Godwin, their prayers go to the real Almighty God.